UNIVERSITY OF OKLAHOMA

GRADUATE COLLEGE

EVALUATION OF SURFACE PREPARATION AND BOND ANGLE COMBINATIONS FOR JOINT REPLACEMENT USING ULTRA-HIGH PERFORMANCE CONCRETE

A THESIS

SUBMITTED TO THE GRADUATE FACULTY

in partial fulfillment of the requirements for the

Degree of

MASTER OF SCIENCE

By

CHANDLER K. FUNDERBURG
Norman, Oklahoma
2018

EVALUATION OF SURFACE PREPARATION AND BOND ANGLE COMBINATIONS FOR BRIDGE JOINT REPLACEMENT USING ULTRA-HIGH PERFORMANCE CONCRETE

A THESIS APPROVED FOR THE
SCHOOL OF CIVIL ENGINEERING AND ENVIRONMENTAL SCIENCE

BY

_____
Dr. Royce W. Floyd, Chair

_____
Dr. Jeffery S. Volz

_____
Dr. Philip S. Harvey Jr.

This thesis is dedicated to my parents—Jami and Leonard Braxton—for their continued love and support, and my grandparents—Gene and Jackie Funderburg—for always supporting and believing in me.

Acknowledgements

First and foremost, I would like to express my sincere gratitude to my advisor, Dr. Royce Floyd, for his continuous support of my research, for his patience, motivation, guidance, and positivity. I would also like to thank Dr. Jeffery Volz and Dr. Philip Harvey for providing guidance as committee members.

A big thank you to the Oklahoma Department of Transportation (ODOT) for supporting this project as part of SPR 2276, to the students who helped throughout the project –Connor Casey, Amy McDaniel, Dr. Cameron Murray, and Stephen Tanksley—and to Mike Schmitz and Donald G. Fears Structural Engineering Laboratory for providing support for the testing. I would also like to thank Lafarge North America for donating Ductal® and Dolese Bros. Co. for donating cement, aggregate, and Glenium.

Last, but certainly not least, I would like to thank my friends and family for being a continuous and unwavering support system throughout this process.

Table of Contents

List of Tables

List of Figures

Abstract

Deterioration of bridges is often attributed to declining performance of the longitudinal connections between precast members or transverse deck joints. Ultra-high performance concrete (UHPC) is a cementitious composite with mechanical and durability properties far exceeding those of conventional concrete, making it an ideal material for bridge deck joints. This project included a multi-faceted evaluation of the proprietary UHPC material, Lafarge Ductal®, to determine best practices for placing UHPC joints and to better understand their behavior. Composite modulus of rupture (MOR) specimens were tested in flexure to determine the effects of varying interface angles and levels of surface roughness on bond strength. Slant shear tests were performed on composite cylinders to provide a baseline of bond strength with no surface manipulation. Static and fatigue flexural testing was performed on three medium-scale slabs with heat cured UHPC joints to determine their flexural capacity and the effects of cyclic loading on the joint interface. The MOR specimens exceed the flexural strength of the base concrete, and most did not experience interface failure. Two slabs, tested statically in flexure, had experimental capacities exceeding the estimated capacity. The third slab, loaded cyclically, achieved 3 million cycles of a load less than the cracking load and experienced degradation in performance. It then failed at a much lower number of cycles after the load was increased. These results indicate that UHPC provides superior structural performance for slab joints and is worth studying further in future research.

1.0 Introduction

This thesis describes a project involving the evaluation of ultra-high performance concrete (UHPC) as a repair material for bridges in Oklahoma. UHPC is a type of concrete that has high compressive and tensile strength, high durability, low permeability, and increased potential for longer-lasting repair applications. Although UHPC is more expensive than other types of concrete, there is potential for a clear benefit when using it in small quantities for applications that will have a long-lasting impact. The use of UHPC can potentially give new concrete structures a longer life and extend the life of existing structures. It therefore can limit the cost and frequency of repairs, maintenance, and rehabilitation in comparison to normal strength concrete (NSC). Because UHPC is a fairly new material, more research is needed to study its behavior and possible applications.

1.1 Purpose of Study

The Oklahoma Department of Transportation (ODOT) is looking for information on the feasibility of UHPC as a solution for replacing deteriorated bridge joints. The short required steel embedment lengths and high impact resistance allow for a small quantity of highly durable material to be used in the vicinity of the joint. This has the potential to reduce the amount of material that must be removed and to replace steel angles used to protect the corners of the joint. In addition, difference in elevation between a UHPC repair and existing concrete can be corrected by grinding when no steel is used. UHPC has been

used in many precast applications, but the primary interest of ODOT is to assess the most efficient method of using UHPC as a repair material after old bridge joints have been sawn out, and limited data on this application are available. The results obtained from testing both the composite specimens and the medium-scale slab specimens will be used to make recommendations for field applications of UHPC in bridge joint repair.

1.2 General Overview

The use of UHPC is a fairly recent stride in the realm of high strength concrete. First introduced in the year 2000, UHPC is now being considered for more widespread use. It has been proven to solve issues commonly encountered with aging or deteriorated NSC including cracking, shrinkage, low durability, and freeze-thaw degradation. A primary advantage of UHPC is that it achieves extremely high strengths; compressive strengths are typically greater than 21 ksi and tensile strengths are typically greater than 0.72 ksi (Graybeal 2011). It is also highly flowable and more durable than other types of concrete (Graybeal 2011). UHPC has a negligible permeability; therefore, it is considered to be suitable as a protective barrier and repair material. UHPC achieves its high strength, enhanced durability, and workability with a mix composed of a wide range of aggregate sizes with a reduced amount of coarse aggregate, a water-cement ratio that is typically less than 0.25, and small fibers for reinforcement. The mix requires high-range water reducer (HRWR) to increase workability without adding more water to the mix. Table 1 outlines some typical properties of UHPC for reference.

Table 1. Typical UHPC Properties (Graybeal 2014)

Material Characteristic	Average Result
Density	155 lb/ft^3
Compressive strength (28-day)	21 ksi
Modulus of elasticity (28-day)	7,000 ksi
Direct tension cracking strength	1.2 ksi
Tensile strain capacity before crack localization and fiber debond	>0.003
Long-term creep coefficient	0.78
Long-term shrinkage	555 microstrain
Total shrinkage	790 microstrain
Coefficient of thermal expansion	$8.2*10^{-6}$ in/in/°F
Abrasion resistance	0.026 oz. lost
Freeze-thaw resistance	RDM = 99%

Construction using UHPC requires a number of different procedures than for NSC. It requires a higher mixing energy input and a longer mixing time, and it is important to make sure it does not overheat during mixing. Because UHPC is typically considered to be self-consolidating and contains steel fibers, internal vibration is not necessary during placement, nor recommended, as it may re-orient fibers. The compressive strength value at which the concrete has reached an acceptable level of hydration to allow the concrete to be put into service is typically 14 ksi. UHPC also has a longer set time than typical NSC. For this reason, heat curing is often used. Due to its differing properties from NSC, different quality control testing procedures are required for UHPC. For example, rather than the typical range of 28 to 42 psi/s for compressive testing of NSC, 150 psi/s is a more feasible stress rate that ensures the test is not unnecessarily prolonged (Graybeal 2011). Cube compression tests are also a

viable method to assess UHPC strengths. Because UHPC is self-consolidating and flows freely, mortar flow tests are more appropriate than slump tests.

1.3 Previous Implementation

While UHPC is a relatively new material, substantial previous research has been performed on UHPC properties and there have been multiple applications that serve as examples of its properties and methods of implementation. Table 2 shows different instances of UHPC use in practical applications. The most common applications thus far employed when considering bridges tend to be the use of UHPC for tee beams and girders of multiple shapes, as well as for joints between precast deck panels and longitudinal and transverse deck joints. The use of UHPC in joints between precast members in new construction has been extensively studied and implemented according to the literature. It has not, however, been extensively explored and implemented as a repair material for bridge joints (initially made of NSC) that have been removed or sawn out and require replacement. Although there has been a limited amount of research on UHPC as a repair material, its feasibility in this capacity is supported by previous research for other applications, which is a reasonable starting point to motivate further research.

Table 2. UHPC Applications in the United States (Graybeal 2013)

Name	Year	Application	Reference
Mars Hill Bridge, Wapello County, IA	2006	Three 45 in.-deep bulb tee beams	Bierwagon et al. Endicott
Route 624 over Cat Point Creek, Richmond County, VA	2008	Five 45 in.-deep bulb tee girders	Ozyildirim & Volgyi
Jakway Park Bridge, Buchanan County, IA	2008	Three 33 in.-deep pi-shaped girders	Keierleber et al.
State Route 31 over Canandaigua Outlet, Lyons, NY	2009	Joints between full-depth bulb tees	Shutt
State Route 23 over Otego Creek, Oneonta, NY	2009	Joints between full-depth deck panels	Royce
Little Cedar Creek, Wapello County, IA	2011	Fourteen 8 in.-deep waffle deck panels	Moore
Fingerboard Road Bridge over Staten Island Expressway, NY	2011-2012	Joints between deck bulb tees	Royce
State Route 248 over Bennett Creek, NY	2011	Joints between deck bulb tees	Royce
U.S. Route 30 over Burnt River and UPRR bridge, OR	2011	Haunch and shear connectors & transverse joints	Bornstedt
U.S. Route 6 over Keg Creek, Pottawatomie County, IA	2011	Longitudinal and transverse joints between beams	Graybeal
Ramapo River Bridge, Sloatsburg, NY	2011	Joints between full depth deck panels	Anon
State Route 42 Bridges (2) near Lexington, NY	2012	Joints between full depth deck panels and shear pockets	Anon
State Route 31 over Putnam Brook near Weedsport, NY	2012	Joints between full depth deck panels	Anon
I-690 Bridges (2) over Peat Street near Syracuse, NY	2012	Joints between full depth deck panels	Anon
I-690 Bridges (2) over Crouse Avenue near Syracuse, NY	2012	Joints between full depth deck panels	Anon
I-481 Bridge over Kirkville Road near Syracuse, NY	2012	Joints between full depth deck panels	Anon
Windham Bridge over BNSF Railroad on U.S. Route 87 near Moccasin, Montana	2012	Joints between full depth deck panels	Anon

1.4 Research Conducted

In order to meet the stated goals and objectives, the major areas of research conducted in this study focused on bond strength, interface angles, and surface preparations between the base concrete and a UHPC repair. Composite specimens composed of half normal strength portland cement concrete and half UHPC were tested in flexure to evaluate bond strength. These composite specimens were comprised of different combinations of surface preparation and bond angle to determine the resulting effects of these variables on the interface strength. Larger specimens (medium-scale slabs) were then statically and cyclically tested to determine flexural capacity and observe the effects of fatigue loading on flexural strength over time. The specific UHPC material examined in all testing is the Lafarge product Ductal®.

1.5 Hypotheses

Although this research will explore several combinations to determine the best surface preparation and bond angle for UHPC to base concrete connections, there is a preconceived idea of which combination may work best, based on related research found in the literature. The hypotheses for this study are as follows:

1. As seen in other research, a rougher bonding surface tends to yield the best results when assessing bond strength between two concrete materials. The roughest surface preparation implemented in this study will likely have the highest bond strength.

2. Orienting the bonding surface at some angle, either 45 or 60 degrees, or utilizing a shear key, will yield better results during testing of the composite specimens than a 90-degree bond angle (vertical interface).
3. Behavior of the medium-scale slab will be reasonably predicted by the smaller-scale composite MOR results.

1.6 Goals and Objectives

The study described in this thesis is part of a multi-phase project sponsored by ODOT (Floyd et al., 2016) with the overall goal of implementing UHPC as a repair material in Oklahoma and extending the service life of bridges with deteriorating joints. The objectives of the project are to identify appropriate mix design for UHPC made with local materials for use in joints, evaluate joint details, evaluate long-term performance of trial joints, and create specifications for UHPC construction in Oklahoma. The study was focused on the following objectives:

- Determine the best bond angle based on performance during composite MOR flexural interface testing
- Determine the best surface preparation based on performance during composite MOR flexural interface testing
- Assess the feasibility of using the best tested combination for field applications
- Apply the knowledge gained during small-scale testing to perform larger-scale testing of slab sections to determine initial cracking

moment, flexural capacity of the joint, and joint failure mode

- Make recommendations to ODOT about the best practice for UHPC replacement joints and develop a baseline standard to which future research can be compared to predict UHPC joint behavior and strength

2.0 Literature Review

UHPC is a cementitious composite material with increased durability and strength properties compared to NSC. UHPC was first developed in the late 20th century and is a product of advancements in superplasticizers, fiber reinforcements, supplementary cementitious materials, and optimized gradation of dry materials (Graybeal 2014). Its properties differ from those of typical portland cement concrete, so many of the methods for casting UHPC and determining its fresh and hardened material properties have been modified from the methods used for conventional concrete. Connections that are cast using UHPC can extend the life of a structure and allow for less maintenance over time. The use of UHPC for connecting precast elements has been the focus of many case studies and research projects. It has also been studied as an overlay material to repair and/or extend the life of existing bridges. However, the use of UHPC as a repair material for existing joints in bridges has not been extensively studied.

2.1 Placement, Curing, and Strength Gain

UHPC can be mixed in mortar/grout mixers as well as in traditional concrete mixers; however, traditional concrete mixers and ready-mix trucks may be less efficient than mixers with higher shear (Graybeal 2014). Higher shear mixers can decrease the duration of the mixing process, since they impart greater energy into the mix. It should also be noted that, typically, the maximum amount of UHPC that should be mixed in any mixer is about half the volume of conventional concrete that could be mixed (Graybeal 2014). It is typically placed

and moved using wheelbarrows or buckets. When there are two successive pours, the new UHPC should be poured directly over the most recently poured layer; sometimes rodding is necessary to limit the amount of separation between layers.

UHPC does not require the same type of finishing as traditional concrete. Because of its flowability and viscid nature, finishing with a trowel is not effective or necessary. UHPC should be poured into closed forms to provide a smooth top surface and minimize dehydration (Graybeal 2014). It can also be ground after curing to the desired surface texture or appearance.

For curing, the UHPC should be sealed in some way that does not allow moisture to escape and cause dehydration; moist curing is also an option. Multiple factors contribute to the extended initial set time of UHPC: temperature at time of placement, ambient temperature, admixtures, cement type, and constituent material properties (Graybeal 2014). Heat can be added to the UHPC after placement to accelerate strength gain. This is usually done by using external sources such as heating mats or lamps, or internal sources like resistance heating wires (Graybeal 2014). Figure 1 shows UHPC being mixed in the field with typical mixers. Figure 2 depicts the process for transporting UHPC from the mixer to the site of the pour and the pouring procedure for a longitudinal connection.

Figure 1. UHPC mixing operations (Graybeal 2014)

Figure 2. UHPC placement into longitudinal connection (Graybeal 2014)

2.2 UHPC as a Repair Material

The strength and durability properties of UHPC make it a good candidate to be a repair material that may provide a longer life to structures that are deteriorated or have been weakened. Both Sarkar (2010) and Denarie and Bruhwiler (2006) explored the feasibility of UHPC as a repair material. In both studies, UHPC was considered as an overlay repair material to be poured as a thin top layer on an existing roadway or bridge. While conducting research on the process of field implementation of a 3 cm thick UHPC overlay on a bridge in Switzerland, Denarie and Bruhwiler (2006) found that implementing UHPC in this capacity could “simplify the construction process, increase the durability of structures and their mechanical performance (stiffness and resistance), and decrease the number of interventions during their service life”. They performed analysis of the rehabilitation by noting the construction process and performing compressive and uniaxial tensile tests, ultimately determining that the benefits of implementing UHPC far outweigh the costs and surpass those of lower quality traditional solutions (Denarie and Bruhwiler 2006). Sarkar (2010) performed extensive evaluation of UHPC and its feasibility as an overlay material by performing slant shear tests, splitting tensile tests, and third point loading flexural tests on specimens with a 1 in. thick UHPC overlay. This study found that, based on its mechanical properties and the tensile properties exhibited during testing, UHPC achieves adequate bond strength to other concrete materials and is likely feasible as a repair material. Habel et al. (2004) also performed testing on a UHPC composite overlay configuration to

determine the bending behavior of the composite element. The study used a four point loading system, seen in Figure 3.

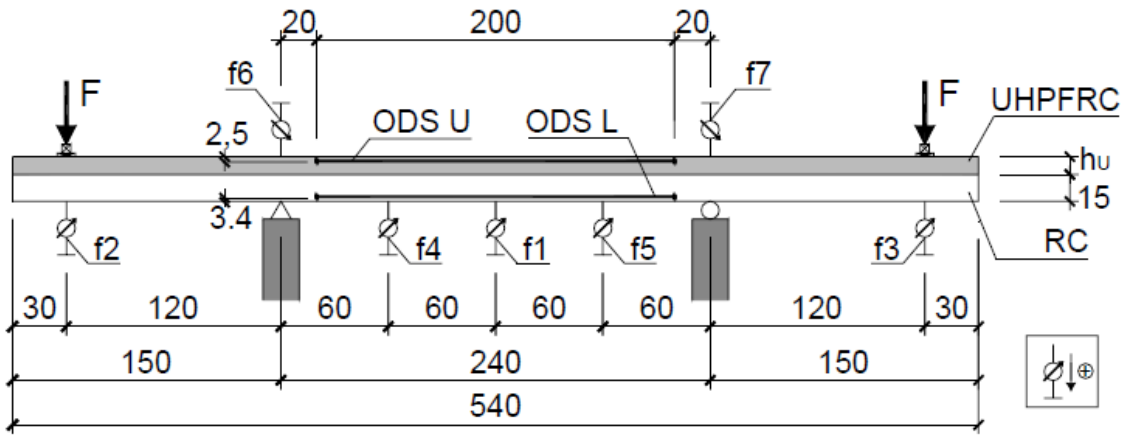

Figure 3. Four point loading system for Habel et al. (2004) experiments. Notations f1-f7 are LVDT locations, and dimensions are given in cm.

Three different types of overlays were studied (each having different depths and rebar configurations), and the following conclusions were made: (1) the enhanced mechanical properties of UHPC contribute to improved structural response of composite elements due to its strain-hardening behavior under uniaxial tension (2) the stiffness of the composite elements was increased under service loads, and no large cracks formed until the maximum force was reached, and (3) the addition of tensile reinforcement in the UHPC layer increased resistance and stiffness of the composite elements and delayed localized macrocracks (Habel et al., 2004).

2.3 UHPC Bond Strength as Determined by Slant Shear Tests

Sufficient bond strength between the existing concrete and repair material is one of the requirements for successful repair of any concrete

structure. There are multiple ways to assess bond strength, but the American Society for Testing and Materials (ASTM) has not specified a standardized method for applying slant shear to a regular concrete substrate and a repair concrete rather than epoxy for a composite specimen. Most researchers use a modified version of ASTM C882 and adaptations to other applicable standards, often referred to as slant shear tests, as a method to evaluate the behavior of composite specimens. Climaco et al. (2001) performed tests on prisms of different sizes and proportions, finding that the size of the specimens had little to no effect on the results obtained from testing. Carbonell Munoz et al. (2014) used prismatic slant shear specimens with an 89 mm by 89 mm cross-section and a height of 356 mm based on the British Standard (BS EN 12615:1999) of using prisms with a cross-section length and width that are one quarter of the height. In this study, the dimensions remained constant, while the interface angles were varied between 55, 60, and 70 degrees. Tayeh et al. (2013) performed experiments on prismatic slant shear specimens with a cross-section length and width of 100 mm, height of 300 mm, and interface angle of 60 degrees from the horizontal. Figure 4 shows an example of a prismatic specimen.

Some researchers that have adapted tests for slant shear have used a larger cylindrical version of the original ASTM C882 slant shear test. ASTM C882 specifies the cylinder size to be 3 in. by 6 in. for assessing mortar bonds, but researchers like Diab et al. (2017) used larger composite cylinders with diameters that were half of the height, finding smaller coefficients of variation

and results that were more consistent. Sarkar (2010) also performed slant shear tests on cylindrical specimens, seen in Figure 5. This study utilized 3 in. by 6 in. composite cylinders composed of half normal-strength concrete and half UHPC at a 30-degree angle.

Figure 4. Prismatic specimen and testing setup for Tayeh et al. (2013) experiments

Figure 5. Cylindrical specimen and testing setup for Sarkar (2010) experiments

According to Climaco et al. (2001), the stress state in slant shear tests at failure depends on the quality of the bond. In many of the experiments in previous research, the composite specimen failure occurred within the normal concrete substrate rather than the bond, indicating that these bonds could have resisted higher stresses and demonstrating the superior bond behavior of UHPC (Tayeh et al. 2013; Carbonell Munoz et al. 2014). In the Carbonell Munoz et al. (2014) experiments, the specimens “obtained a bond capacity, at the age of 3 days, greater than the [strength] requirements given by ACI 546-06 [Guide for Repair of Concrete Superstructures] (ACI 2006) at 7 days and also satisfies the requirements at 28 days.”

Momayez et al. (2005) performed a study on the bond strength between concrete substrates and various repair materials. This study included several types of tensile and shear testing, including pull-off tests, splitting prism tests, slant shear, and bi-surface shear testing. Although the study did not use UHPC as a repair material, the six repair materials used (each with a different mix design) provided useful information on the factors that affect bond strength, especially when using slant shear tests. Momayez et al. (2005) drew the following conclusions:

- The measured bond strength is highly influenced by the type of test performed. Each test that was conducted had an acceptable coefficient of variation, but it is crucial to select tests that represent the stress state of the structure or configuration in the field.
- Slant shear testing typically yields the highest measured bond strength.
- Bond strength between the repair material and the concrete substrate increases with the amount of silica fume in the repair material.
- Preparation of the concrete substrate surface that increases the roughness leads to a higher bond strength—about 25% higher for slant shear tests.

2.4 Surface Preparation

Preparation and alteration of cast concrete surfaces provides an increase in roughness and texture that allows materials subsequently cast against the prepared surface to adhere more thoroughly and form a better bond. The International Concrete Repair Institute (1997) provides a concrete surface preparation (CSP) index that describes nine different rubber profiles representing different degrees of roughness. There is also a macrotexture depth test in ASTM E965 that measures different degrees of roughness. In the experiments carried out by Carbonell Munoz et al. (2014) to test the effects of surface preparation on bond strength, the researchers examined six different surface preparations: smooth, slightly brushed; chipped; brushed; sandblasted; grooved; and rough, exposed aggregate. Figure 6 depicts the different surface preparations used in this study. The specimen with a deeply grooved substrate was the only one that had increased strength in the ambient dry substrate condition. In this case, the UHPC fit into the grooves rather than relying on bond strength alone. In slant shear testing, all specimens with a brushed surface (brushed during finishing) failed in the bond, which is to be expected for a surface with low roughness (Carbonell Munoz et al., 2014).

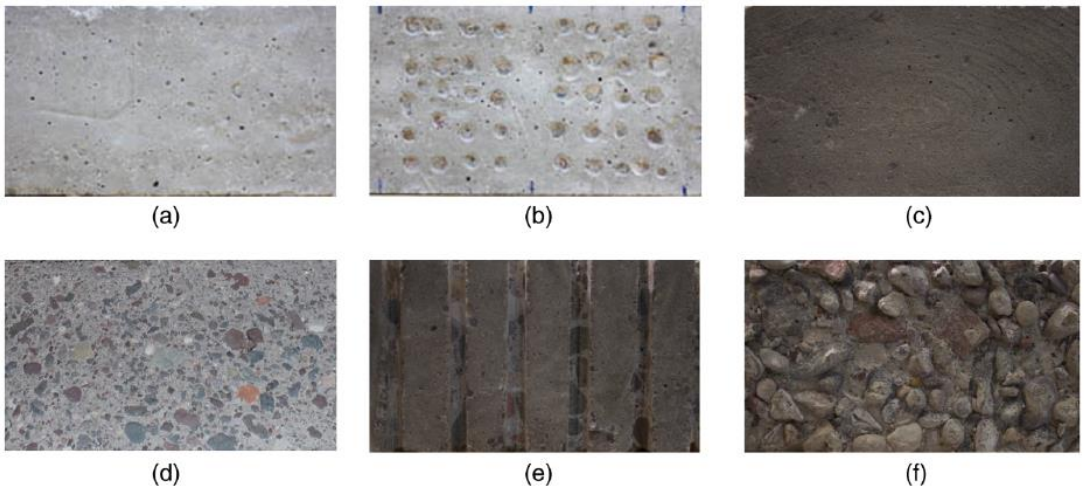

Figure 6. Substrate Surfaces: (a) smooth, slightly brushed; (b) chipped; (c) brushed; (d) sandblasted; (e) grooved; (f) rough, exposed aggregate (Carbonell Munoz et al., 2014)

All the bond strengths observed during testing by Carbonell Munoz et al. satisfied or exceeded bond requirements as outlined by the ACI 546-06 Guide to Concrete Repair (ACI 2006), but proved to be weak in comparison to the stand-alone strength of UHPC (Carbonell Munoz et al., 2014). Carbonell Munoz et al. (2014) also found that Ductal® performs better with concrete substrate that is saturated, and stated that “If the appropriate wetting conditions of the substrate are achieved, the degree of roughness . . . is not a critical factor to obtain good bond strength”. One important characteristic discovered in these experiments is that the bond and the strength of the UHPC had an important measurable turning point around the time that the concrete reached 2 to 3 days of age, where there was a significant increase in strength. At 2 days of age, the strength was significantly lower than at 3 days of age, and then from 3 days onward there was little to no change in strength (Carbonell Munoz et al., 2014).

This follows the pattern of the UHPC hydration process in which there is a dormant period followed by a significant energy release.

The results of the experiments carried out by Tayeh et al. (2013) and Sarkar (2010) also showed that a rougher surface yields a higher bond strength. When using split cylinder testing to determine tensile strength, as specified in ASTM C496, the sand blasted and grooved surface preparations performed the best, while the wire brushed surfaces failed prematurely (Tayeh et al., 2013). Sarkar (2010) found that in slant shear tests, specimens that had a smooth surface at the interface failed in the bond, while specimens with prepared surfaces—grooves and shear keys—failed in the substrate. The results of this study indicated that bond strength in shear/compression was increased by preparing the specimen surface, and that “UHPC can achieve adequate bond strength to other concretes so long as the surface preparation is appropriate for the loading conditions” (Sarkar 2010). Similarly, other research confirms that, typically, smooth brushed surfaces are too smooth to replicate real world situations of repair (Climaco et al., 2001).

2.5 Development Length

The development length required for reinforcing bars embedded in UHPC is much less than for NSC. Extensive research confirming the minimal development length required when using UHPC was conducted by Graybeal (2014), and is not uncharted territory due to the known effect of high compressive strength on reducing required development length. The shorter development length is considered an advantage because structural elements

can be connected using a smaller quantity of steel with less complicated bends and a smaller joint width and resulting amount of material can be used to make the connection. Cost and complexity of the joints both decrease with shorter development length. One example of implementation focuses on a set of bridges built in Syracuse, New York in 2013. The top and bottom mats of slab reinforcement only required a 6 in. wide connection (Graybeal 2014). Another example of implementation was carried out for a bridge on County Road 47 in Stockholm, New York, where yet again, the specification required a minimum lap splice length of only 6 in. for two precast slabs connected by a UHPC joint (Graybeal 2014).

2.6 Previous Laboratory Testing on UHPC Slab Joints

Apart from studying the behavior of interface bond for small-scale composite specimens, it is also beneficial to consider the bond behavior of UHPC and NSC in a slab-joint configuration. This information can be applied to similar configurations for bridges in the field and can connect small-scale testing data with field performance. Graybeal (2010) conducted research on six slab-joint configurations representing both transverse connections between precast deck panels and longitudinal connections between deck bulb-tee girders. The specimens were constructed with precast half-panels connected by a UHPC joint after about three weeks of curing. The UHPC joint was poured and cured for two weeks before being statically and cyclically tested in flexure. Cyclic loading was performed for at least 7 million total cycles at a maximum frequency of 6 Hz. Figures 7 and 8 depict the testing setup for both types of

joint (transverse and longitudinal). From this testing, several promising conclusions were made (Graybeal 2010):

- Performance of the connections tested equaled or exceeded what would be anticipated from a monolithic slab with no joint at mid-span.
- The development length of the reinforcement (#5 mild steel reinforcing bars) proved to be less than or equal to 5.9 in. and no debonding was observed.
- The cracking behavior of the specimens was not greatly affected by cyclic loading below the cracking moment, and cyclic loading just above the cracking moment did not greatly influence the structural behavior.
- The bond performance between the precast half-panels and the UHPC joint indicate that the precast panel bridge decking system (transverse) tested is unlikely to leak along the connection interface under cyclic service loads or static overloads.

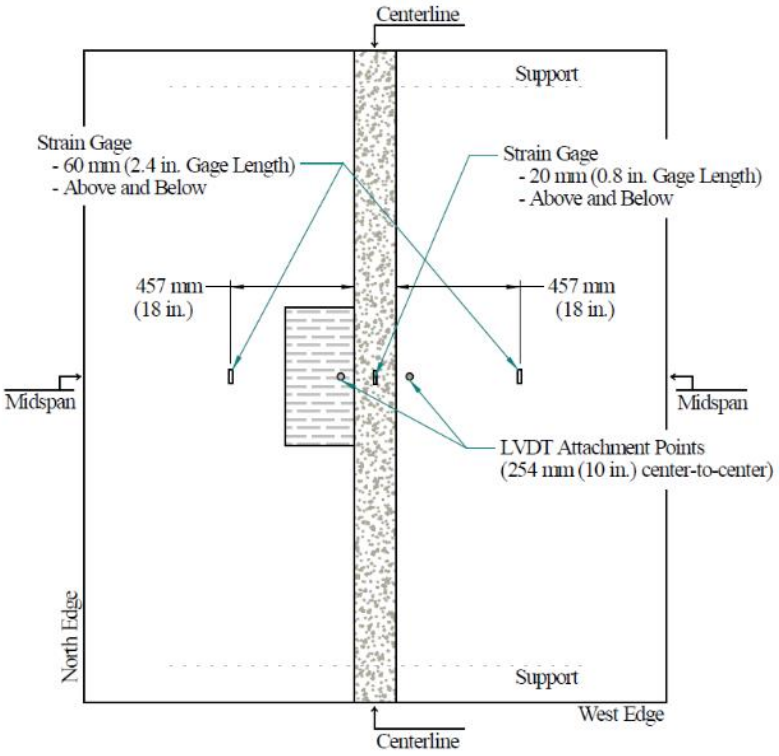

Figure 7. Layout for transverse joint specimen (Graybeal 2010)

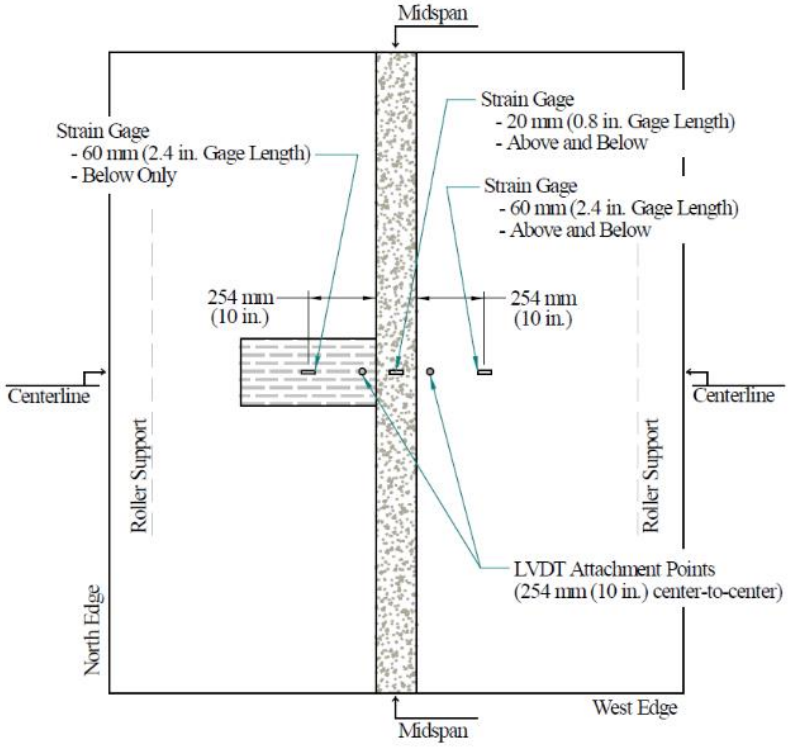

Figure 8. Layout for longitudinal joint specimen (Graybeal 2010)

2.7 Summary

UHPC has been extensively studied and implemented for use in precast applications and new construction. Its material properties, overall behavior, and placement techniques are fairly well known and have been tested time and again. However, assessments of the flexural strength of composite specimens based on the MOR test have not been widely conducted. The effects of surface preparation on bond strength have been studied as well, but not exclusively for the application of UHPC as a joint repair material. There is limited information about UHPC used for repairs at all, save for the few studies done to explore UHPC as an overlay material. A limited number of studies exist focused on determining the behavior of a UHPC joint in a slab under static and cyclic loading in flexure, and these considered specific joint reinforcing details for new construction, not retrofits. These gaps in information serve as a starting point for the research done in the current study.

3.0 Experimental Program

The purpose of this section is to outline the methods that were utilized to conduct the research described in Chapter 1. All research took place at Donald G. Fears Structural Engineering Laboratory unless otherwise specified. Additional photos of testing procedures and specimens are provided in Appendix B.

3.1 Composite MOR Specimens

To determine the effect of interface angles and surface preparations on flexural strength, 36 composite UHPC and NSC MOR specimens were cast and tested. Three surface preparations and four interface configurations were combined in order to construct the specimens.

3.1.1 Preliminary NSC Mix Design

This study began with identifying a suitable mix design meeting ODOT specifications for bridges and that is similar to the typical Dolese Bros. Co. mixes delivered to construction sites. The final NSC mix design chosen was intended to meet the ODOT Standard Specifications (2009) for Class AA concrete, seen in Table 3. The mix design was adapted using a spreadsheet previously developed by the research group and was based on past Class AA mixes obtained from Dolese Bros. Co. The purpose of meeting these parameters was to ensure a concrete substrate suitable for further comparison and easily replicable for implementation in the field.

Table 3. ODOT Standard Specifications (2009) for Concrete Related to Bridge Repair

Concrete Class	Min. Cement Content, lb/yd^3	Air Content, %	Water/Cement Ratio lb/lb	Slump, in.	Min. 28-Day Strength (f'c) psi
AA	564	6.5 ± 1.5	0.25 – 0.44	2 ± 1	4000
A	517	6.0 ± 1.5	0.25 – 0.48	2 ± 1	3000
HDC	825	6.5 ± 1.0	< 0.35	0.5 ± 1	4000
VES I	900	± 1.5	< 0.30	1 – 8	3000
VES III	600	6.0 ± 1.5	< 0.35	1 – 8	3000

Several trial batches were conducted to determine appropriate amounts of constituent materials and concrete properties to satisfy required specifications. These trial batches were mixed individually, and each had a volume of 1.5 ft^3. A chemical air-entraining agent, MasterAir AE90, was used to obtain the desired air content. Glenium 7920, a high-range water reducer, was added to increase the flow and workability of the concrete without increasing the water-cement ratio. Five trial batches were conducted over a period of three weeks, with varying water-cement ratios, amounts of high-range water reducer, and amounts of chemical air entraining agent, until the required fresh and hardened concrete properties were obtained. The first four trial batches were conducted to identify consistent mix proportions that yielded the appropriate values for the desired ODOT parameters for class AA concrete. Every time a new mix design was tested, only one variable was altered to isolate the effect of that specific variable. Each batch was tested for temperature, slump, air content, and compressive strength (in accordance with ASTMs C1064, C143,

C231, and C39, respectively). The fifth batch was conducted as a control batch to double check that the chosen mix design was consistent and behaved as expected. The trial mix designs and their corresponding data are shown in Table 4. The final mix design chosen was mix design 4, which satisfied the required standard. Although the slump for this mix was slightly higher than ODOT specifications, it was achieved through the use of high-range water reducer, and the overall performance was satisfactory. This mix design was used for the normal strength portion of the composite specimens.

Table 4. Trial Mix Designs

Mix Design	Cement Content, lb/yd^3	Air Content, %	Water/Cement Ratio lb/lb	Slump, in.	28-Day Strength (f'c) psi
1	588	7.80	0.31	9.50	8020
2	588	12.75	0.37	4.75	3700
3	588	3.20	0.37	1.25	6900
4	588	6.50	0.37	4.00	4220

3.1.2 Casting of NSC for Composite MOR Specimens

After choosing mix design 4, it was then used to batch the NSC that comprised half of each composite MOR specimen. Twelve full-length NSC MOR specimens with dimensions based on ASTM C78 (6 in. by 6 in. by 20 or 21 in.) were initially cast along with twelve half-length NSC MOR specimens in four different batches. Each batch included casting of 4 in. by 8 in. cylinders to be tested and to monitor compressive strength over time. Due to the slight

variance in compressive strength between specimens cast from different batches, MOR test results were normalized in such a way that they can be compared equitably. The normal strength specimens were cast in either wood or metal forms, some of which were modified to achieve a specific interface angle and surface roughness. The specimens were cast such that three surface preparations could be examined: wire-brushed, sandblasted, and exposed aggregate. The surface preparations were combined with four specified interface configurations: 90 degrees, 60 degrees, 45 degrees, and a shear key. The different surface preparations and configurations were later combined with UHPC to create a total of 36 composite specimens.

Due to limited production capacity in the lab, the specimens were cast in separate groups based on interface configuration. The 90 degree specimens were cast in batch N1, 60 degree specimens were cast in batch N2, 45 degree specimens were cast in batch N3, and the shear key specimens were cast in batch N4. Each specimen that was set to be wire-brushed or sandblasted were cast in their forms as full-length specimens that were later saw cut at the specified angle at 28 days of age. Each specimen that was set to have an exposed aggregate finish was cast as a half specimen because the exposed aggregate surface roughness condition cannot be carried out as efficiently after the concrete has cured. A list of the different combinations and their casting types can be seen in Table 5. Completed specimens and their companion cylinders were cured wrapped in wet burlap and plastic sheeting at 72°F. Figure 9 depicts the standard layout used to cast each batch.

Table 5. NSC Casting Types and Quantities

Configuration	Surface Preparation	Casting Type and Quantity	Resulting # Composite Specimens
90 degrees	Sand-Blasted	2 full specimens	4
90 degrees	Wire-Brushed	2 full specimens	4
90 degrees	Exposed Aggregate	3 half specimens	3
60 degrees	Sand-Blasted	2 full specimens	4
60 degrees	Wire-Brushed	2 full specimens	4
60 degrees	Exposed Aggregate	3 half specimens	3
45 degrees	Sand-Blasted	2 full specimens	4
45 degrees	Wire-Brushed	2 full specimens	4
45 degrees	Exposed Aggregate	3 half specimens	3
Shear Key	Exposed Aggregate	3 half specimens	3

Figure 9. Layout of formwork ready for concrete to be cast. From left to right: two for sandblasted specimens, two for wire-brushed specimens, and three for exposed aggregate specimens

3.1.3 Surface Preparations

Surface preparations were carried out in conjunction with saw cutting at the 28-day mark, at which time the specimens had reached a compressive strength of at least 4,000 psi.

Cutting Full Length Specimens

All specimens that required cutting were cut with a diamond blade concrete table saw, as seen in Figure 10. The saw was used to cut each full specimen into two halves, each having the same interface angle. A completed cut is shown in Figure 11. This same process was performed on all 45 degree, 60 degree, and 90 degree specimens (minus those with exposed aggregate). The standard for MOR specimens is to rotate them for testing so that the trowel-finished top surface of the specimen is on the side, and the smoother portions of the specimen become the top and bottom of the testing surface. The specimens were cut in such a way that the angled interface was measured clockwise from the top of the testing surface. This can be seen in Figure 12.

Figure 10. Concrete table saw used to cut MOR specimens

Figure 11. 45 degree specimen immediately after cutting

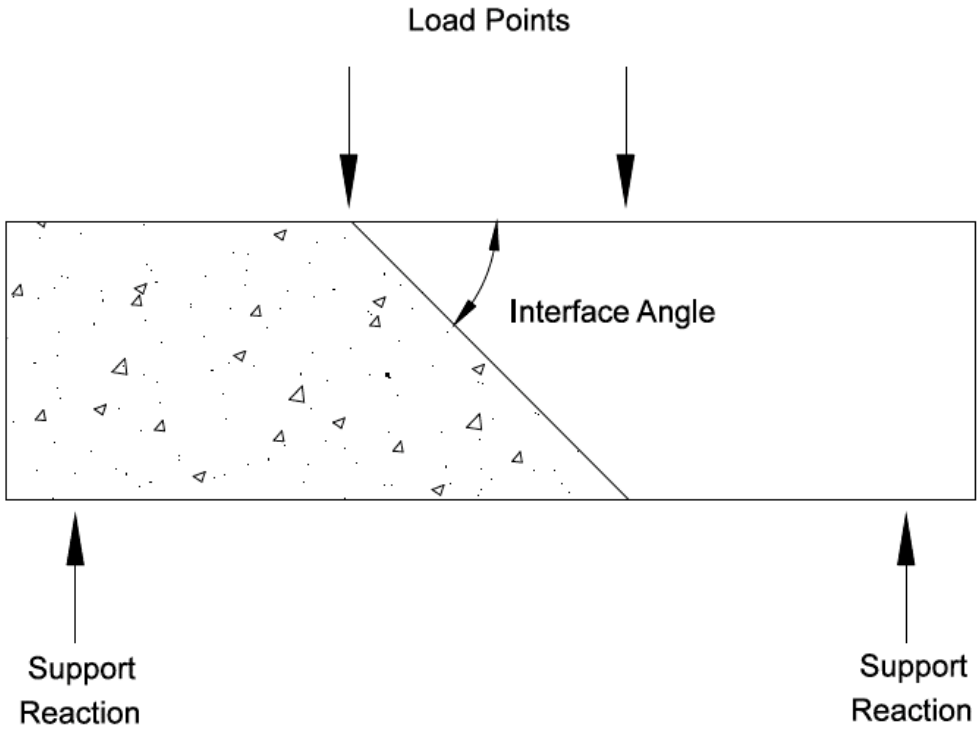

Figure 12. Relationship of interface angle to loading direction at top of testing surface

Creating the Shear Key

The specimens with shear keys required wooden inserts to form the shape of the shear key. A triangular shear key was used to create this shape in the exposed aggregate specimen. The wooden formwork insert is shown in Figure 13, and a completed specimen half is shown in Figure 14. The orientation of the shear key in relation to the testing direction is shown in Figure 15. The shear key specimens had an exposed aggregate surface only—this interface configuration was not combined with wire-brushed or sandblasted preparations.

Figure 13. Wood insert for shear key

Figure 14. Shear key specimen after being de-molded

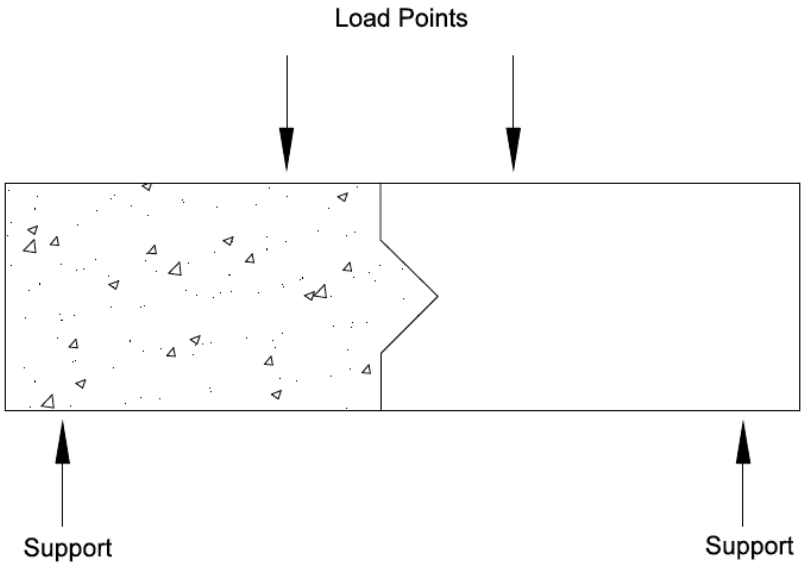

Figure 15. Relationship of shear key direction to loading direction

Exposed Aggregate Surface Preparation

All exposed aggregate specimens were cast as half specimens in the same forms used for the full NSC MOR specimens. Wooden inserts were used to create each of the four interface configurations (45 degree, 60 degree, and 90 degree as well as a shear key). The face of each wooden insert, seen in Figure 13, was coated with a general purpose spray adhesive and subsequently coated in sugar. Sugar naturally retards the curing process of concrete. This prevented the face of each concrete specimen in contact with the sugar from fully curing, allowing excess pieces of unhardened cement and aggregate to be removed. The excess material was removed by power washing the exposed face of the specimen at 28 days of age, thus exposing the remaining aggregate. A completed exposed aggregate surface is shown in Figure 16. This surface preparation, intuitively, provides the highest amount of material interlock between the NSC substrate and the UHPC.

Figure 16. Exposed aggregate surface after power washing

Sand-Blasting

Each interface surface for sand-blasted specimens was sand-blasted until a uniform surface roughness was visually observed. This took place in a standard sand-blasting cabinet. This preparation provides a roughness level that is in between the exposed aggregate and the wire brushed (smooth) finishes.

Wire Brushing

Wire brushing was performed on the smooth cut surface of the wire brushed specimens to clean away any debris. This surface preparation has no appreciable roughness and is considered smooth in comparison to the other surface preparations.

3.1.4 Casting and Curing of UHPC for Composite MOR Specimens

The UHPC portion of the composite specimens was cast after all of the surface preparation was completed (with all specimens no more than 35 days of age). This was the second and final step to complete casting of the composite MOR specimens. As previously mentioned, the UHPC used is the pre-mixed proprietary product, Ductal®. A high shear mortar mixer is best for mixing UHPC. A 4.25 ft^3 Imer Mortarman 120 Plus mortar mixer that could mix approximately 100 lb of material per batch without overloading the mixer was used for all UHPC batches. Flow measurements were not taken, but the specific mixing procedure for Ductal® as specified by the manufacturer, Lafarge North America, was followed in order to achieve the intended final product and maintain consistency between batches. Figures 17-20 depict various stages of the mixing process. The mixing steps were:

1. Ductal® premix dry components were mixed for 2 minutes
2. Half the amount of specified high range water reducer was combined with the water
3. Water-high range mixture was added slowly over the course of 2 minutes
4. After one minute the remaining amount of high range water reducer was added
5. Mixing was continued until the material reached a consistency similar to that seen in Figure 20

6. Steel fibers were added to the mix, and mixing was continued until they were dispersed evenly

Figure 17. Beginning stages of mixing after water was added to dry premix

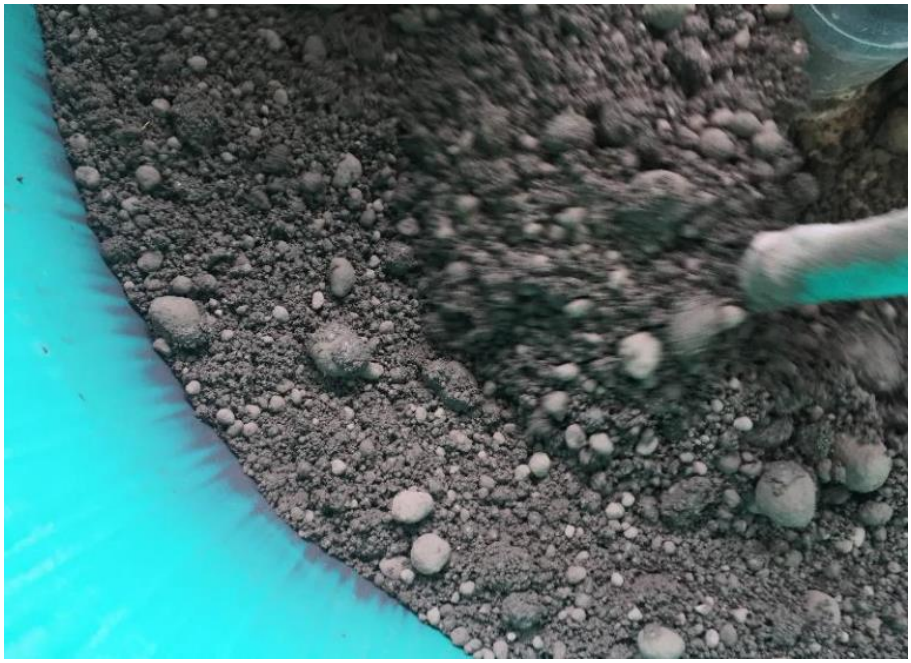

Figure 18. Progression of mix immediately after all high range water reducer was added

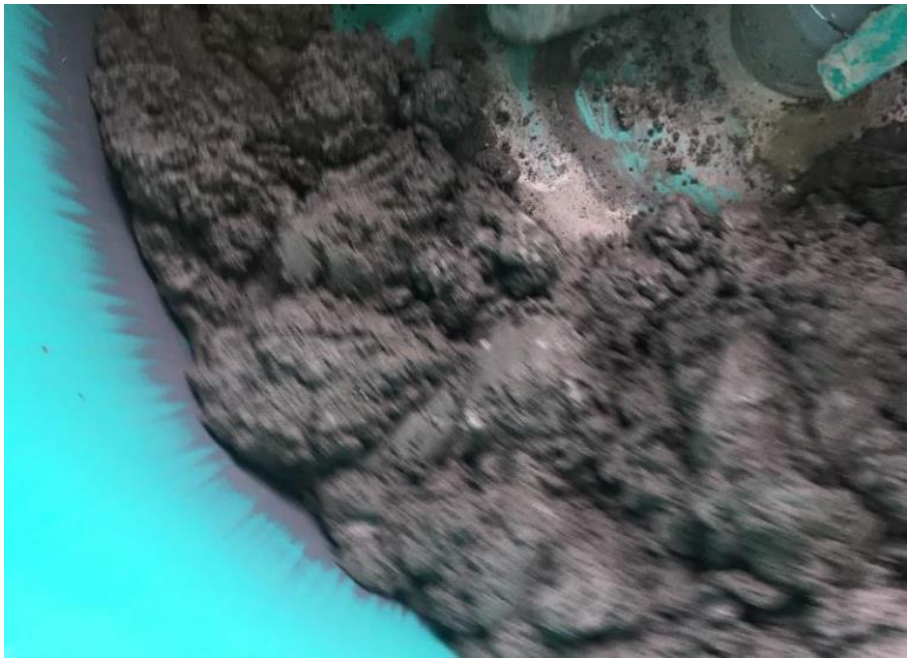

Figure 19. Consistency after several minutes of mixing beyond final addition of high-range water reducer, no additional components were added to reach this point

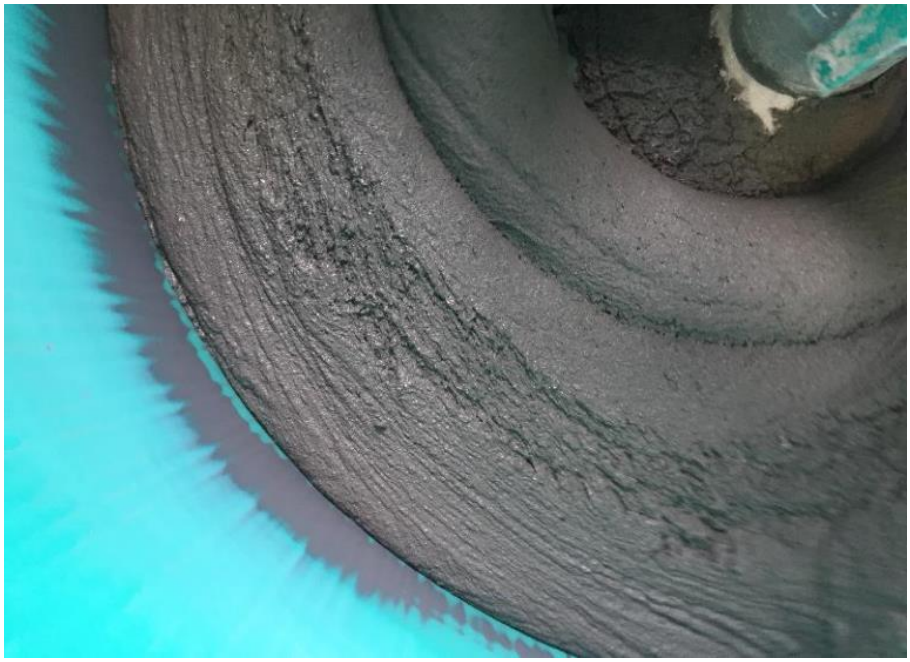

Figure 20. Final consistency of UHPC mixture prior to adding steel fibers

Because of the limited volumetric capacity of the mortar mixer used, each set of MOR specimens required four individual UHPC batches for completion. There were eleven specimens per set. The UHPC portion of the specimens was cast in the same groupings as the NSC specimens to maintain consistency of testing age. The 90 degree specimens were cast in batch U1, 60 degree specimens were cast in batch U2, 45 degree specimens were cast in batch U3, and shear key specimens were cast in batch U4. No consolidation measures were utilized during casting. Once the UHPC was cast, the composite specimens were allowed to cure for 28 days in an environmental chamber at 72°F covered with moistened burlap before being tested in flexure in accordance with ASTM C78. Figure 21 shows composite specimens immediately after casting, and Figure 22 shows specimens after curing. For the NSC portion of the specimens, 4 in. by 8 in. cylinders were tested in compression at 1 and 28 days as well as the day of flexural testing. For the UHPC portion, 3 in. by 6 in. cylinders were tested in compression at 3 and 28 days (test day).

Figure 21. Composite specimens immediately after casting

Figure 22. Composite specimens after curing

3.2 Composite MOR Testing

All of the composite MOR specimens were tested as simple beams with third-point loading in accordance with ASTM C78 once the UHPC portion reached 28 days of age. This testing was done using a Forney testing machine and the apparatus shown in Figure 23. The purpose of this test was to determine flexural strength and evaluate the effects, if any, each tested variable had on the flexural strength at the interface. At failure, a caliper was used to take measurements of the exact length and width of the failure surface. If the specimen failed along the interface, length and width measurements were taken for both sides of the specimen. These measurements were used to calculate the flexural stress at failure. In the instance of interface failure with two sets of measurements, the lowest flexural stress value was recorded.

Figure 23. Testing setup for composite MOR specimens

3.3 Slant Shear Specimens

A total of five slant shear specimens were cast to evaluate the feasibility of using the test for quality control in UHPC joint application. The slant shear specimens were cast as 6 in. by 12 in. cylinders, similar to those used by Sarkar (2010). The NSC portion of the slant shear specimens was cast using the same mix design as the composite MOR specimens. The UHPC portion of the slant shear specimens was cast using Ductal® and the same procedure as the composite MOR specimens. No additional surface preparation was conducted to the as-cast surface. The slant shear specimens underwent the same curing regimen as the composite MOR specimens to ensure consistency. A completed slant shear specimen is shown in Figure 24.

Figure 24. Composite slant shear specimen after curing

3.4 Slant Shear Testing

For slant shear specimens, testing was performed in accordance with ASTM C882. There were five total specimens tested at a loading rate of 35 ± 7 psi/second. The slant shear specimens were two times the size specified in ASTM C882. Because of this difference, bond strength values were determined by dividing the maximum failure load by the elliptical area of the interface, rather than using the area given in ASTM C882.

3.5 Construction of Medium-Scale Slab Specimens

3.5.1 Casting and Reinforcement

A total of three composite slabs were constructed to examine the effectiveness of UHPC connections. These slabs were NSC on either side, with a UHPC joint running through the slab at mid-span, and were intended to represent a connection between two sections of concrete bridge deck. Each slab consisted of two 4 ft by 4 ft by 8 in. thick reinforced concrete slab panels connected by a 1 ft wide UHPC joint. The slab panels were reinforced with #5 Grade 60 steel reinforcing bars as flexural reinforcement and temperature and shrinkage steel approximately matching the standard bridge deck reinforcement for Oklahoma bridges. The flexural reinforcing bars were spaced 12 in. on center. The reinforcement layout can be seen in Figure 25. The panels were cast with a portion of the reinforcing steel (5 in.) sticking out beyond the slab face (Figure 26). This exposed reinforcing steel was intended to represent the steel that may be exposed in the field after an existing deck joint is sawn out to be replaced, and the length was chosen based on the short development

lengths expected for UHPC. The concrete for casting the slab panels was supplied by Dolese Bros. Co. due to the large quantity needed for this portion of the study. The mix design for this concrete and a comparison to the concrete used for the composite MOR specimens can be seen in Table 6.

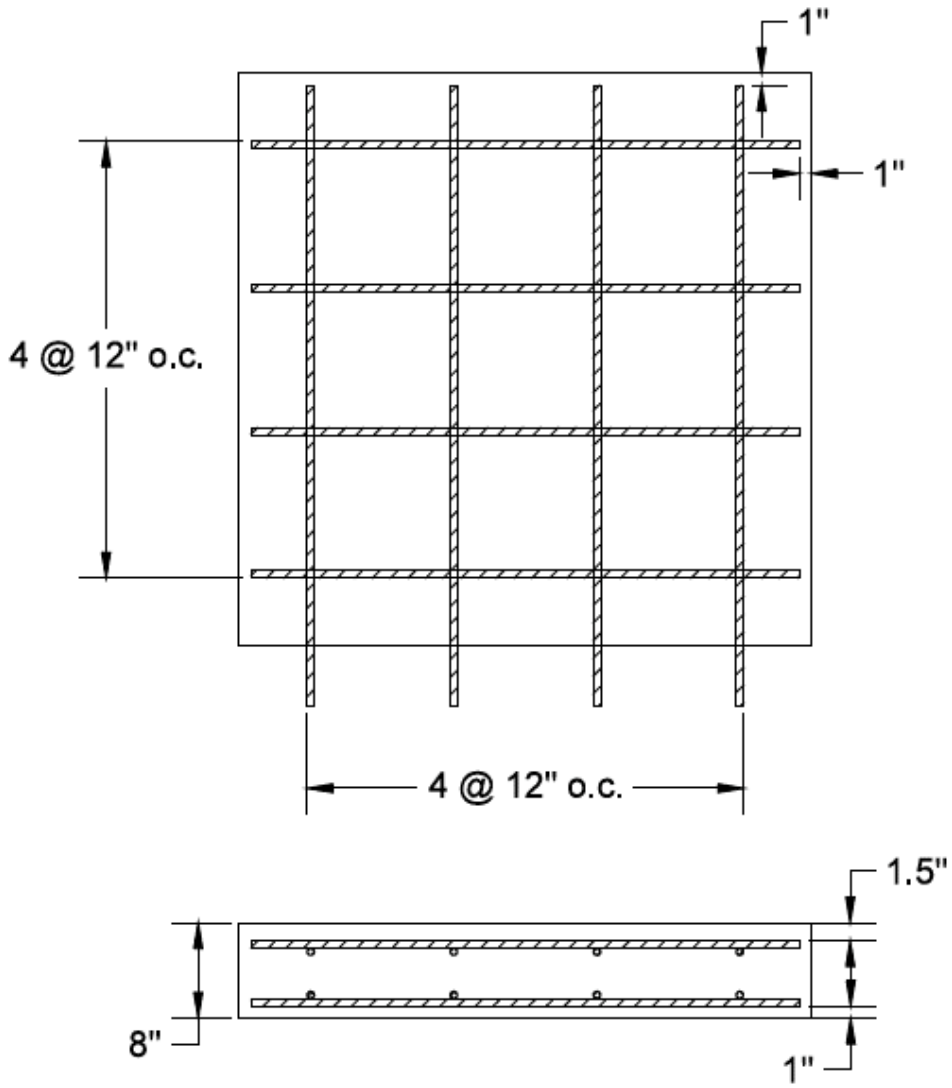

Figure 25. Overhead and cross-sectional view of rebar layout for slab specimens

Table 6. Concrete Mix Designs for Slabs and MOR Specimens

Material for Slabs	Quantity for Slab Mix Design	Quantity for MOR Mix Design
Cement (lb/yd^3)	470.0	588.0
Fly Ash (lb/yd^3)	118.0	0
Water (lb/yd^3)	153.3	218.0
Aggregate (lb/yd^3)	1858.9	1855.0
Air Entraining Agent (oz/yd^3)	3.3	4.1
Glenium 7920 (oz/yd^3)	17.6	20.6

Slab reinforcement prior to casting is shown in Figure 26. Similarly to the composite MOR specimens, the slabs were cured for 28 days. The slabs were cured in the ambient temperature conditions of the lab high bay. For the first week of curing, the concrete was covered with burlap and kept damp, as shown in Figure 27. The surface preparation for the slabs was wire-brushed. After curing, the UHPC joints were poured between two slab panels, resulting in three 4 ft by 9 ft slab specimens. Prior to the UHPC being poured, the protruding steel from each slab panel was joined together with a 10 in. long #5 splice bar to ensure proper development of forces between the two panels. The complete joint reinforcement before casting the UHPC is shown in Figure 28. The UHPC was mixed and poured through one end into closed forms and allowed to flow to the opposite end. The UHPC joints were formed over and left ¼ in. high, as is the practice recommended by the manufacturer. No consolidation measures were utilized. For compressive strengths, the NSC portion of the slab was tested with 4 in. by 8 in. cylinders at 1, 7, and 28 days as

well as test day. For the UHPC portion of the slab, 3 in. by 6 in. cylinders were tested at 12 hours (immediately after heat curing), 28 days, and test day.

Figure 26. Rebar layout prior to casting slab panels

Figure 27. Slab panels curing covered in burlap

Figure 28. Rebar layout for UHPC joint

3.5.2 Heat Curing

Immediately after pouring the UHPC, each joint was heat cured using a radiant heat lamp for 12 hours. The target internal concrete temperature was 190°F, and temperature data showed that internal temperature reached approximately 180°F. This heat curing regimen was chosen based on conclusions from a prior study done by fellow graduate student Connor Casey. Thermocouples were used to monitor the internal temperature at different depths within the joint and evaluate effectiveness of the heat curing. When the joint had been heat cured for 12 hours, the heat lamp was removed and the

joint was allowed to cure in ambient conditions for the remainder of 28 days. A completed and cured joint is shown in Figure 29.

Figure 29. Completed UHPC joint after curing

3.6 Slab Testing under Static and Cyclic Loading

Each slab specimen was tested in a steel portal frame and loaded using a hydraulic ram and pump. Each specimen was supported by a 6 in. wide concrete beam at either end with rubber pads between the slab and the support beam. The span length of each specimen was 8 ft 6 in., and the load point was located 5 ft 2 in. from the west end of the slab. Measurements of deflection were taken manually with a steel ruler at the load point during static load testing as well as digitally using 7 linear variable differential transformers (LVDTs) placed beneath the slab (locations shown in Figure 30). LVDTs 4, 6, and 7 were

placed 2 in. away from supports and slab edges. LVDTs 2, 3, and 5 were placed 2 in. from slab edges and 5 in. from the joint interface. Concrete strain was measured using 4 strain gages on the sides of the slab (locations shown in Figure 30). Strain gages 2 and 4 were placed directly in the center of the UHPC joint. Strain gages 1 and 3 were placed on either side of strain gage 2, approximately 1 in. from each joint interface. Each strain gage was approximately 0.4 in. from the bottom of the specimen. Load was measured using a load cell. All sensors were connected to a single data acquisition system collecting data at 20 Hz. The load was applied and distributed to each slab through a 10 in. by 20 in. metal load plate on top of a 1 in. thick rubber pad directly adjacent to the joint interface as seen in Figure 30. Each slab had the same support conditions and testing setup.

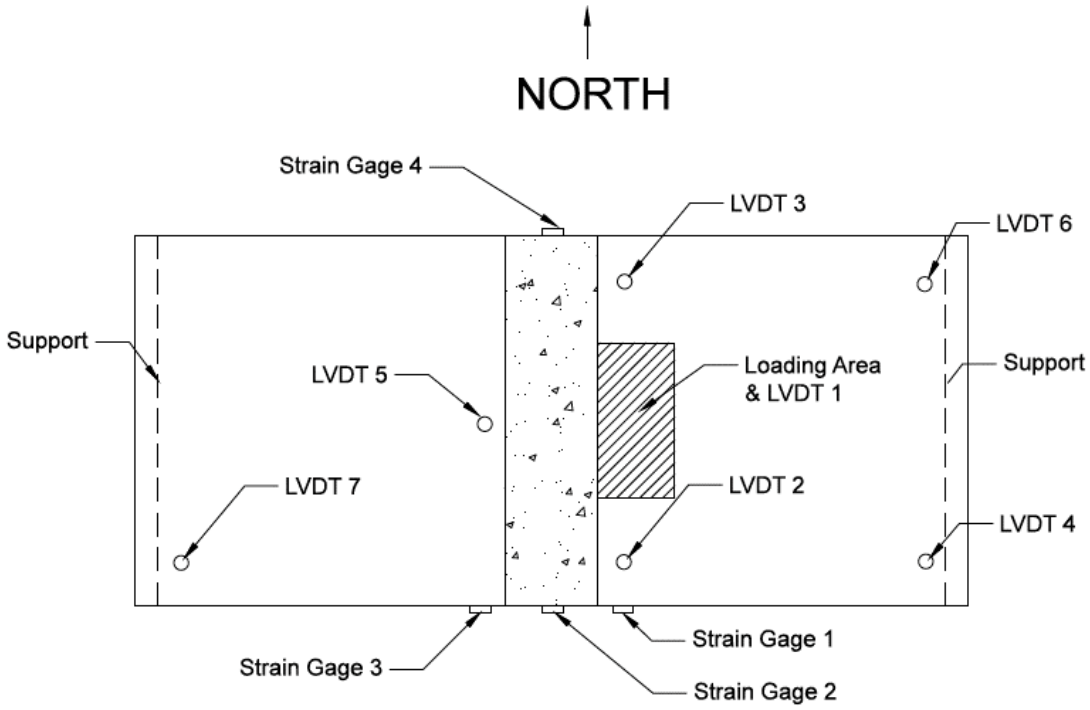

Figure 30. Instrumentation and layout for slab testing

3.6.1 Slabs 1 and 2

Slab 1 and Slab 2 were tested initially using a 22 kip capacity electronically controlled servo valve MTS hydraulic ram to produce a static load. Each slab was loaded in this manner at increments of 1 kip until the threshold of the machinery was reached. After each load increase, the slab specimens were visibly inspected for cracks and any observed cracks were marked with the load increment. After reaching approximately 22 kips, the specimen was unloaded and the electronically controlled system was switched out with a manually controlled hand pump (with a higher loading capacity of 50 kips). Before resuming the test, all LVDTs were removed from underneath the slab, and LVDTs 2, 3, and 5 (see Figure 30) were replaced with wire potentiometers (pots) with a longer stroke to prevent the instrumentation from being damaged if the slab were to deflect beyond the stroke of the LVDTs or collapse during testing. Once the manually controlled system was in place, the slab was loaded using the same 1 kip increments until failure occurred. Failure was considered to be the point at which the specimen could no longer support any increase in load.

3.6.2 Slab 3

Slab 3 was tested using the same electronically controlled hydraulic ram used for the initial portions of the static tests to induce a cyclic load. The load cycled from a 0.5 kip minimum to a specified maximum load using a haversine waveform with a frequency of 1 Hz. For the first 3 million cycles, it was planned to load the slab to a maximum load of 90% of the load corresponding to the

calculated cracking moment. Initially, the calculated cracking moment was determined to be 13.9 kips, for which the applied cyclic load was 12.5 kips. Because the testing setup varied slightly from that assumed for initial calculations, the load was lowered to 9 kips for the first 3 million cycles. After the first 3 million cycles, the load was to be increased to a maximum load 5% greater than the load corresponding to the calculated cracking moment (14.6 kips) with the same instrumentation for 2 million more cycles (or until failure). Testing was stopped and restarted once each day due to data storage limitations. After 5 million total cycles, the slab was to be statically loaded to failure (if not already failed). Figure 31 depicts one of the slabs prior to testing.

Figure 31. Testing setup for slabs

4.0 Test Results and Discussion

4.1 Compressive Strength Results

Tables 7-11 contain the results for compressive strength testing done in accordance with ASTM C39 for each concrete type. All testing for NSC was performed on 4 in. by 8 in. cylinders. Testing for UHPC was performed on 3 in. by 6 in. cylinders because the high strengths of the UHPC would require high loads. The compressive strength of concrete is the most recognized property and is important to document for use in comparisons and for establishing a baseline standard. Note that all strengths are given as averages of multiple values (given 3 specimens) and all strength values can be found in Appendix A.

4.1.1 NSC Trial Batches

Table 7. Compressive Strengths for Trial Batches

Age	Mix Design 1 Strength (psi)	Mix Design 2 Strength (psi)	Mix Design 3 Strength (psi)	Mix Design 4 Strength (psi)
1 - day	4130	2160	3490	2000
7 - day	6630	3420	N/A	3690
28 - day	8020	3700	6900	4220

In the process of conducting trial batches to determine the best mix design, mix design 4 most closely matched the properties listed in the ODOT specifications for class AA concrete. Slump, air content, and compressive strength were all factors that were taken into account (refer to Table 4). As shown in Table 6, the compressive strength of mix design 4 was just greater than the 4,000 psi target at 28 days of age.

4.1.2 Composite MOR NSC

Table 8. Compressive Strengths for MOR NSC

Age	N1 (psi)	N2 (psi)	N3 (psi)	N4 (psi)
1 - day	2350	1730	2390	2960
28 - day	4990	3550	4650	5850
Test Day	N/A	3760	4730	6570

Because the NSC for the composite MOR specimens was batched separately for each group of specimens, the different groups (N1, N2, N3, and N4) have different measured compressive strengths. The 28-day strengths have a standard deviation of 825 psi. The reason for these variations is unclear, but it may be attributable to human error and the fact that each batch was done on separate days. Due to these differences, the final results of the MOR testing are normalized to represent an equitable comparison. Three out of four batches (N1, N3, and N4) reached the minimum target strength of 4,000 psi.

4.1.3 Composite MOR UHPC

Table 9. Compressive Strength for MOR UHPC

Age	U1 (psi)	U2 (psi)	U3 (psi)	U4 (psi)
3 - day	11,620	11,650	12,360	12,600
28 - day	21,740	22,040	21,690	21,630

Each UHPC mix was performed in the same manner, which is reflected by the results of the compressive testing. The consistency of the results shown in Table 8, as compared to the NSC, is a product of the Ductal premix used, and the lack of aggregate moisture effects during mixing. The compressive

tests reveal that the UHPC, without heat curing, typically achieved a compressive strength of over 21 ksi at 28 days of age. The target strength was approximately 21 ksi, simplified from the 21.7 ksi potential strength referenced in the literature (Graybeal 2011).

4.1.4 Medium-Scale Slab NSC

Table 10. Compressive Strength for Slab NSC

Specimen	1 – Day (psi)	7 – Day (psi)	28 – Day (psi)	Test Day (psi)
All Slabs	3080	4790	5980	5780

All small-scale slabs were poured at the same time using the same mix. The measured compressive strengths more than satisfy the ODOT requirement of a minimum 28-day compressive strength of 4,000 psi for class AA concrete. Contrary to the strengths for the MOR specimens, these strengths are more consistent because all three slabs were poured at the same time. This will likely result in more consistent results than those obtained for the MOR specimens.

4.1.5 Medium-Scale Slab UHPC

Table 11. Compressive Strength for Slab UHPC

Specimen	12 - Hour (psi)	28 – Day (psi)	Test Day (psi)
Joint 1	21,430	22,870	22,680
Joint 2	16,390	20,460	24,360
Joint 3	17,310	20,590	23,000

The compressive strength testing results for the UHPC used for the medium-scale slab joints are slightly higher than for the UHPC used for the

composite MOR specimens. This UHPC was heat cured for 12 hours and generally had a higher compressive strength at test day because it was allowed to gain strength beyond 28 days. The compressive strength measurements were all greater than 22 ksi by the time flexural testing was carried out. The compressive strengths for the heat cured UHPC used for the joints had more variation than was observed for the UHPC used for the composite MOR specimens. Differences in the rate of strength gain can possibly be attributed to variations in cylinder placement under the heat lamps during the heat curing process. Overall, the UHPC for the slab specimen reached an acceptable strength by the 28-day mark.

4.2 Slant Shear Test Results

As previously mentioned, slant shear testing was performed using 6 in. by 12 in. cylinders—a modification to ASTM C882. The bond strength was determined by dividing the maximum load by the area of the interface. Because the specimens were twice the size of that specified in ASTM C882, the area of the interface was quadruple the value given in the ASTM. This was confirmed by calculating the area of the elliptical interface using the specimen dimensions. All specimens failed at the interface. The results are shown in Table 12.

Table 12. Maximum Load and Bond Strength for Slant Shear Specimens

Specimen	Maximum Load (lb)	Bond Strength (psi)	Corresponding Compressive Strength (psi)	NSC 28-Day Compressive Strength (psi)
Cylinder 1	122,670	2170	4340	5850
Cylinder 2	146,840	2600	5190	
Cylinder 3	177,245	3130	6270	
Cylinder 4	154,800	2740	5480	
Cylinder 5	153,430	2710	5430	
Average	150,997	2670	5340	
Std. Deviation	17,487	308	619	

These bond strength results, while generally within the same range, vary by up to 31%. This is attributable to the small sample size and the potential variations in the NSC surface for each specimen.

4.3 Composite MOR Test Results

The composite MOR specimens were tested on the day that the UHPC reached 28 days of age (NSC was 53 days of age). Testing was done in four groups, based on the age of the specimens and the configurations. The MOR (maximum tensile stress at failure) was determined by inputting measured values into Equation 1 taken from ASTM C78. The results are also compared to would-be results for a monolithic NSC MOR specimen of the same compressive strength as determined by Equation 2 taken from ACI 318 (2014).

$$R = \frac{PL}{bd^2} \quad (1)$$

where

R = MOR, psi

P = maximum observed load, lb

L = span length of the specimen from support to support, in.

b = width of the specimen at location of failure, in.

d = depth of specimen at location of failure, in.

$$fr = 7.5\sqrt{f'c} \quad (2)$$

where

fr = flexural tension strength, psi

$f'c$ = compressive strength of NSC, psi

Tables 13-16 contain the results for each individual specimen with relation to its interface configuration and surface preparation. For each specimen, WB indicated wire brushed, SB indicates sand blasted, and EA indicates exposed aggregate. Almost all specimens failed in the base concrete. The three specimens that failed at the interface were all 90 degree wire brushed specimens. The 90 degree specimens had 5 wire brushed specimens and 3 sand blasted specimens, contrary to the original casting plan seen in Table 5. Figure 32 shows the two different failure types.

Figure 32. Interface failure (left) and base concrete failure (right)

Table 13. 90 Degree Composite MOR Specimen Results

90 Degree Specimens	Failure Type	Peak Load (lb)	Flexural Stress (psi)	Average Flexural Stress (psi)	Std. Deviation (psi)
1-WB-90	Base Concrete	8020	645	584	86.3
2-WB-90	Base Concrete	8335	685		
3-WB-90	Interface	7795	625		
4-WB-90	Interface	5630	460		
5-WB-90	Interface	6220	505		
6-SB-90	Base Concrete	7345	580	563	20.1
7-SB-90	Base Concrete	6705	535		
8-SB-90	Base Concrete	7245	575		
9-EA-90	Base Concrete	8510	675	645	24.5
10-EA-90	Base Concrete	7935	615		
11-EA-90	Base Concrete	8320	645		

Table 14. 60 Degree Composite MOR Specimen Results

60 Degree Specimens	Failure Type	Peak Load (lb)	Flexural Stress (psi)	Average Flexural Stress (psi)	Std. Deviation (psi)
1-WB-60	Base Concrete	7345	590	579	34.3
2-WB-60	Base Concrete	7725	620		
3-WB-60	Base Concrete	6505	525		
4-WB-60	Base Concrete	7085	580		
5-SB-60	Base Concrete	7415	600	596	18.8
6-SB-60	Base Concrete	7525	615		
7-SB-60	Base Concrete	7400	605		
8-SB-60	Base Concrete	7080	565		
9-EA-60	Base Concrete	6100	505	572	51.4
10-EA-60	Base Concrete	8535	630		
11-EA-60	Base Concrete	7115	580		

Table 15. 45 Degree Composite MOR Specimen Results

45 Degree Specimens	Failure Type	Peak Load (lb)	Flexural Stress (psi)	Average Flexural Stress (psi)	Std. Deviation (psi)
1-WB-45	Base Concrete	6865	545	528	30.1
2-WB-45	Base Concrete	5880	480		
3-WB-45	Base Concrete	6810	560		
4-WB-45	Base Concrete	6485	525		
5-SB-45	Base Concrete	6905	560	569	37.8
6-SB-45	Base Concrete	7645	620		
7-SB-45	Base Concrete	6330	515		
8-SB-45	Base Concrete	7070	580		
9-EA-45	Base Concrete	9540	735	510	290.4
10-EA-45	Base Concrete	9230	695		
11-EA-45	Base Concrete	1300	100		

Table 16. Shear Key Composite MOR Specimen Results

Shear Key Specimens	Failure Type	Peak Load (lb)	Flexural Stress (psi)	Average Flexural Stress (psi)	Std. Deviation (psi)
1-EA-SK	Base Concrete	10,810	850	745	118.1
2-EA-SK	Base Concrete	10,855	805		
3-EA-SK	Base Concrete	7250	580		

Figures 33 and 34 depict comparisons of the average flexural stress for each type of composite MOR. Because the concrete for each group of composite specimens had a specific compressive strength value, Figures 35 and 36 depict comparisons of the average flexural stress coefficient, which is a normalized value in relation to the square root of the compressive strength measured for the NSC of each group in order to achieve a more representative comparison.

Within this data set, there was one specimen (11-EA-45) that had an unusually low maximum flexural stress of 100 psi. This lowers the average performance of the 45 degree exposed aggregate specimens, which may mask actual performance. In addition, one 60 degree exposed aggregate specimen (10-EA-60) in this data set had a UHPC portion that extended across the bottom portion of the specimen, which could have strengthened the NSC portion and produced a higher flexural stress of 630 psi. Figure 34 depicts comparisons of the average maximum flexural stress for each type of specimen with these two unusual data points removed.

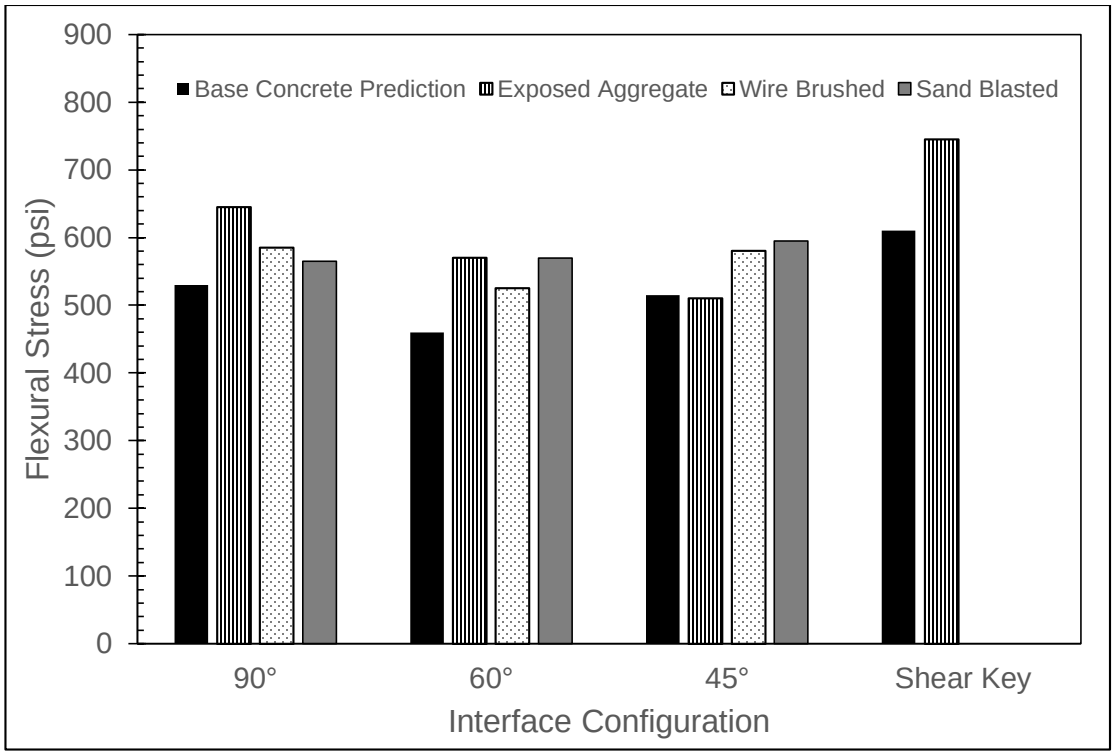

Figure 33. Average Maximum Flexural Stress vs. Interface Configuration including all values

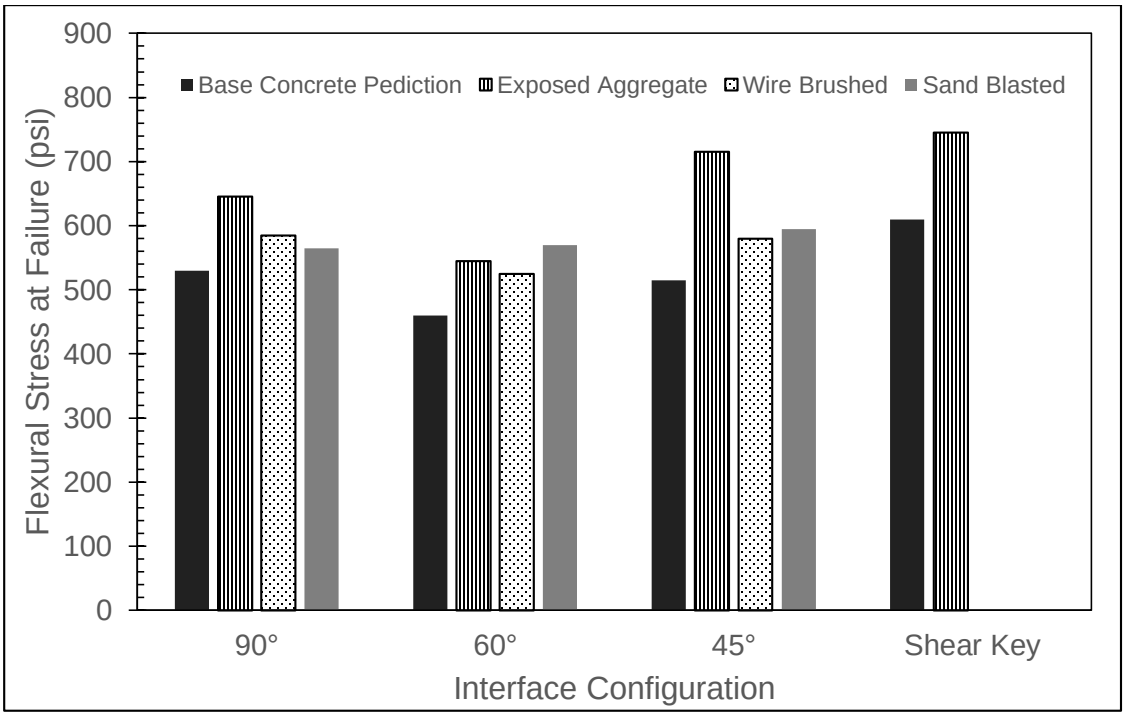

Figure 34. Average Maximum Flexural Stress vs. Interface Configuration with adjusted values

As seen in Figure 34, removing these two unusual data points does not greatly affect comparisons within the data set as a whole. The specimens with the exposed aggregate surface preparation performed better than specimens with other surface preparations, with the exception of the 45 degree specimens. The average values for all specimens reached a higher flexural stress at failure than the flexural stress calculated for a monolithic NSC specimen, indicating that all surface configurations provided a bond strength that was higher than the strength of the base concrete. The wire brushed and sand blasted specimens did not reveal that one surface preparation was superior to the other in increasing overall flexural capacity. However, all of the specimens that failed at the interface were wire brushed. None of the 90 degree sand blasted specimens failed at the interface, while 60% of the 90 degree wire brushed specimens failed at the interface.

In Equation 2, the normalized flexural stress coefficient is 7.5, which is based on a large quantity of experimental results. Figure 35 depicts the normalized flexural stress coefficients for all the values (including the two unusual values previously mentioned) based on the MOR measured for the specimens and the compressive strength of the NSC portion. The MOR calculated from the measured results was divided by the square root of the compressive strength in order to obtain the normalized values. When comparing the normalized results, it appears that the 60 degree specimens had higher average flexural stress coefficients than the other interface configurations indicating slightly better performance.

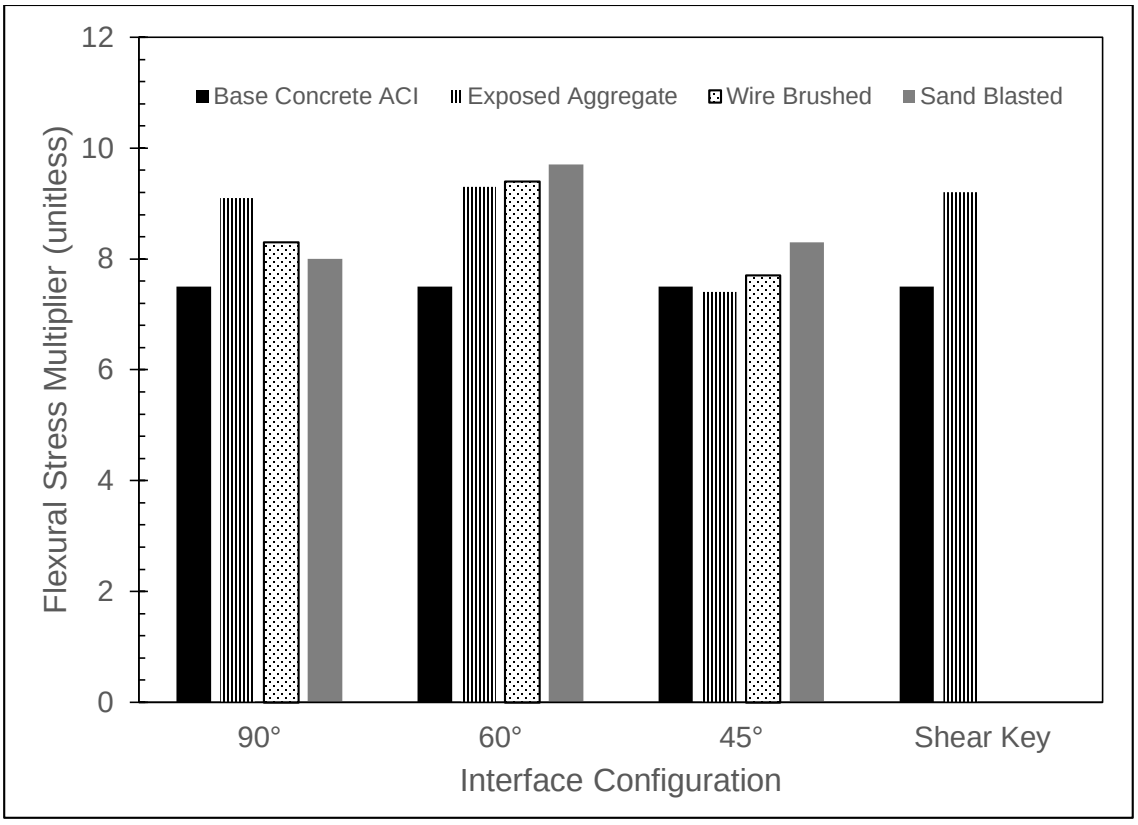

Figure 35. Flexural Stress Coefficient vs. Interface Configuration including all values

After removing the unusual values mentioned previously (Figure 36), the results generally appear the same for the 60 degree specimens, but an increase in the flexural stress coefficient for the 45 degree exposed aggregate specimens is clear. When considering these adjusted results, the specimens with an exposed aggregate surface preparation typically performed better than the 90 degree and 45 degree specimens with other surface preparations. All specimens had a higher flexural stress coefficient than the standard value of 7.5 used for the base concrete calculation. The average of flexural stress coefficients for the 90 degree, 60 degree, 45 degree, and shear key specimens

respectively were 8.5, 9.3, 8.8, and 9.2, respectively. This considered, it can be said that the 60 degree specimens generally performed the best.

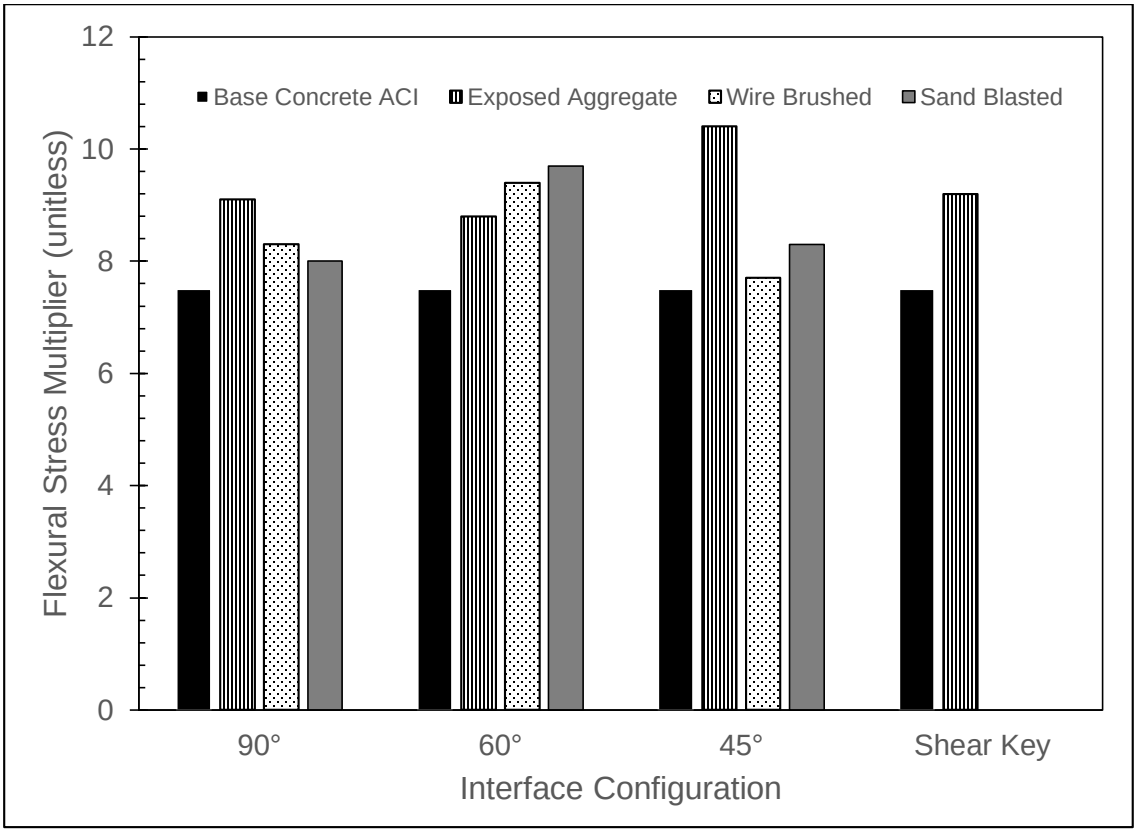

Figure 36. Flexural Stress Coefficient vs. Interface Configuration with adjusted values

4.4 Medium-Scale Slab Test Results

Figures 37-41 show the results of testing (parts 1 and 2) for slab 1. Figures 45-50 show the results of testing (parts 1 and 2) for slab 2. As previously mentioned, slab 1 and 2 were tested in flexure and loaded statically. Part 1 of testing was performed using the MTS loading system and included the elastic range and early post-cracking behavior, while part 2 was performed using a manual hydraulic pump and included behavior at failure.

4.4.1 Slab 1 Static Test Results

The maximum load reached by slab 1 before proceeding to part 2 of testing was approximately 21.3 kips. Because of the loading limitations of the MTS system, the test was stopped at this point. The first cracks were observed in the base concrete during part 1 of the test at a load of approximately 14 kips. This cracking load was determined at the time that the first crack became visible to the naked eye. Further analysis suggests the first crack may have occurred before the load reached 14 kips. Figure 37 depicts the load vs. deflection curve for slab 1 part 1. This curve shows that initial cracking occurred at approximately 10.9 kips, rather than the visually determined 14 kips. This was determined by locating the point in the load vs. deflection curve where the deflection experienced an increase, but load did not. At this point, the slope of the remaining portion of the curve became less steep. The load corresponding to the calculated cracking moment for a monolithic NSC slab with the same reinforcement and dimensions was originally calculated to be 13.9 kips, but after further evaluation, it was estimated to be 11.7 kips (calculations in Appendix C). This calculation was performed using the measured value for the compressive strength of the NSC portion of the slabs and the span of the specimen setup. The graphically determined cracking load of 10.9 kips is less than the expected 11.7 kips. This could potentially be attributed to variability in concrete tensile strength or the method of graphically determining this value. Upon unloading the specimen, the magnitude of total deflection decreased back down to a residual deflection of approximately 0.07 in.

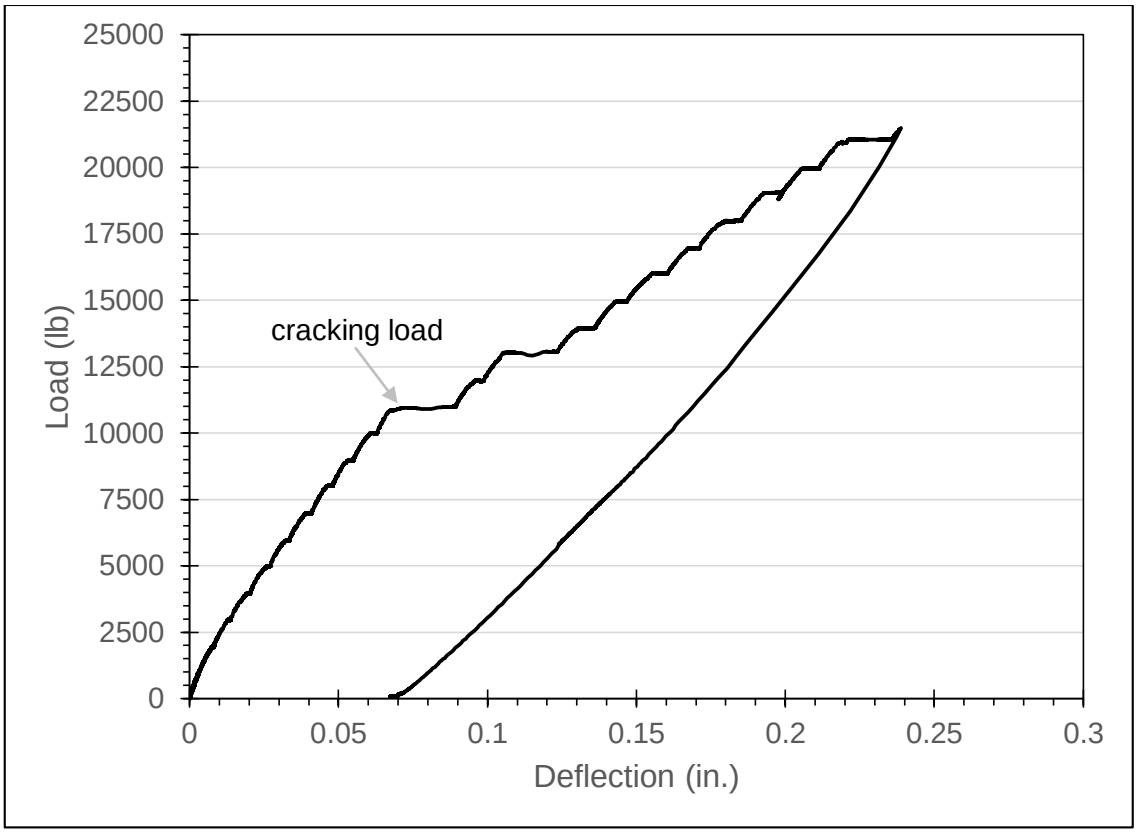

Figure 37. Load vs. Deflection curve for slab 1, part 1

Figure 38 depicts the load vs. strain curve for strain gages 1-3 for the first portion of loading. Refer to section 3.6 for strain gage locations. Strain gage 4 is not included because it produced unreliable results. The general trend for these curves is that the strain increases with increasing load until cracking of the slab releases tension in the area of the gage. The maximum microstrain values for the strain gages are slightly less than the tensile strain in the concrete at cracking, but the values are generally in a reasonable range (less than 100 microstrain). Strain gages 1 and 3 are somewhat unclear, but strain gage 2 shows a good representation of this behavior, confirming that the first crack occurred at approximately 10.9 kips.

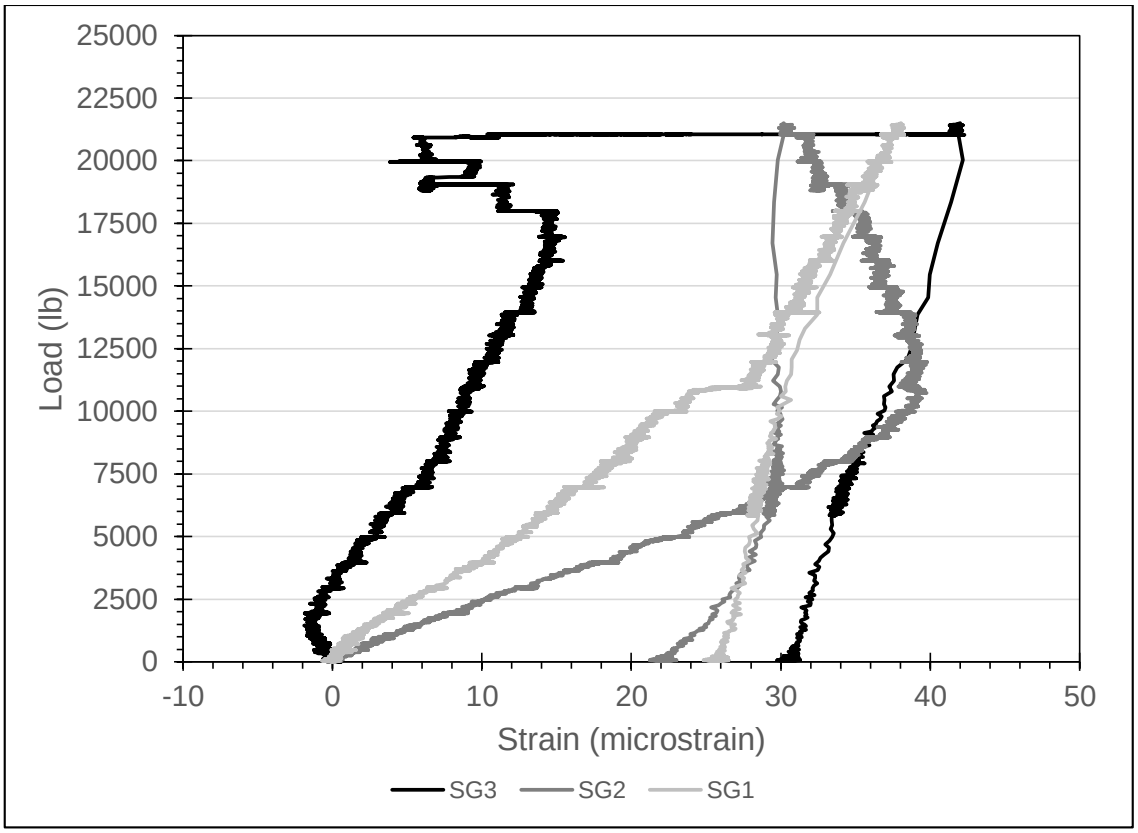

Figure 38. Load vs. Strain curve for slab 1, part 1

Figure 39 depicts the load vs. deflection relationship for part 2 of testing. This portion of the test was performed with a manual hydraulic pump, which was slightly more variable and less precise in terms of the load application increments. The load decreased between each increment of loading due to bleeding pressure in the pump that did not occur using the MTS system. The ultimate load reached for slab 1 was 36.2 kips. The calculated failure load for a monolithic NSC slab with the same reinforcement and dimensions was estimated to be 23.5 kips (Appendix C). The actual failure load of the specimen exceeded estimations by 54%. Failure was determined at the point when the specimen exhibited yielding behavior, was unable to sustain any increasing

load, and concrete crushing was observed at the top compression fiber. Before loading began for part 2, the residual deflection seen in the slab was 0.07 in. After unloading the specimen, the total deflection observed while under load decreased in magnitude from a maximum of 2.02 in. to a residual deflection of approximately 1.58 in. This indicated significant plastic deformation of the specimen. Figure 40 depicts a comparison for slab 1 of the part 1 and part 2 load vs. deflection curves without the residual deflection that occurred after part 1 taken into account. This is to compare the slopes of each curve for loads up to 25 kips. As seen in Figure 40, the slope decreases for the second part of testing, which is to be expected of a slab that has been cracked.

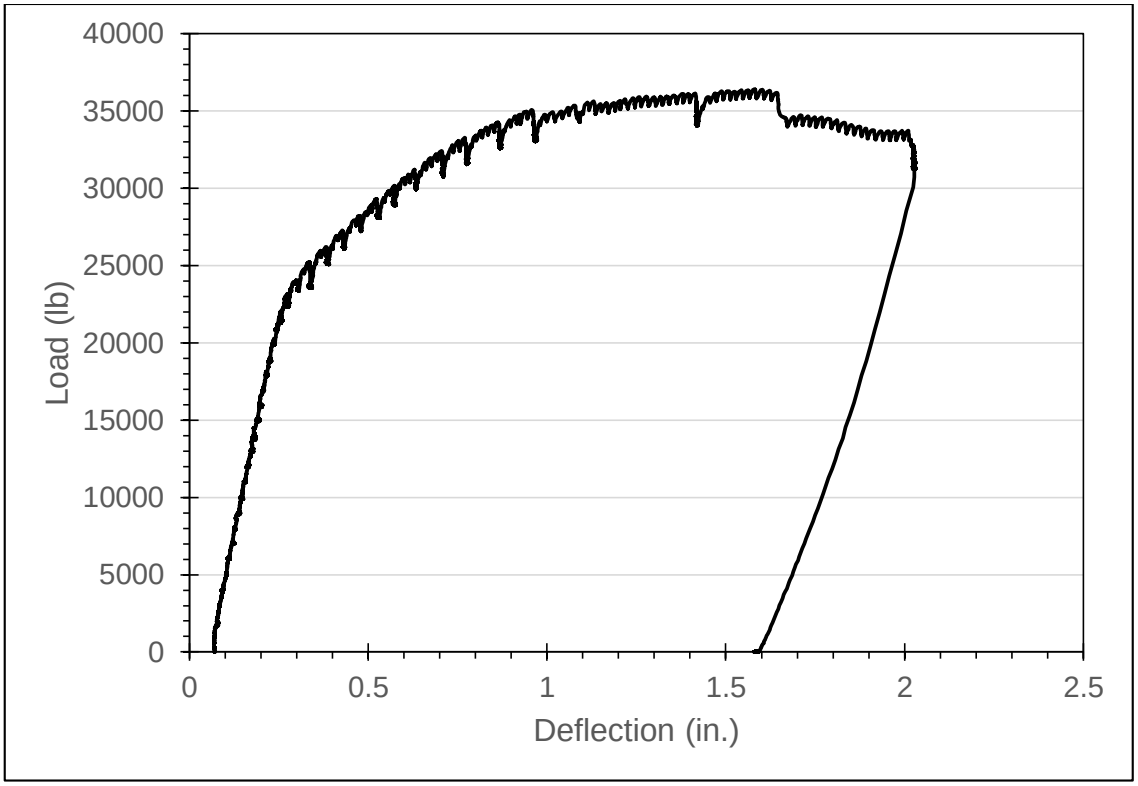

Figure 39. Load vs. Deflection curve for slab 1, part 2

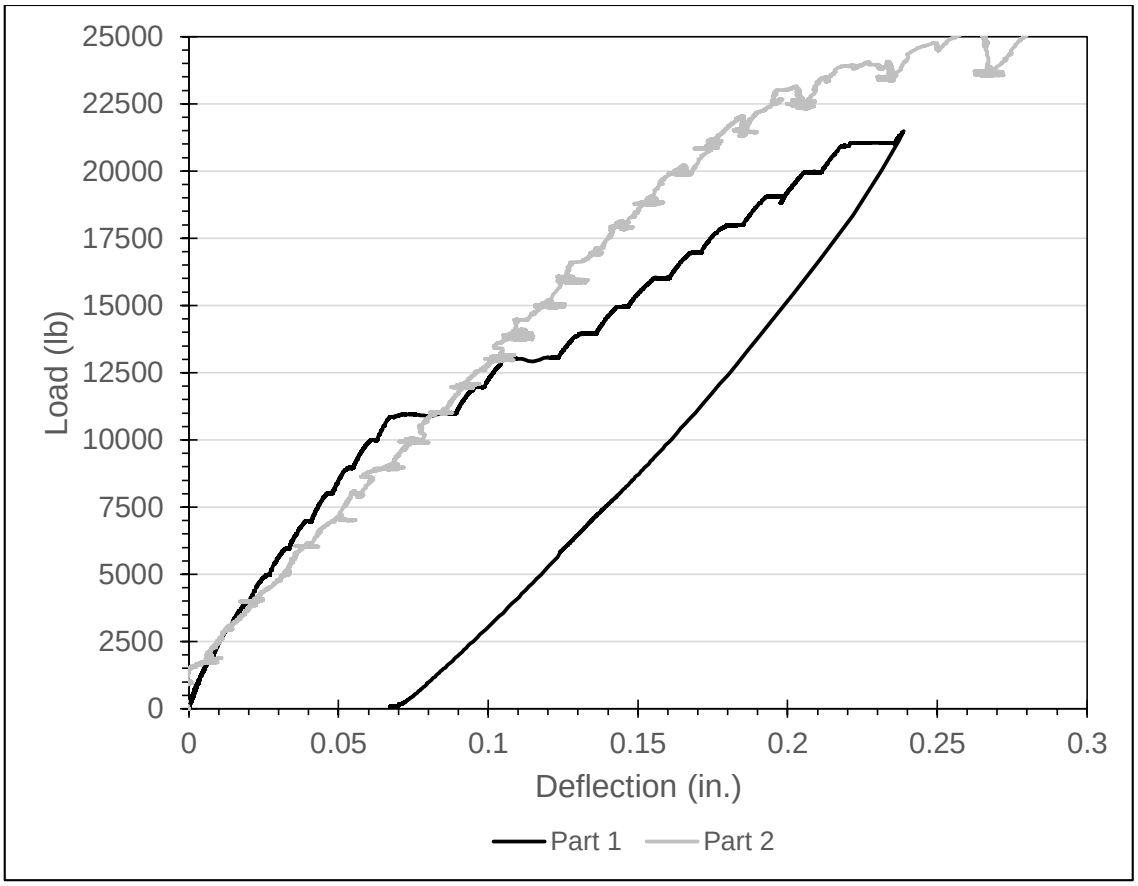

Figure 40. Load vs. Deflection curves for slab 1, parts 1 and 2

At failure, there were no observed cracks within the UHPC joint itself. The major crack at failure occurred in the base concrete directly below the load point, at approximately 5 inches away from the interface between the UHPC and the NSC (directly beneath the load point). There was also minor separation at the interface closest to the load point. Some of the cracks can be seen in Figures 41-43. These cracks followed a logical progression moving outward from the load point as load increased.

Figure 41. Major cracking underneath load point for slab 1

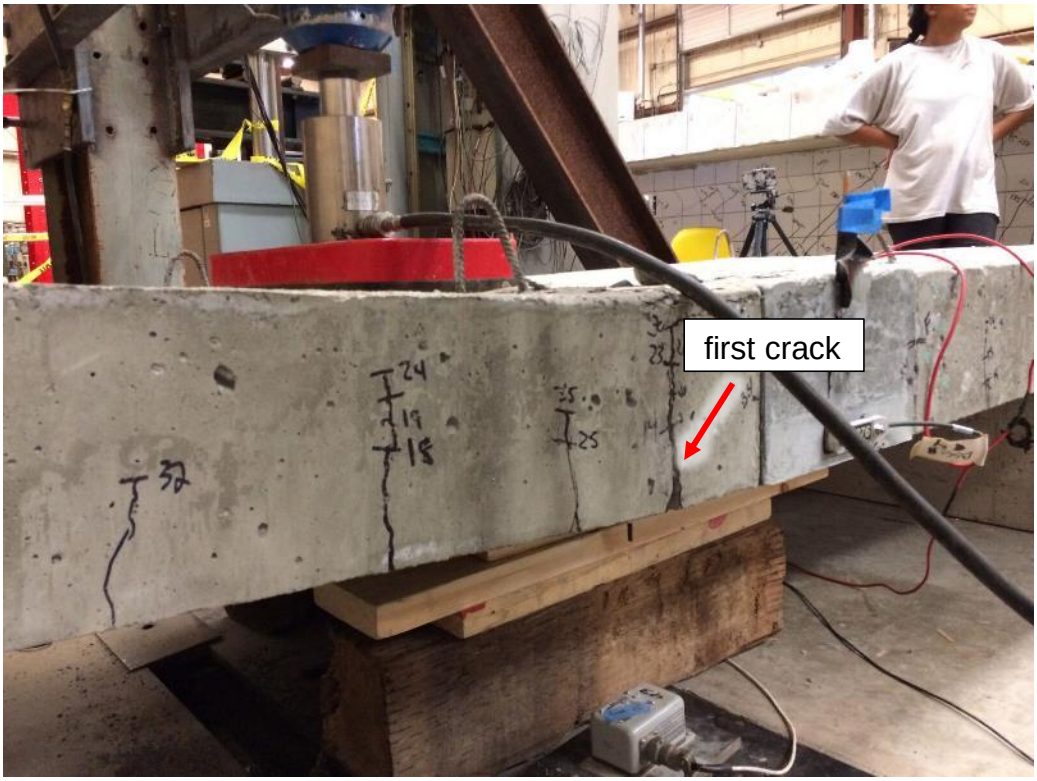

Figure 42. Cracks formed underneath load on north side of slab 1

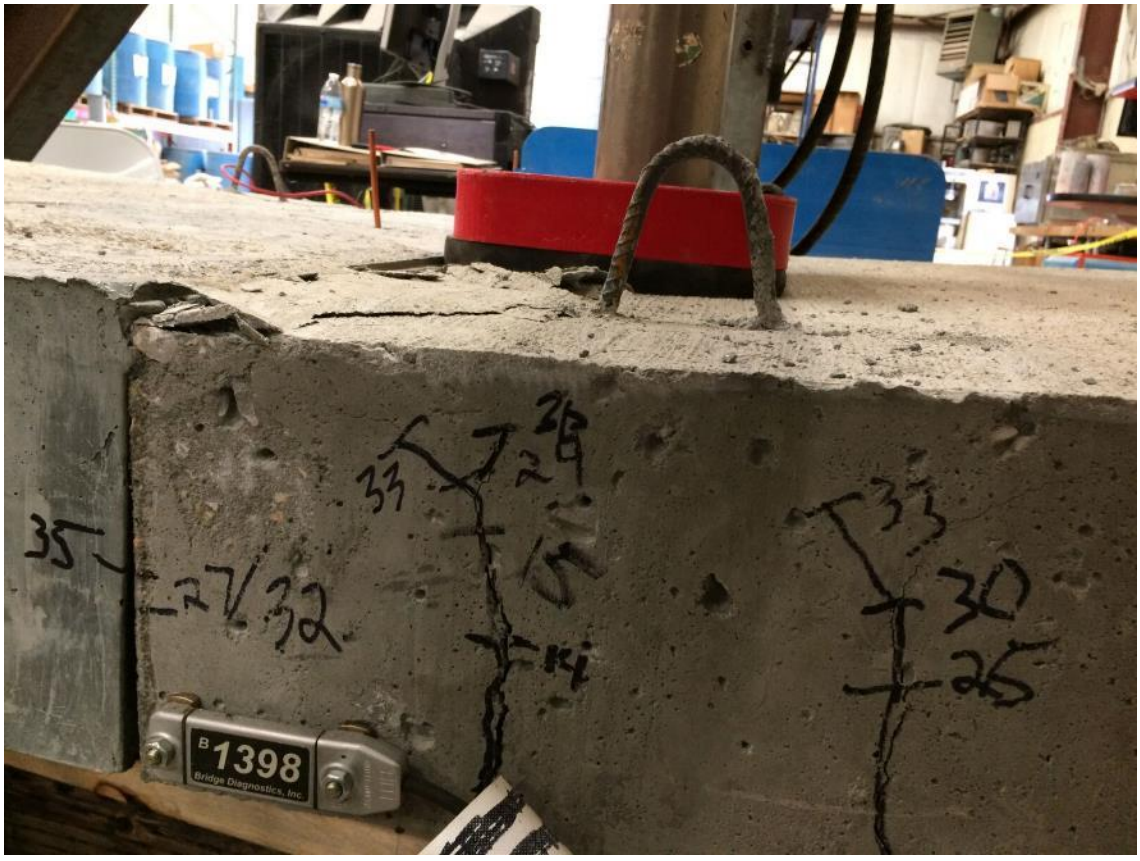

Figure 43. Cracks formed underneath load on south side of slab 1 and concrete crushing at the top compression fiber

4.4.2 Slab 2 Static Test Results

As seen in Figure 44, the maximum load reached by slab 2 before proceeding to part 2 of testing was approximately 22 kips. The first cracks were observed during part 1 of the test similarly to the test for slab 1. The first visually observed cracking occurred in the base concrete directly beneath the load point at a load of approximately 14 kips. This cracking load was determined at the time that the first crack became visible to the naked eye. Further analysis suggests the first crack may have occurred before the load reached 14 kips. Figure 44 depicts the load vs. deflection curve for slab 2 part 1. This curve shows that initial cracking occurred at approximately 13.1 kips, rather than the

visually determined 14 kips. This was determined by locating the point in the load vs. deflection curve where the deflection experienced an increase, but load did not. At this point, the slope of the curve became less steep. The calculated cracking load for a monolithic NSC slab with the same reinforcement and dimensions was estimated to be 11.7 kips. Upon unloading the specimen, the magnitude of total deflection decreased from the maximum observed back down to a residual deflection of approximately 0.067 in. Figure 45 depicts the load vs. strain curve for the first portion of loading for slab 2. Again, while strain gages 1 and 3 are not generally useful, strain gage 2 confirms that initial cracking of the specimen likely occurred at a load of around 13.1 kips, rather than the visually determined 14 kips.

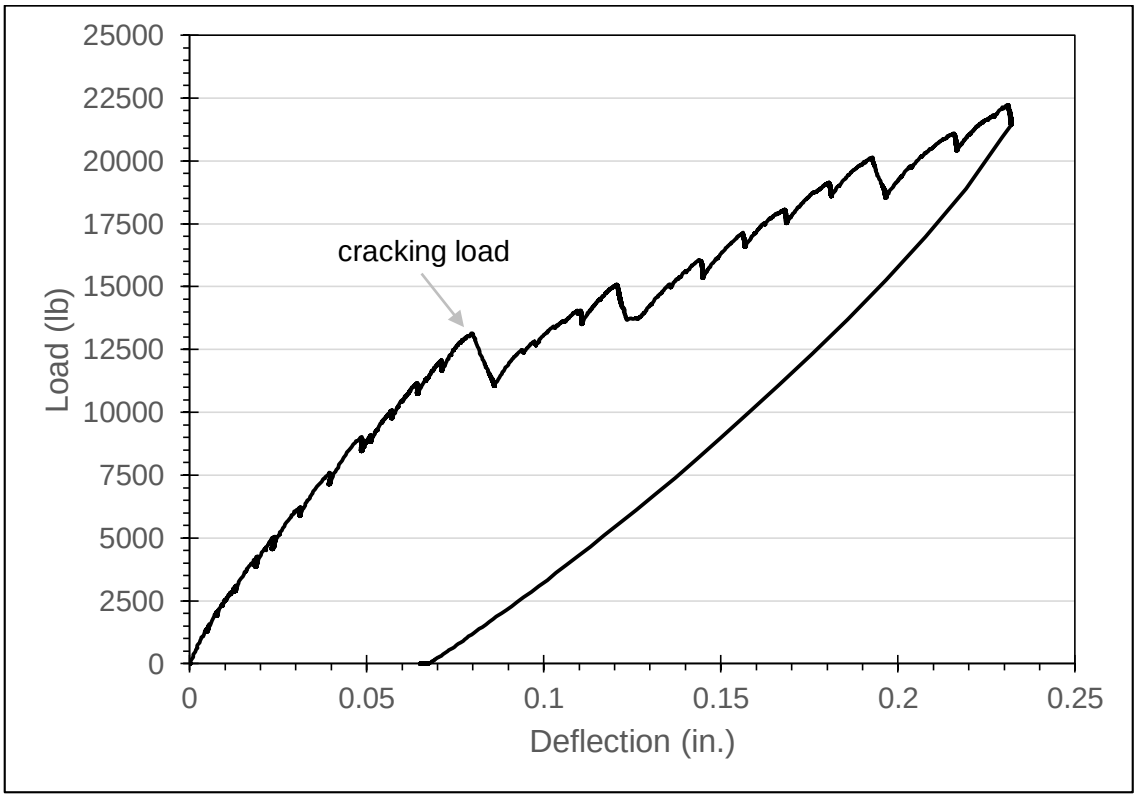

Figure 44. Load vs. Deflection curve for slab 2, part 1

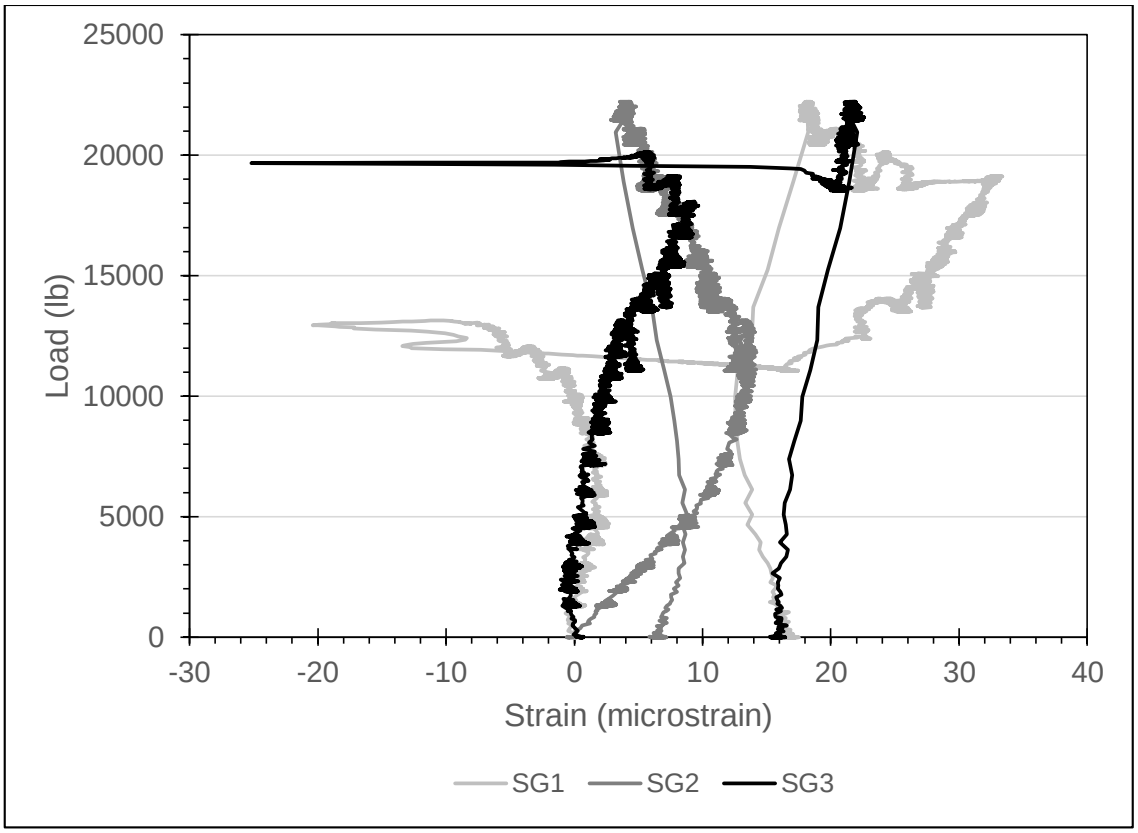

Figure 45. Load v. Strain curve for slab 2, part 1

The ultimate load reached for slab 2 was 37.2 kips. The calculated failure load for a monolithic NSC slab with the same reinforcement and dimensions was estimated to be 23.5 kips. Similarly to slab 1, the actual failure load of the specimen exceeded estimations by 58%. Failure was determined at the point when the specimen exhibited yielding behavior, was unable to sustain any increasing load, and exhibited concrete crushing at the top compression fiber.

Figure 46 shows the load vs. deflection relationship for slab 2 part 2. Before loading began for part 2, the residual deflection seen in the slab was 0.067 in. After unloading the specimen, the total deflection of 2.12 in. observed while under load decreased in magnitude to approximately 1.70 in.

Figure 47 depicts a comparison for slab 2 of the part 1 and part 2 load vs. deflection curves without the residual deflection that occurred after part 1 taken into account. This is to compare the slopes of each curve for loads up to 25 kips. As seen in Figure 47, the slope decreases slightly for the second part of testing, which is to be expected of a slab that has been cracked.

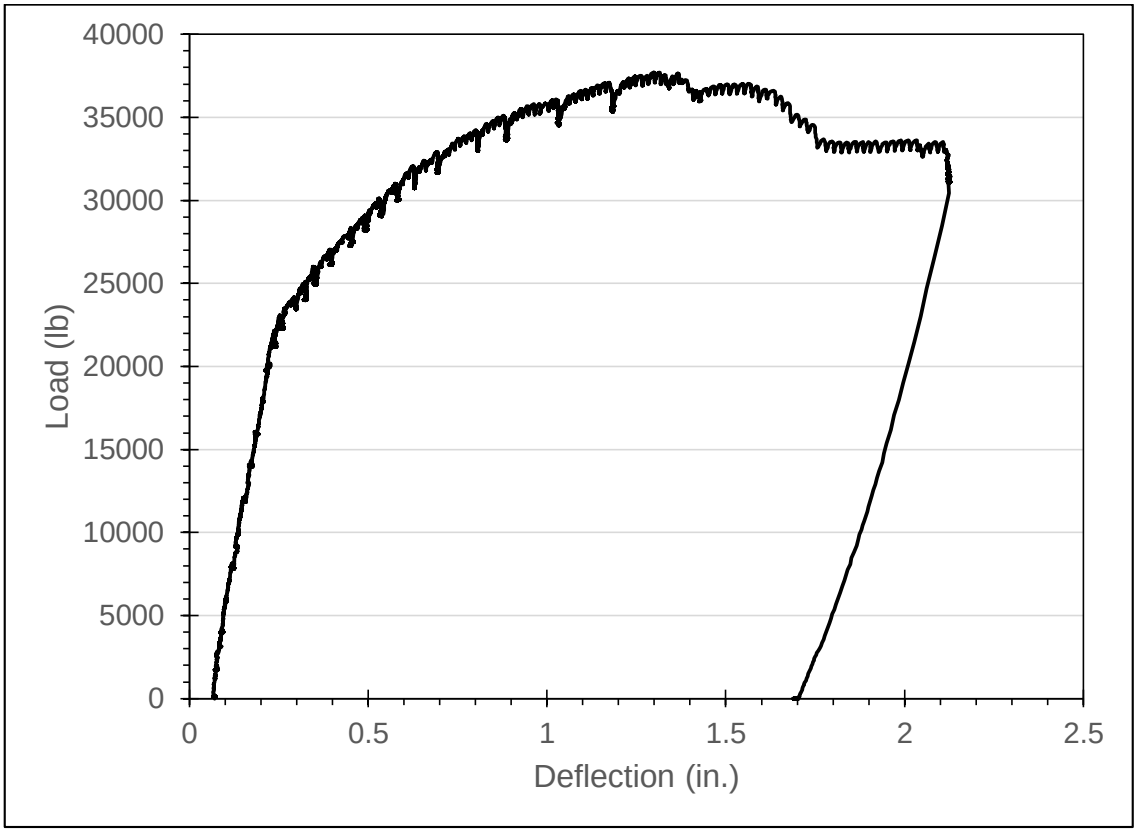

Figure 46. Load vs. Deflection curve for slab 2, part 2

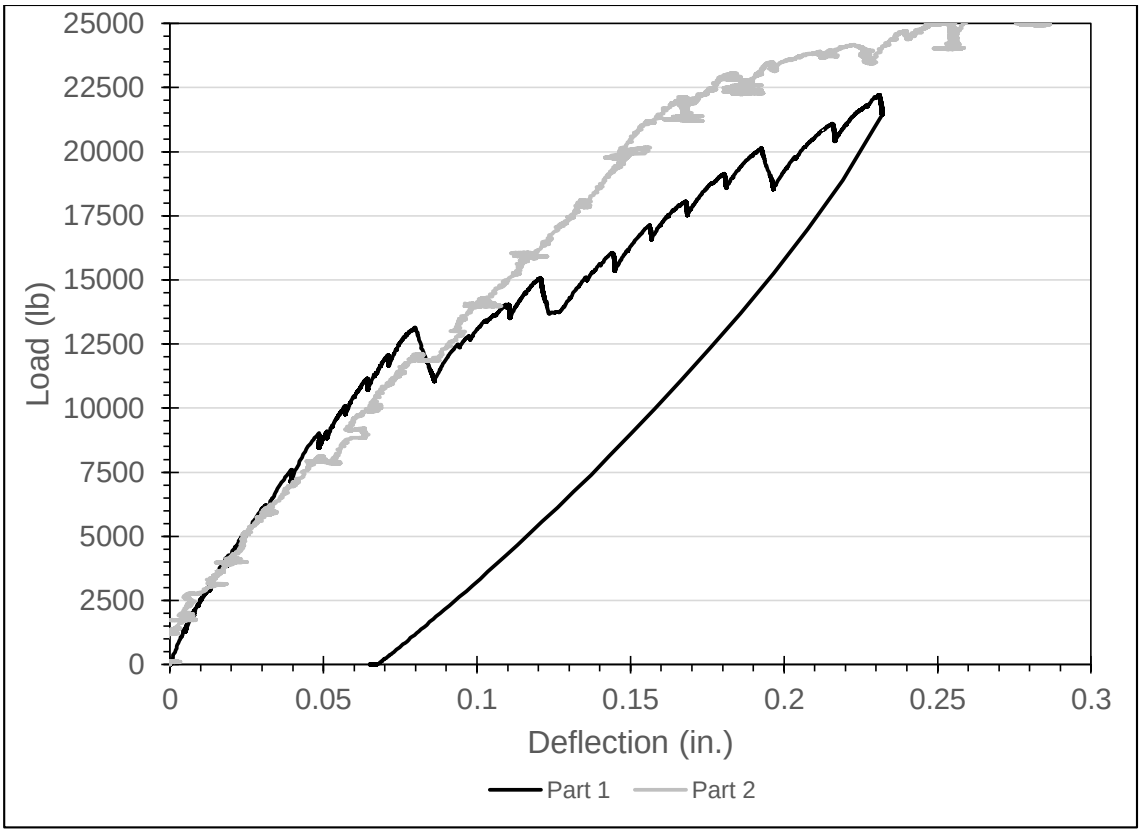

Figure 47. Load vs. Deflection curve for slab 2, parts 1 and 2

At failure, there were no observed cracks within the UHPC joint itself. The major crack at failure occurred in the base concrete near the load point, at approximately 6 in. away from the interface between the UHPC and the NSC (1 in. east of the load point). There was also minor separation at the interface closest to the load point. This separation at the interface was only visible during loading and could not be seen once the load was removed from the slab. Some of the cracks can be seen in Figures 48-50.

Figure 48. Major cracking underneath load point for slab 2

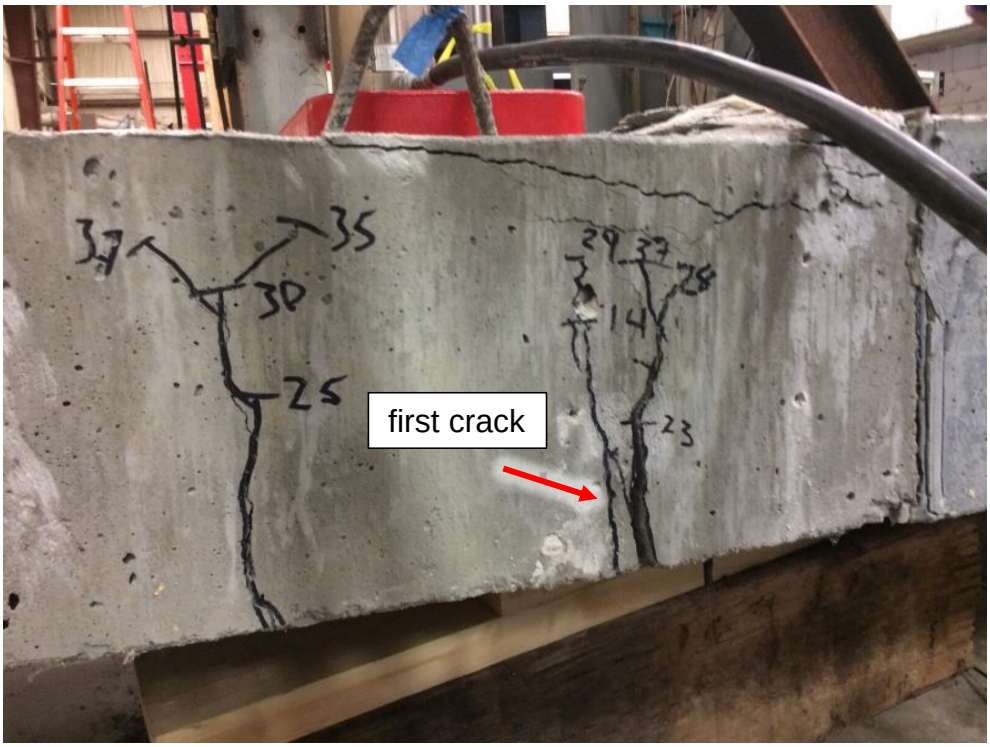

Figure 49. Cracking underneath load on north side of slab 2 and crushing of concrete near load point

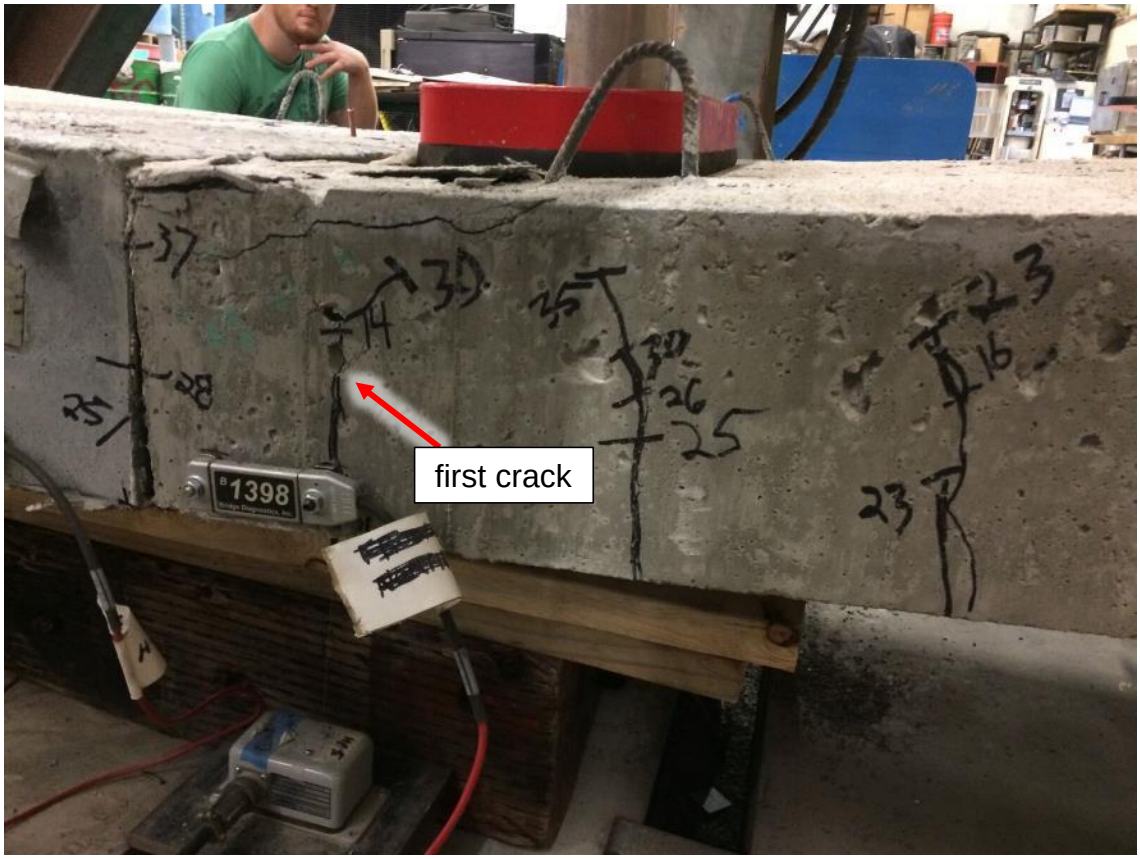

Figure 50. Cracking underneath load on south side of slab 2 and crushing of concrete near load point

4.4.3 Slab 3 Cyclic and Static Test Results

Slab 3 was cyclically tested under fatigue loading. The initial planned test program was to induce a load with a magnitude of 90% of the expected cracking load for the specimen. The visually observed load corresponding to the cracking moment for slab 1 and 2 was approximately 14 kips, 90% of which was approximately 12.5 kips. Using the MTS system, the test was started by applying the 1 Hz cyclic load to the slab in increasing increments up to the 12.5 kip target. Prior to the reaching the predicted cracking load of 14 kips, initial cracking occurred due to the 12.5 kip load, so the load was decreased accordingly to prevent premature fatigue failure of the specimen. The specimen

was cyclically loaded to 9 kips (67% of the estimated cracking load) for the remainder of the first 3 million cycles. Figure 51 depicts the typical cyclic loading over a time period of 10 seconds. Figures 52-71 depict the load vs. deflection curves (for the loading portion of a single cycle) during the first 3 million cycles, analyzed every other day for the duration of initial cycling. All cycles shown are from a period within the first 5,000 cycles on a given day (there were approximately 86,000 cycles per day). The unloading portion of the curves are not shown, but were similar to the loading portion. These curves do not start at zero due to the 500 lb preload that was applied prior to starting the cyclic load. The deflections shown in these curves were adjusted to subtract out deflections of the support. A linear trend line was considered for each load cycle examined, since the slab was expected to have a linear response at the applied load level. The slope of the equation shown is a measure of the stiffness of the slab, which generally decreased throughout the first 3 million cycles. This could be due to the fact that the slab was cracked prematurely during the initial application of the cyclic load. Figure 72 shows multiple cycles from different days for comparison. Even though a gradual decay of stiffness was observed over time, the curves shown in Figure 72 are still nearly on top of one another.

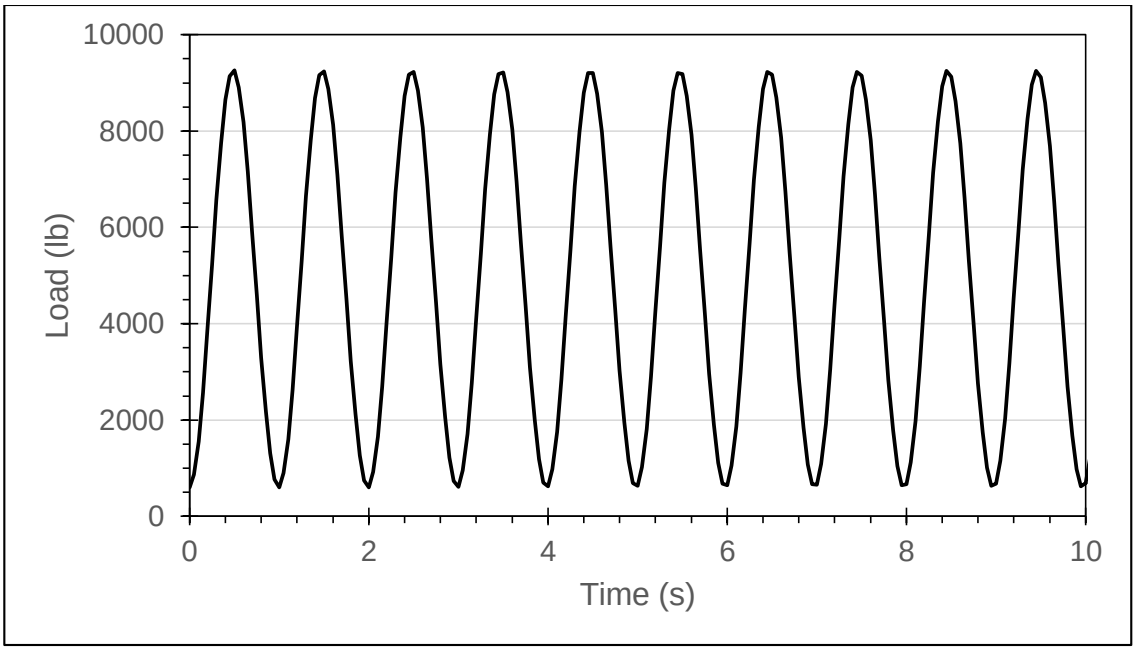

Figure 51. Typical cyclic loading over a short period of time

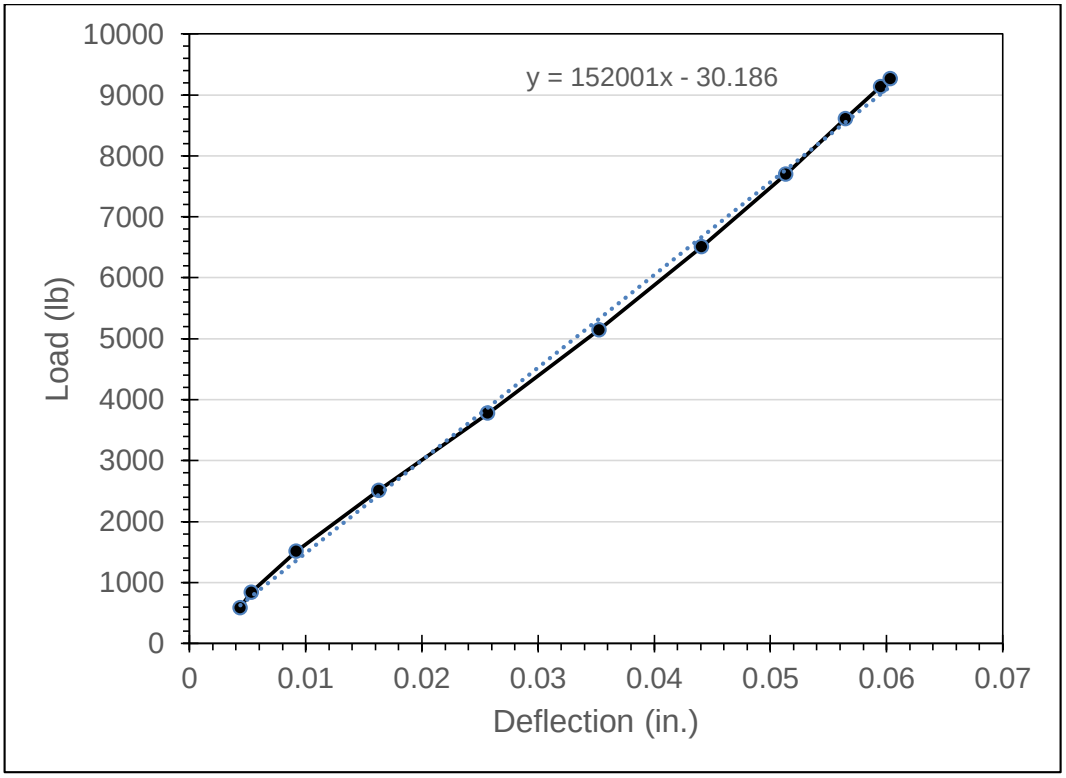

Figure 52. Load vs. Deflection for slab 3, measured from a single load cycle selected from day 1

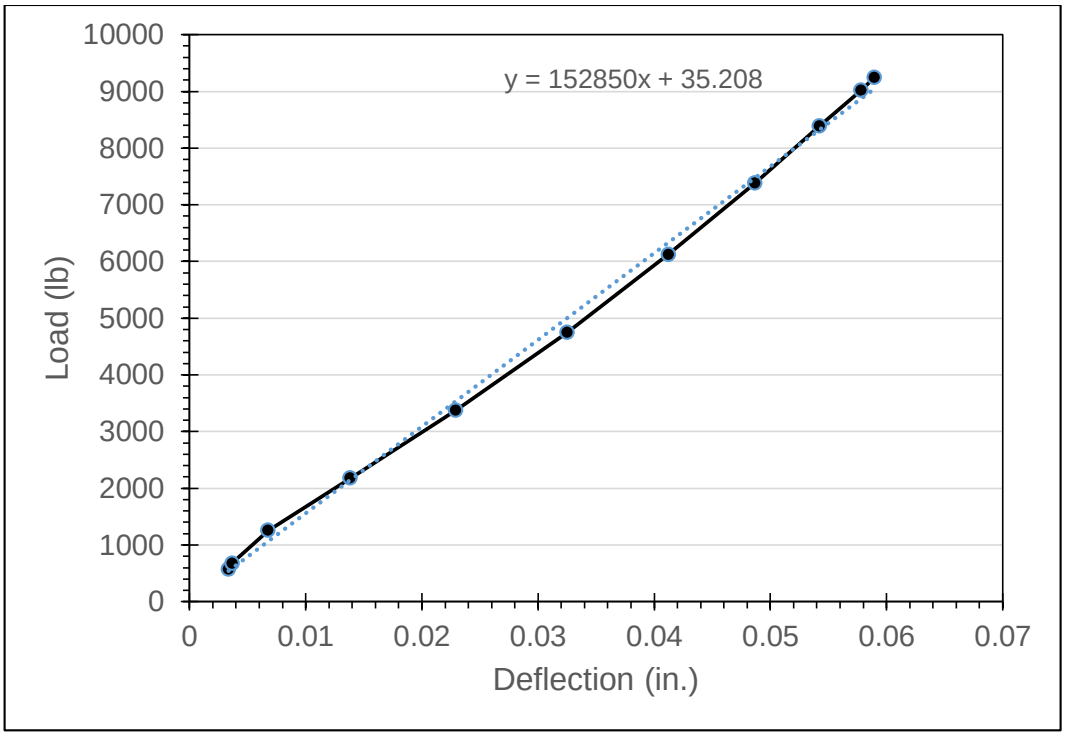

Figure 53. Load vs. Deflection for slab 3, measured from a single load cycle selected from day 3

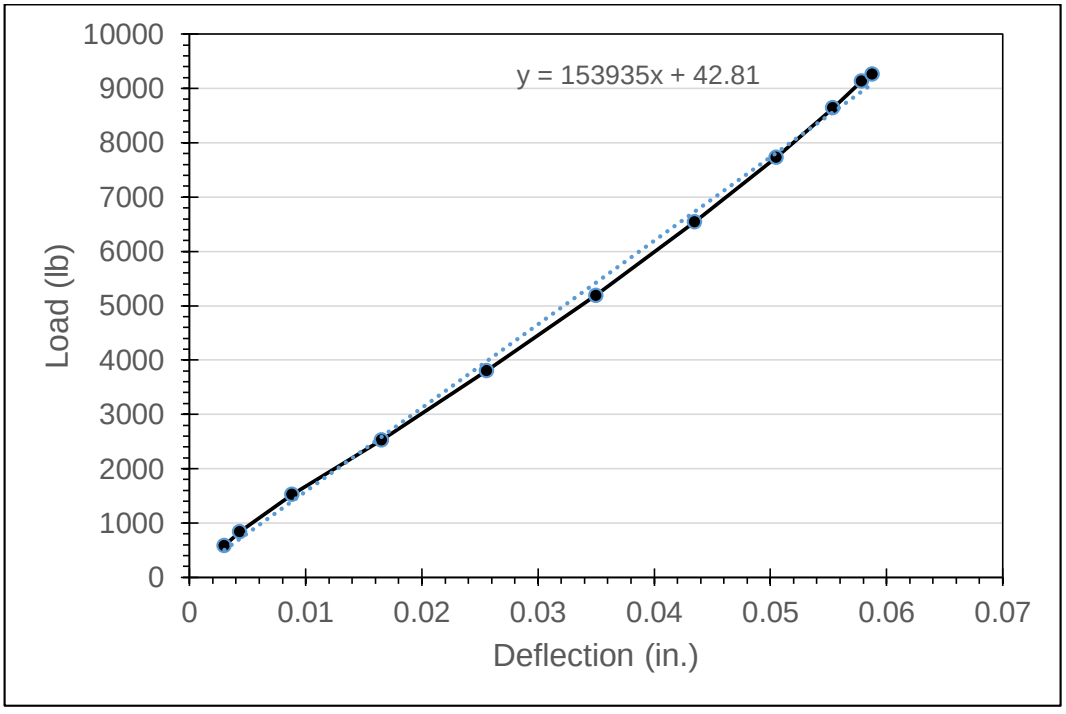

Figure 54. Load vs. Deflection for slab 3, measured from a single load cycle selected from day 5

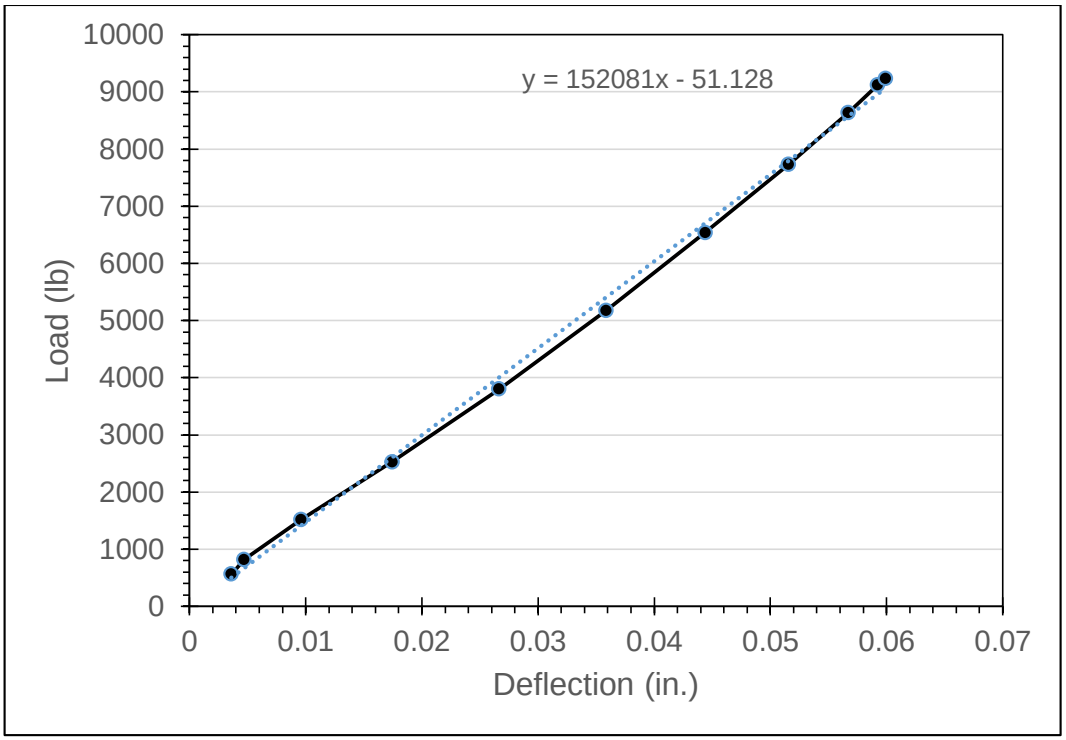

Figure 55. Load vs. Deflection for slab 3, measured from a single load cycle selected from day 7

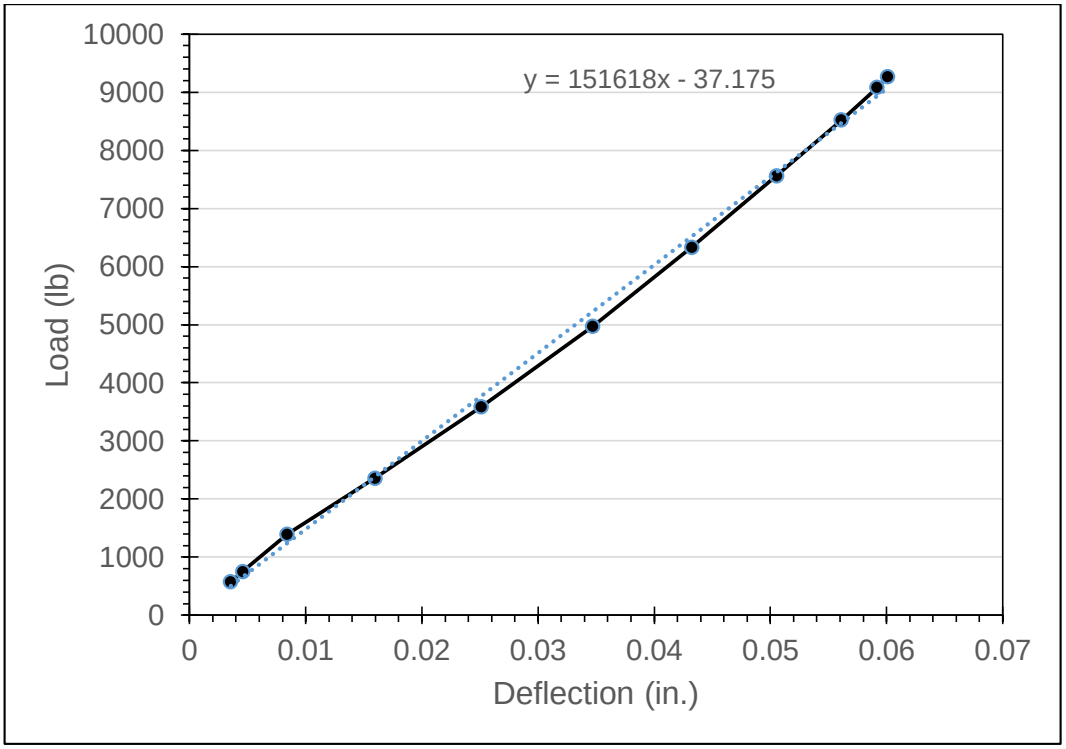

Figure 56. Load vs. Deflection for slab 3, measured from a single load cycle selected from day 9

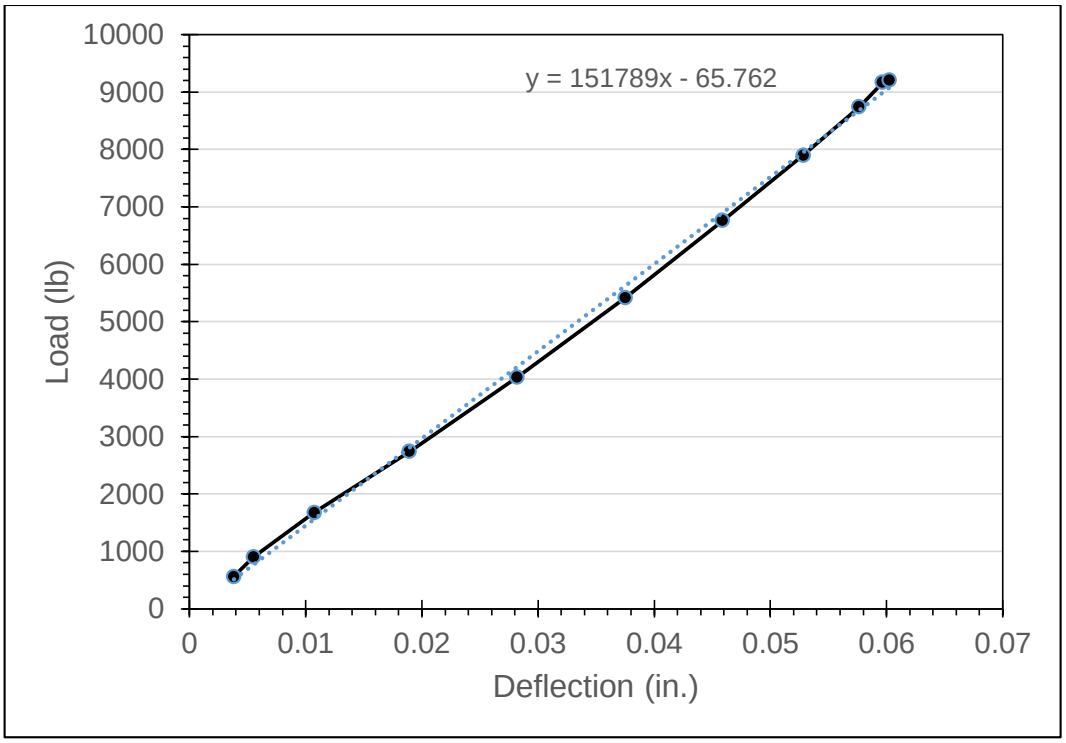

Figure 57. Load vs. Deflection for slab 3, measured from a single load cycle selected from day 11

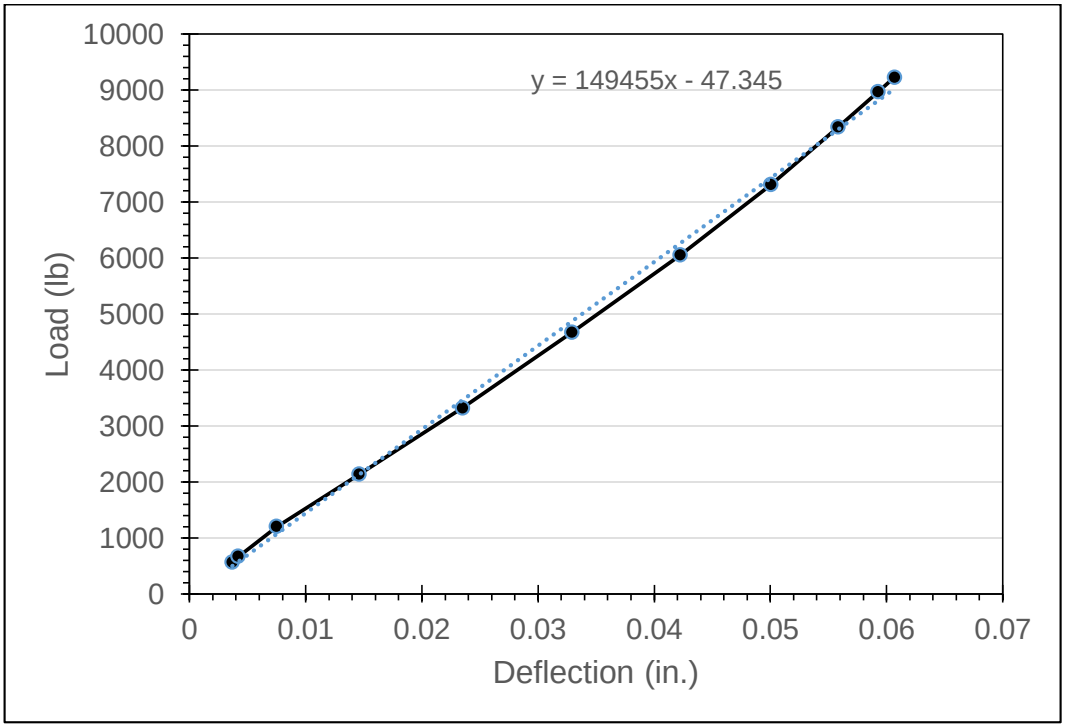

Figure 58. Load vs. Deflection for slab 3, measured from a single load cycle selected from day 13

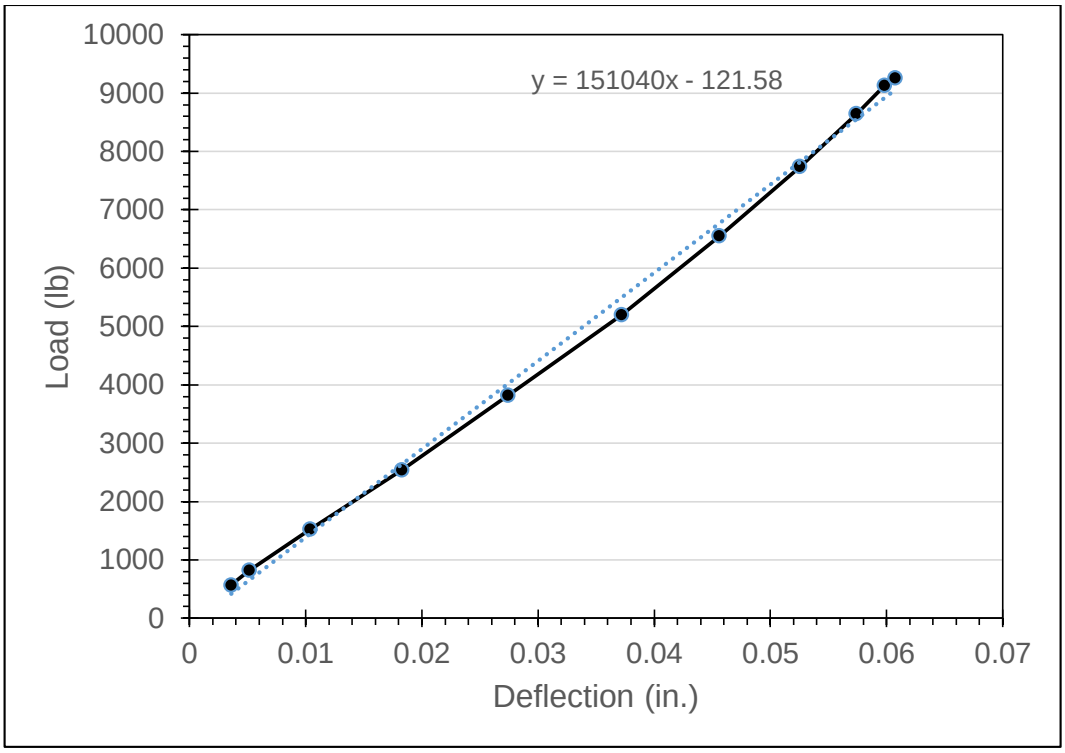

Figure 59. Load vs. Deflection for slab 3, measured from a single load cycle selected from day 15

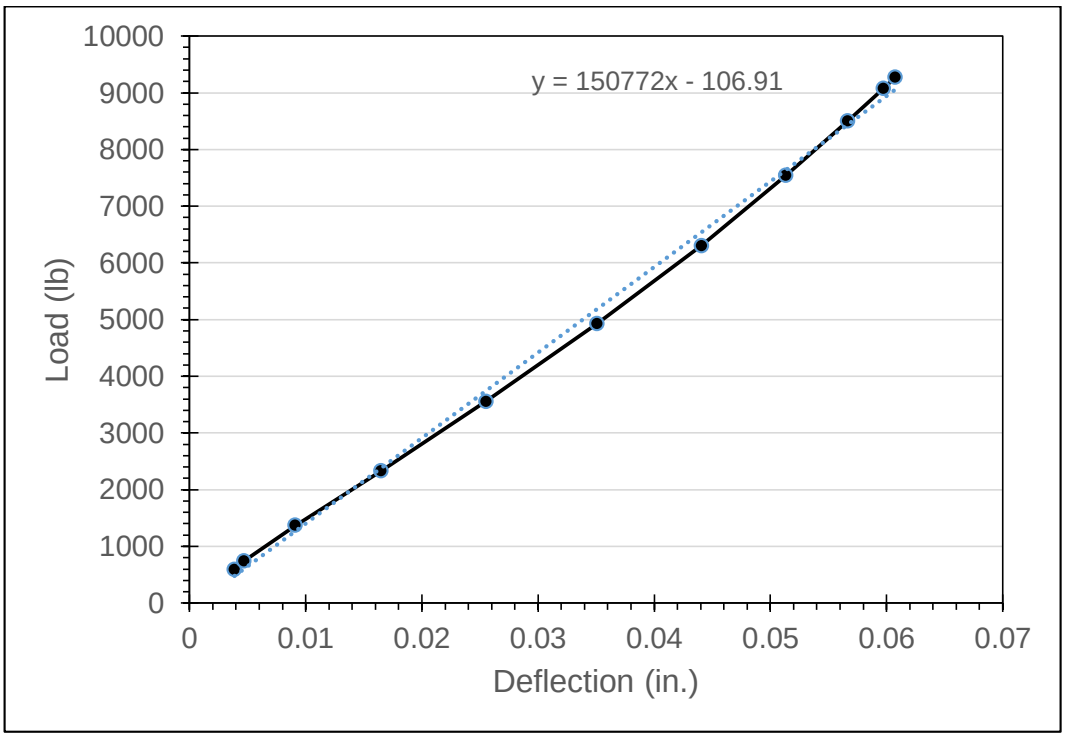

Figure 60. Load vs. Deflection for slab 3, measured from a single load cycle selected from day 17

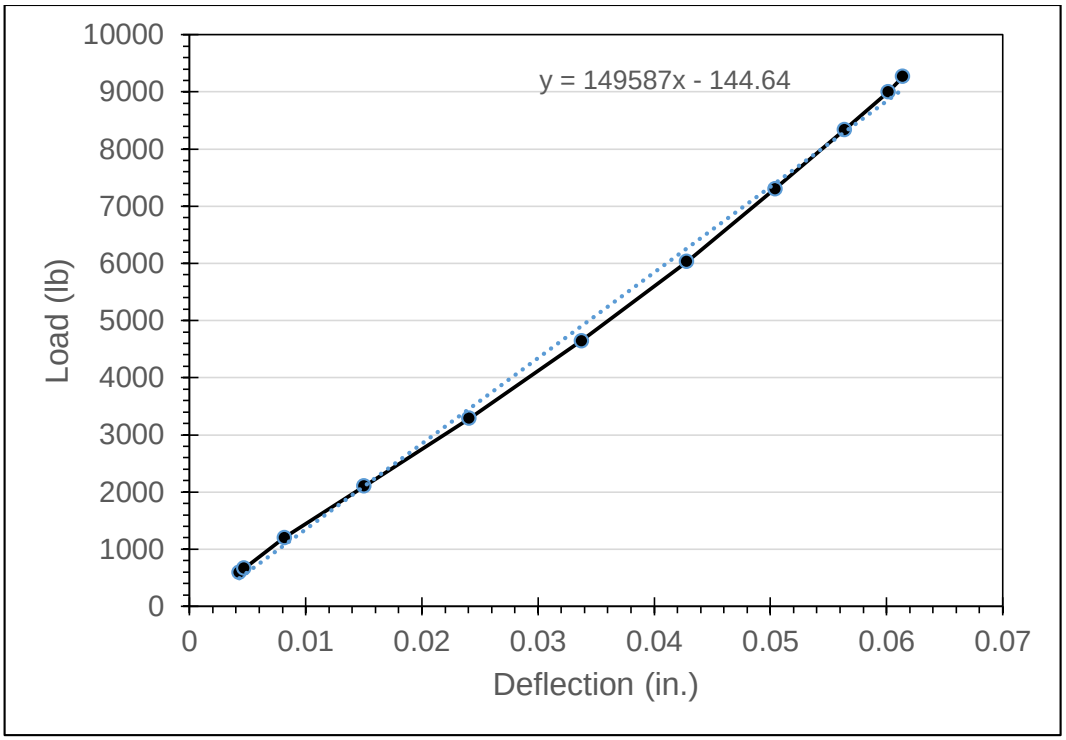

Figure 61. Load vs. Deflection for slab 3, measured from a single load cycle selected from day 19

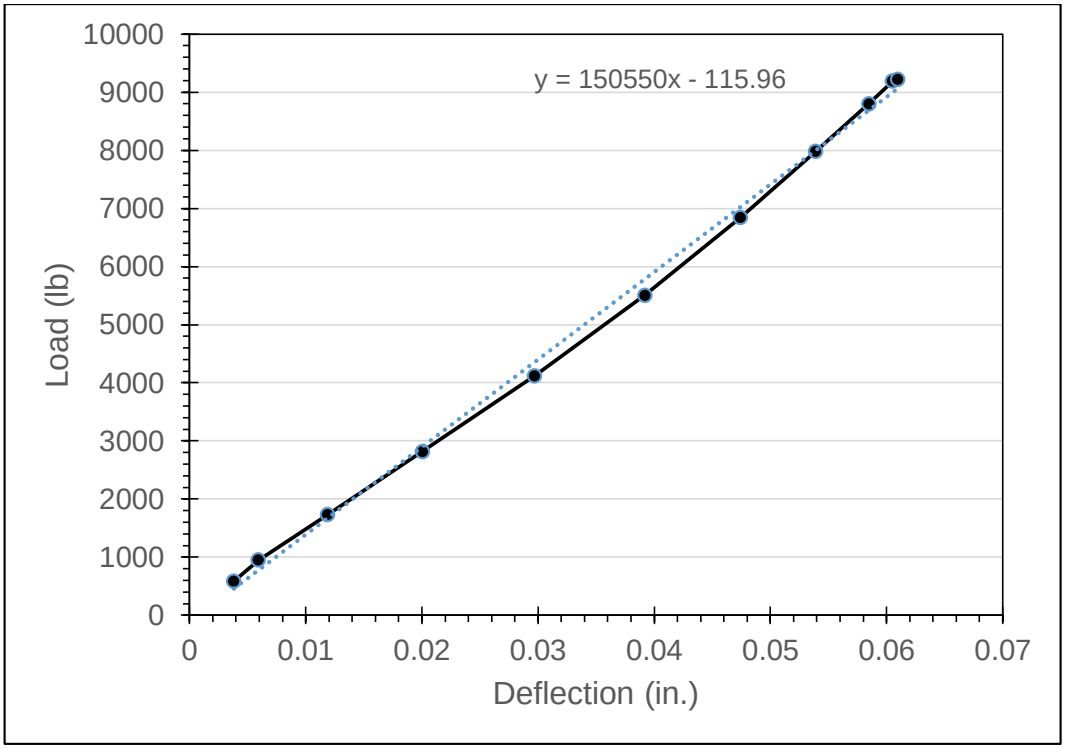

Figure 62. Load vs. Deflection for slab 3, measured from a single load cycle selected from day 21

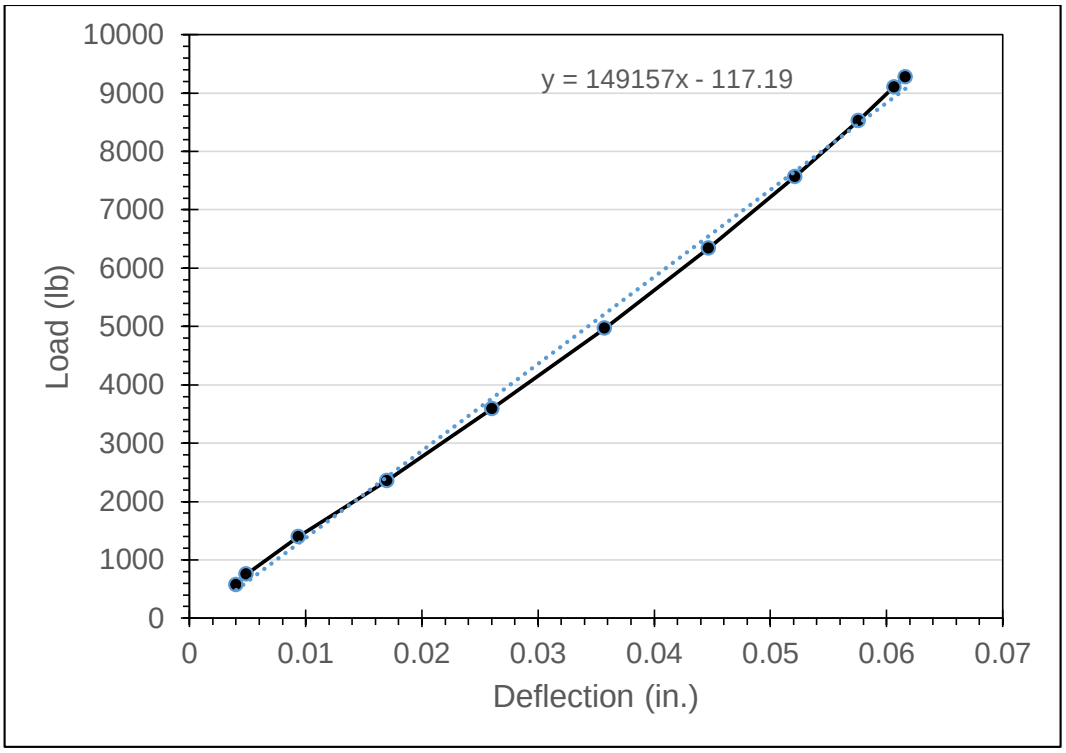

Figure 63. Load vs. Deflection for slab 3, measured from a single load cycle selected from day 23

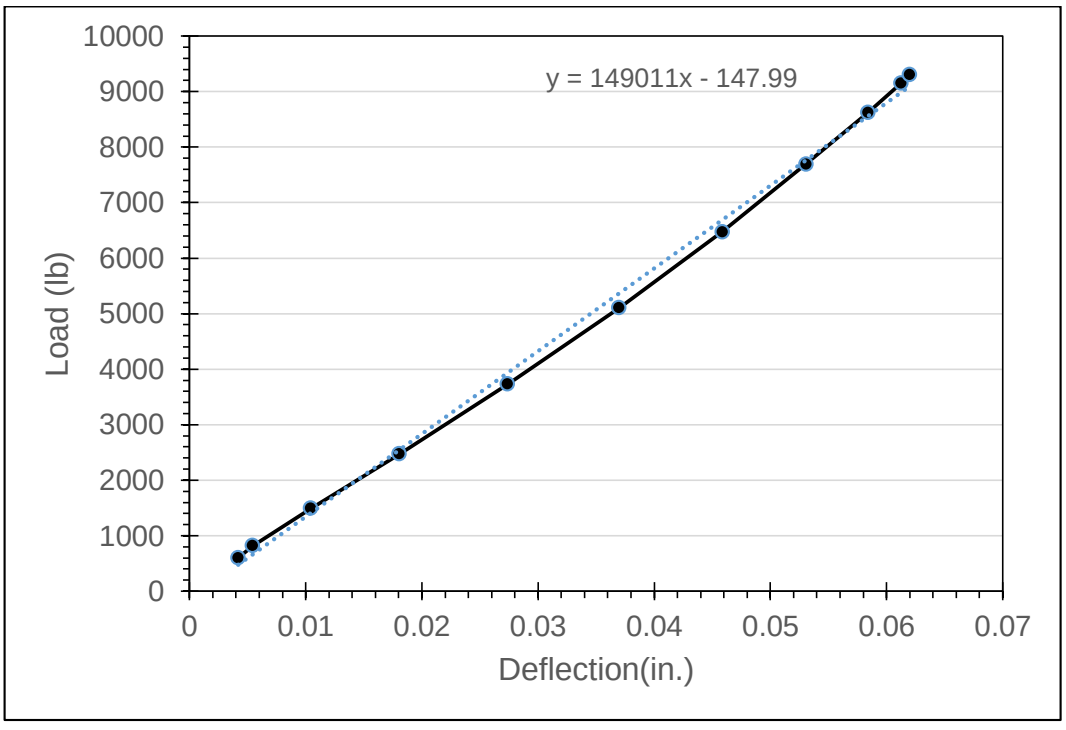

Figure 64. Load vs. Deflection for slab 3, measured from a single load cycle selected from day 25

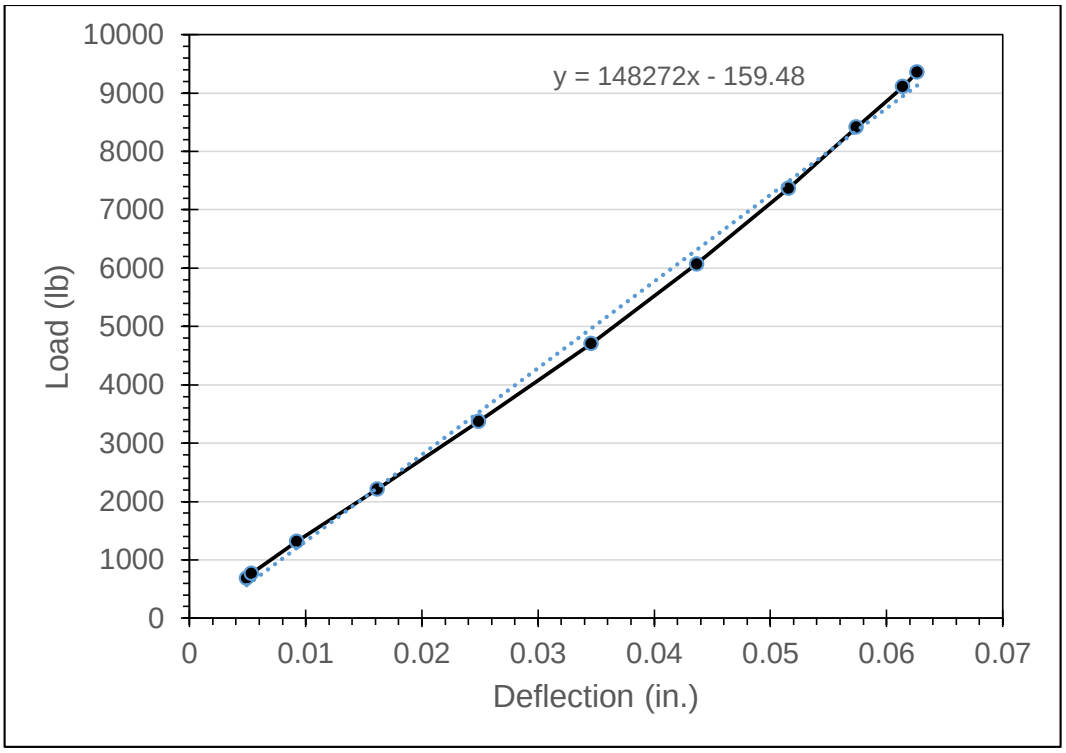

Figure 65. Load vs. Deflection for slab 3, measured from a single load cycle selected from day 27

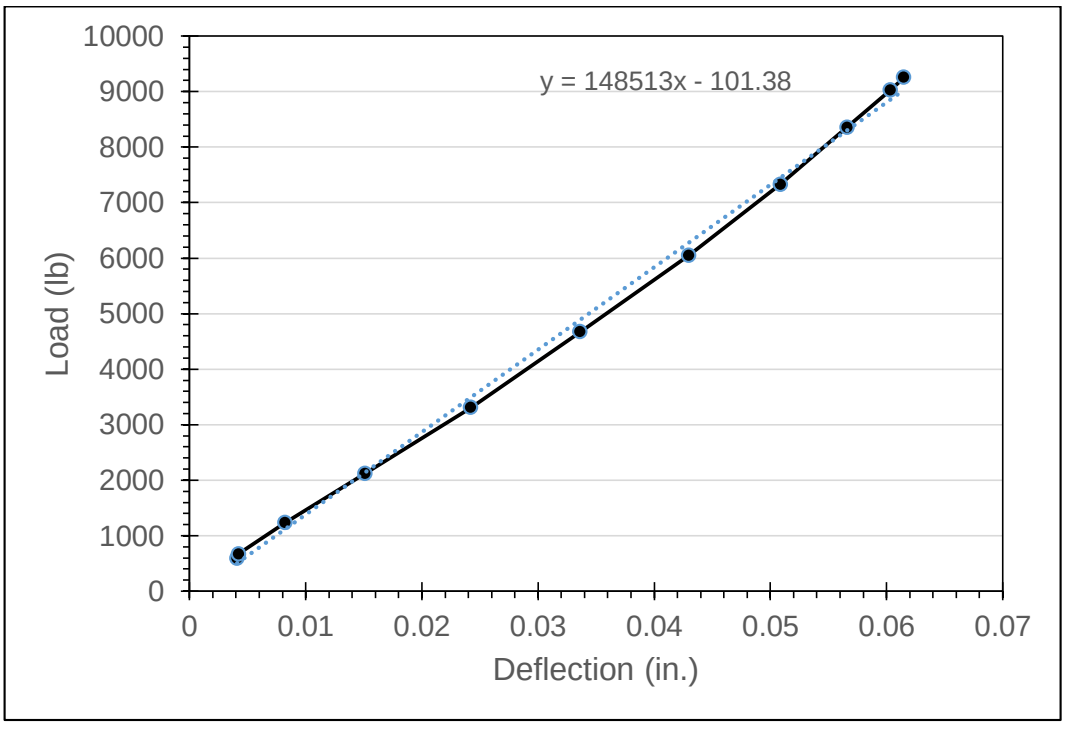

Figure 66. Load vs. Deflection for slab 3, measured from a single load cycle selected from day 29

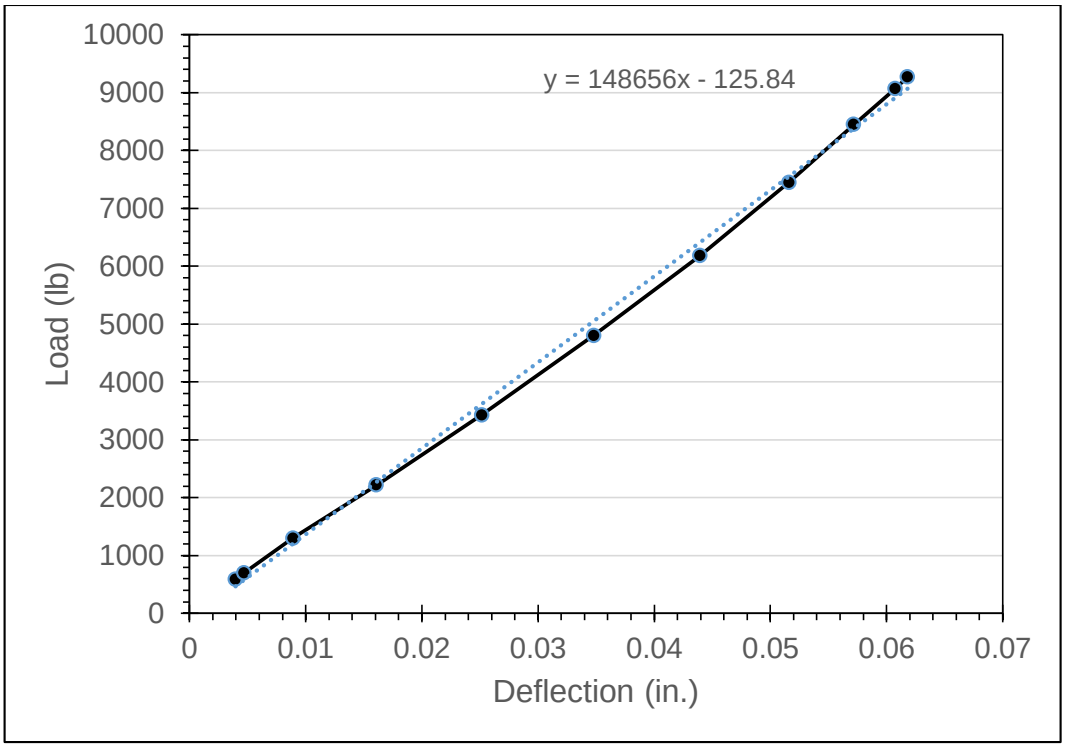

Figure 67. Load vs. Deflection for slab 3, measured from a single load cycle selected from day 31

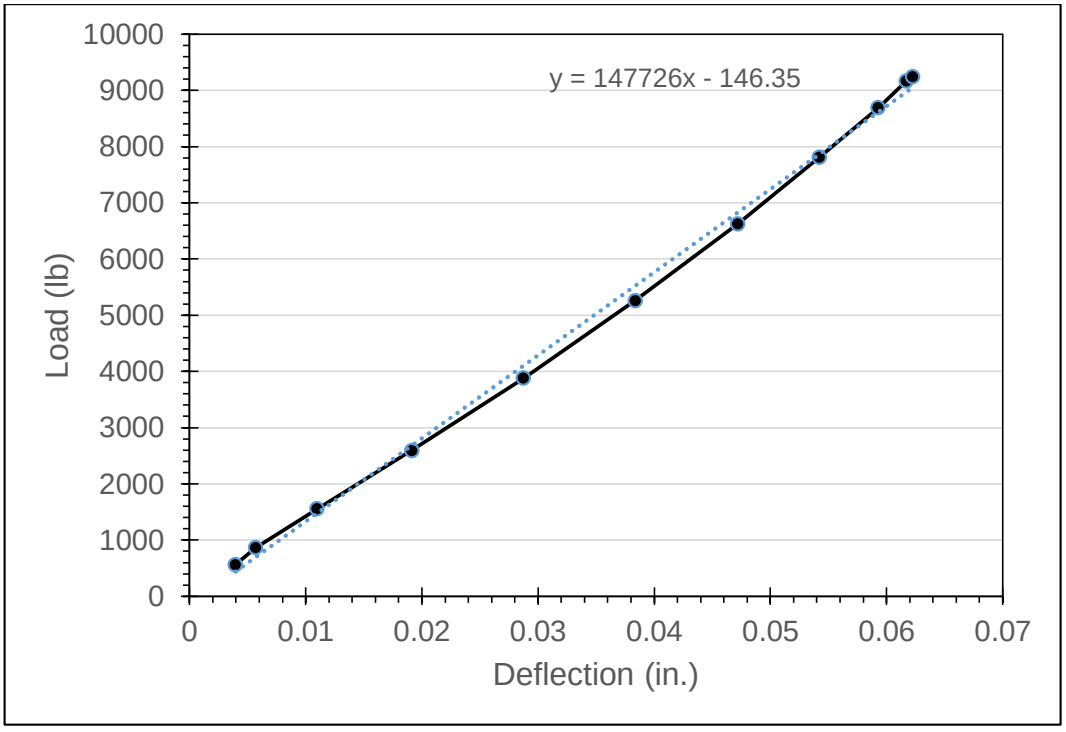

Figure 68. Load vs. Deflection for slab 3, measured from a single load cycle selected from day 33

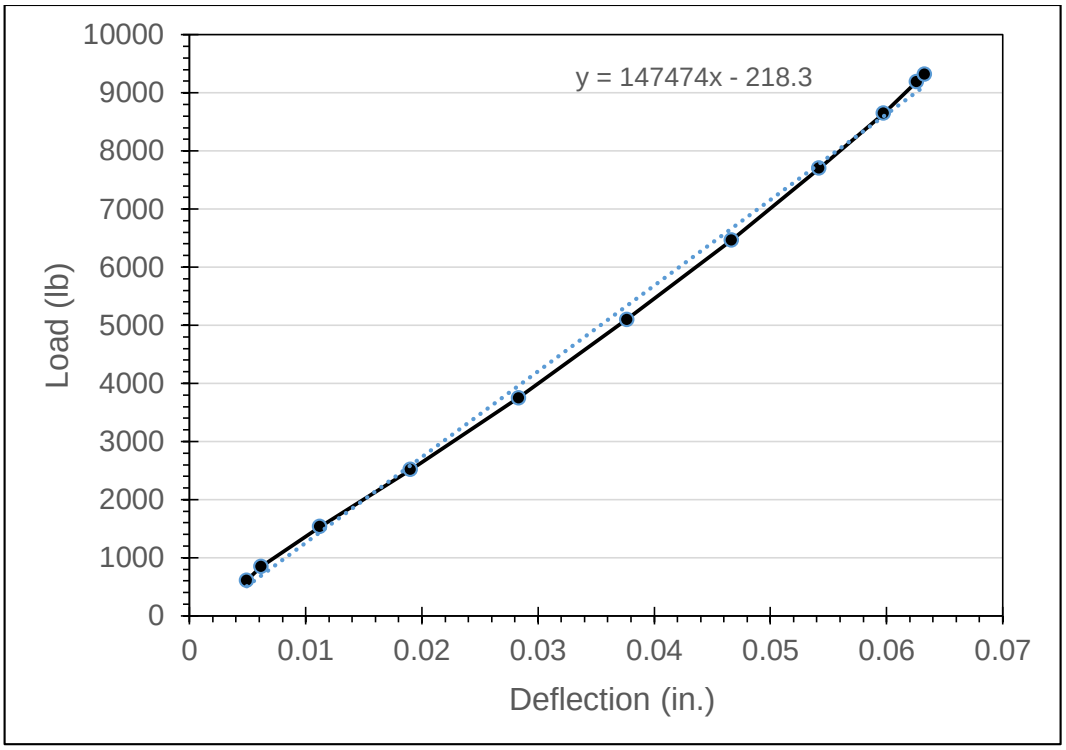

Figure 69. Load vs. Deflection for slab 3, measured from a single load cycle selected from day 35

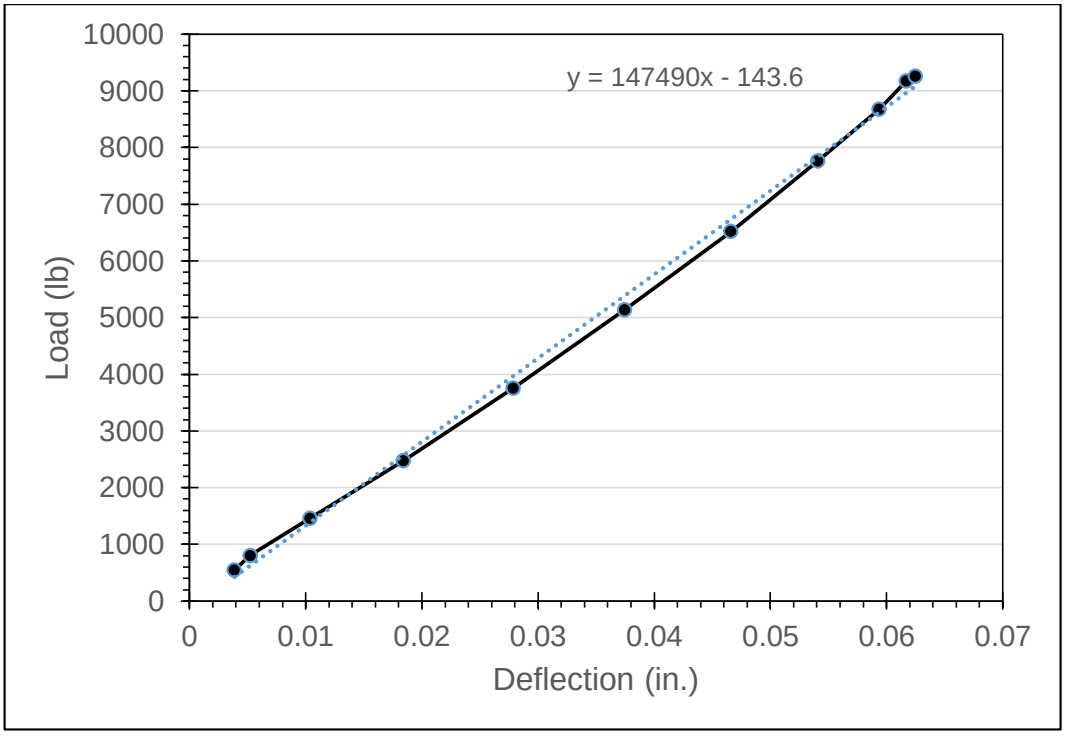

Figure 70. Load vs. Deflection for slab 3, measured from a single load cycle selected from day 37

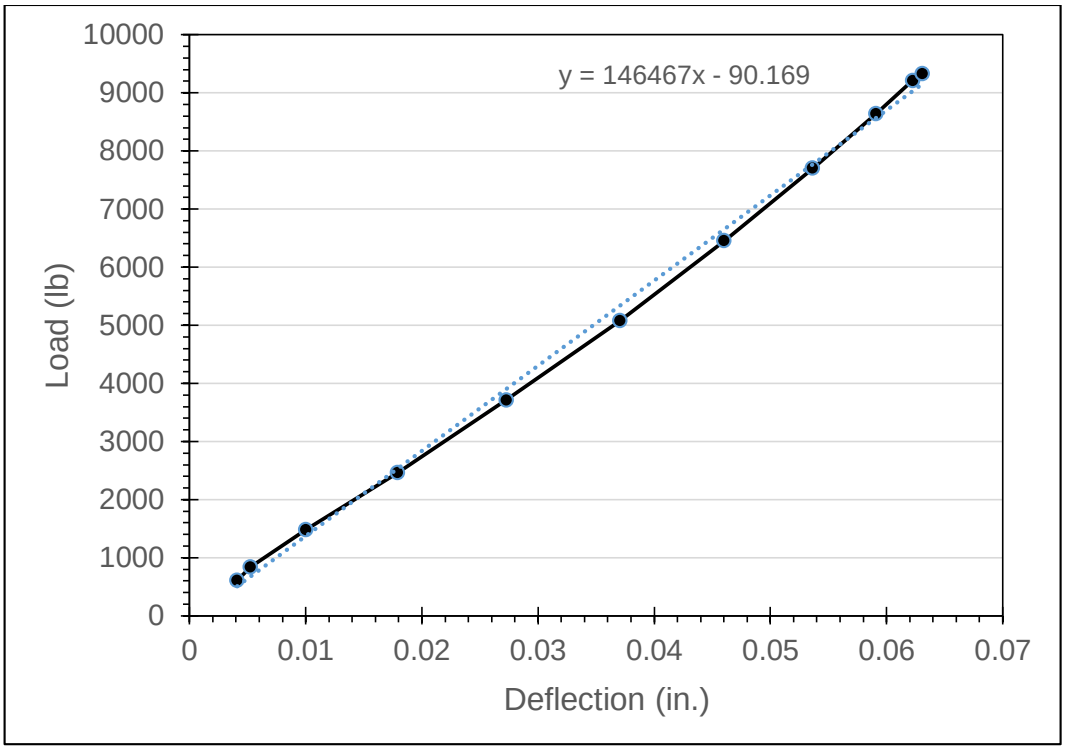

Figure 71. Load vs. Deflection for slab 3, measured from a single load cycle selected from day 39

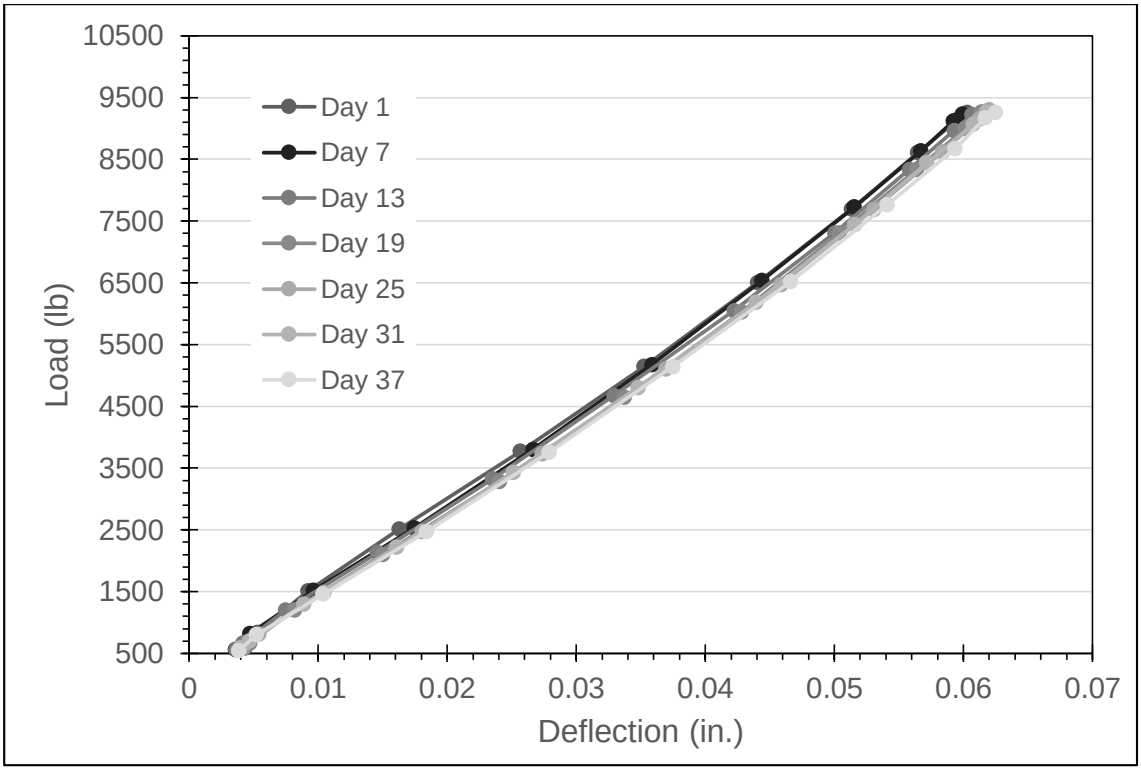

Figure 72. Comparison of load vs. deflection curves for multiple days

After the specimen had been subjected to 3 million load cycles, the load was increased to 14.6 kips (5% more than the expected cracking load) applied cyclically at 1 Hz. The test program called for the specimen to be loaded at this rate and magnitude for 2 million more cycles, or until failure. Figures 73 and 74 depict the load vs. deflection curves (for the loading portion of a selected cycle) during this second portion of testing. A linear trend line is also included in these figures showing the approximate slope of the loading curve.

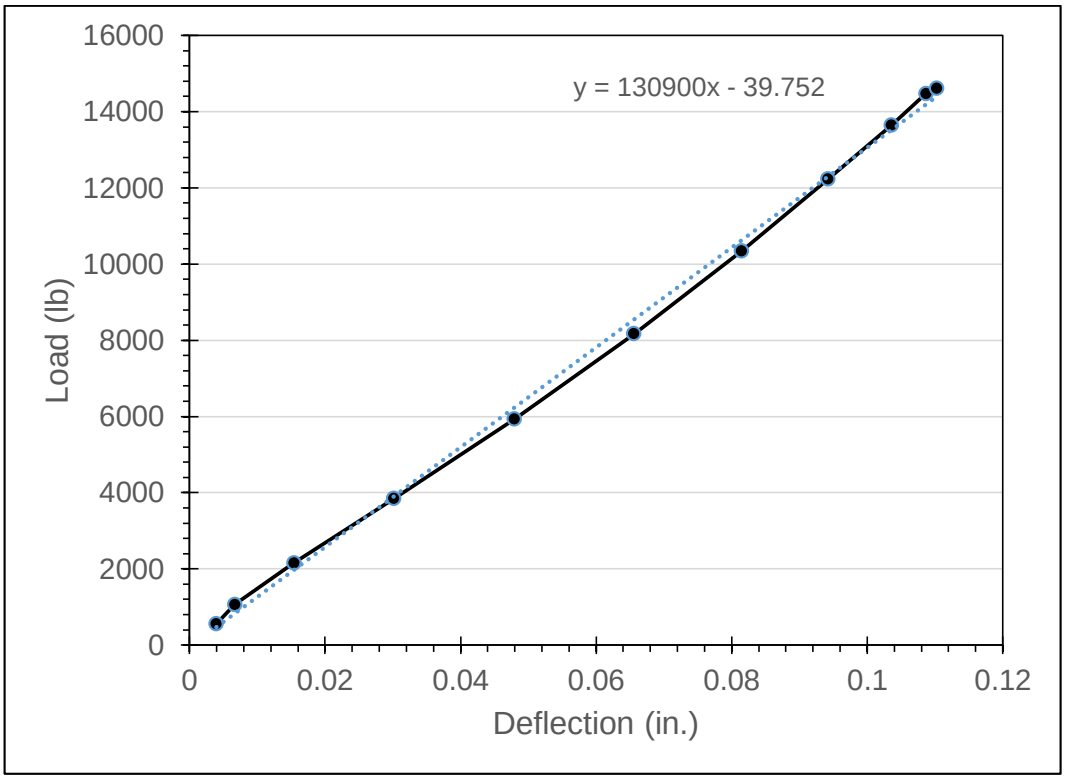

Figure 73. Load vs. Deflection for slab 3, measured from a single load cycle selected from day 40

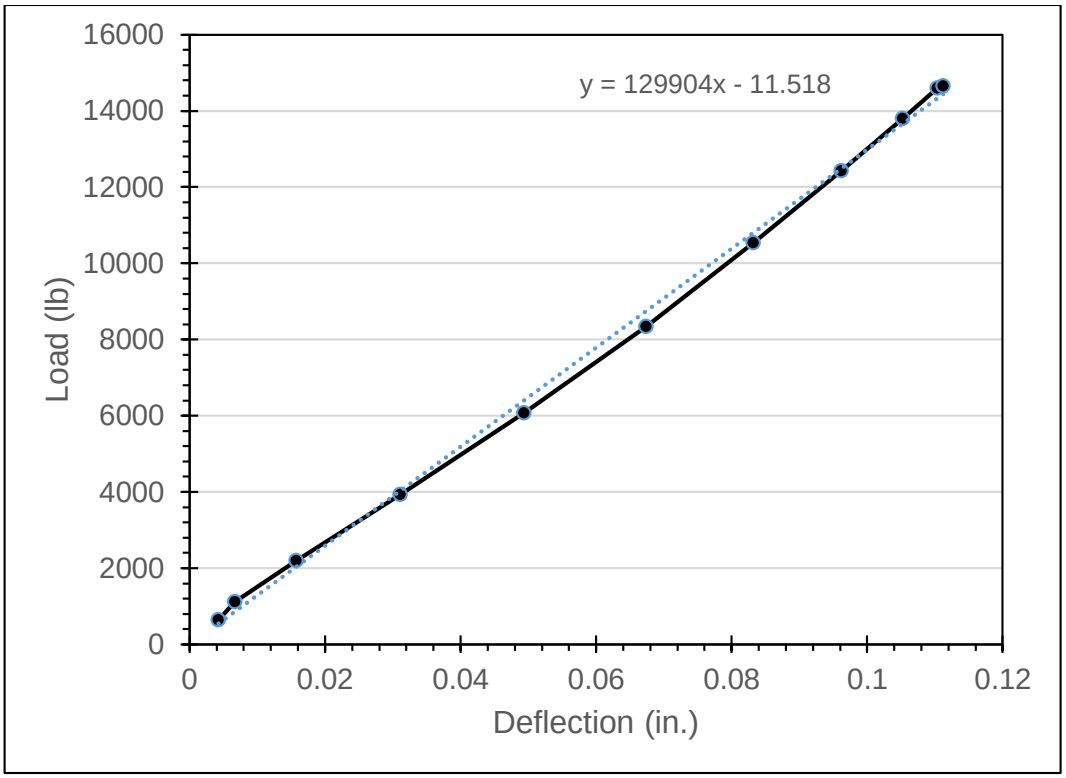

Figure 74. Load vs. Deflection for slab 3, measured from a single load cycle selected from day 41

The specimen failed after undergoing 244,029 cycles of the increased load. This failure was determined by deflection limits set within the MTS loading program, triggered to end the loading if the slab began to deflect excessively (beyond 0.45 in.), signaling that the specimen could no longer sustain the load. Figures 75-78 show the slab after this failure. There was significant visible cracking and a residual deflection of 0.38 in. The major failure crack on the bottom of the slab began on the south side 5.9 in. away from the joint interface closest to the load. Halfway across the slab (in the north-south direction) the crack migrated westward toward the joint and continued along the interface to the north edge. The crack at the interface on the north side after the conclusion of fatigue loading is shown in Figure 76. The crack in the base concrete on the

south side after the conclusion of fatigue loading is shown in Figure 77. Figure 78 shows the path of the crack from the base concrete to the interface.

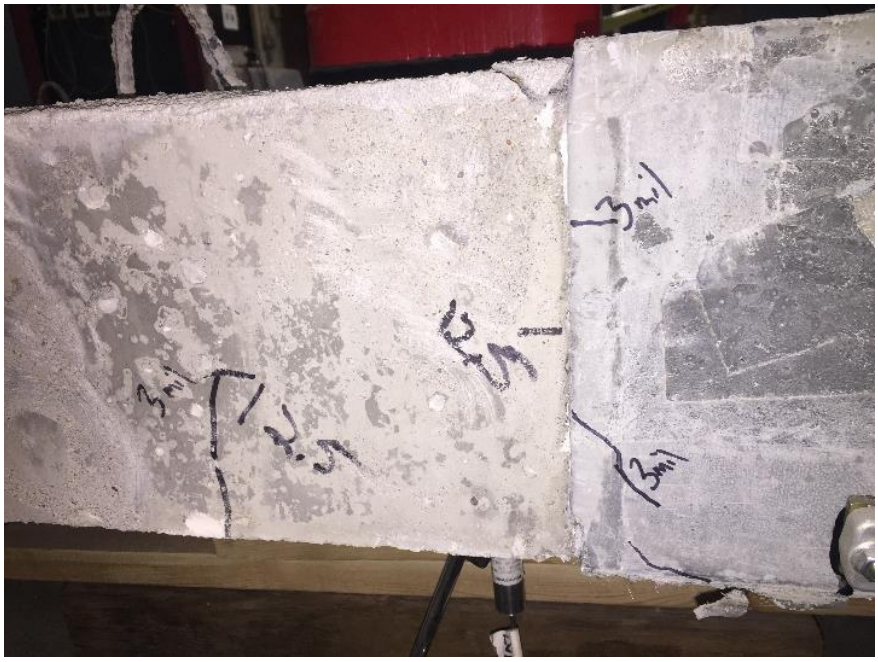

Figure 75. Side view of marked cracks on slab after fatigue loading

Figure 76. Crack at interface on north side of slab after fatigue loading

Figure 77. Crack in base concrete on south side after fatigue loading

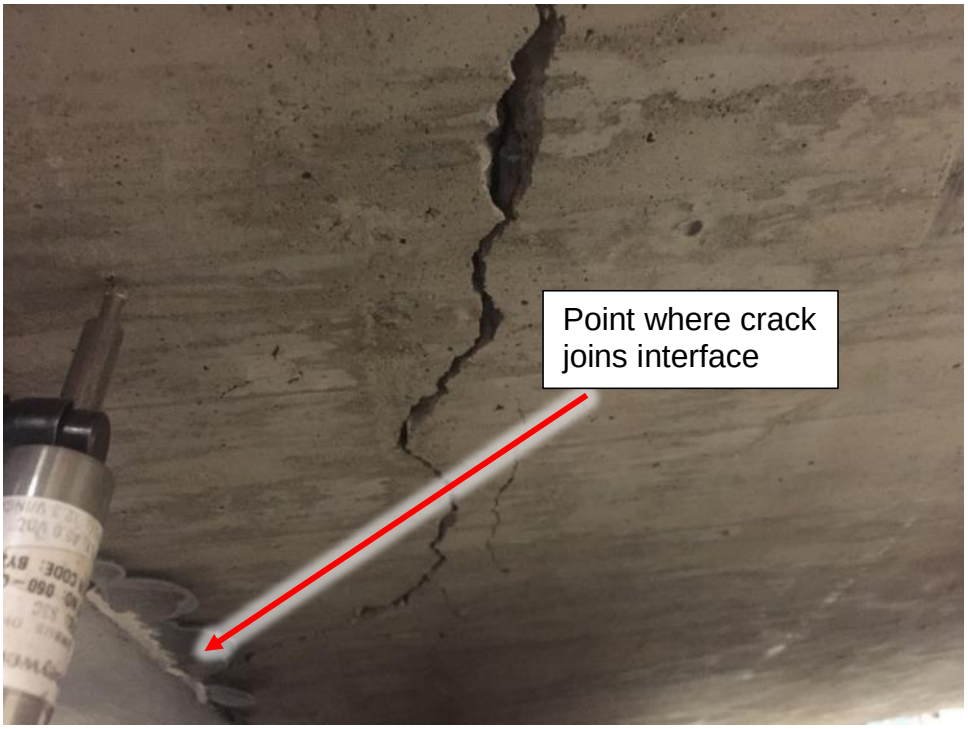

Figure 78. Path of crack underneath slab from base concrete to interface

Figure 79 shows a comparison of the measured stiffness of the slab at the time intervals represented in Figures 52-74. There is a generally steady decrease of 3.6% in the observed stiffness of the slab from day 1 to 39, and a steep decrease of 11.3% between days 39 and 41 when the load was increased and the slab began to fail. Figure 80 shows the residual deflections taken at the end of each day with a final residual deflection of 0.38 in. Due to program malfunction, the first 4 days of testing are not included in this graph. These deflections go hand in hand with the stiffness values shown in Figure 79.

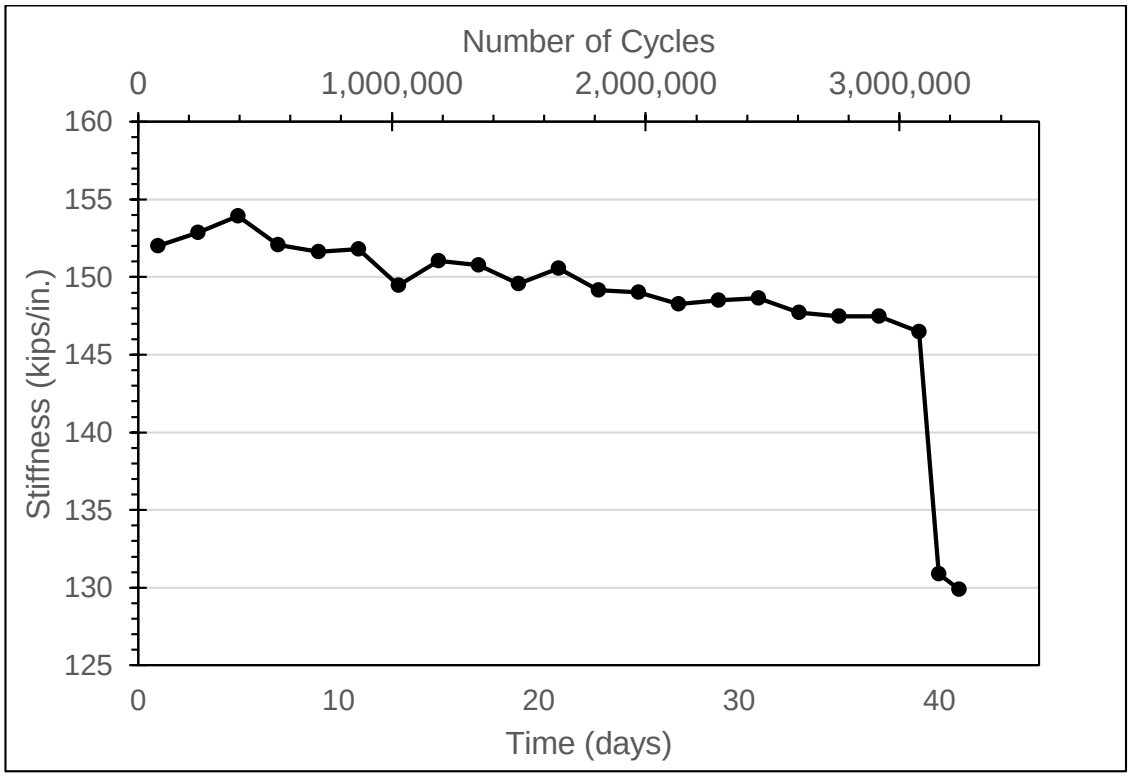

Figure 79. Slab stiffness over loading period

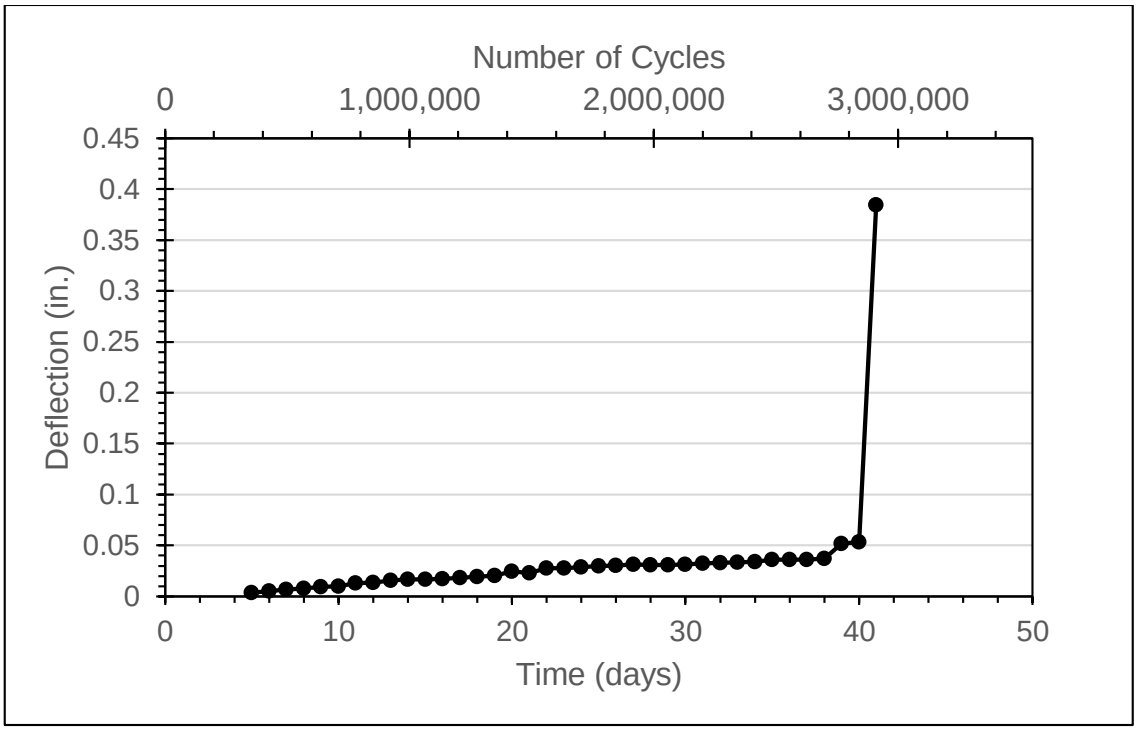

Figure 80. Residual deflections over the course of fatigue testing

After the slab reached the failure point due to the fatigue loading, it was statically loaded to final failure to assess its behavior after being fatigued. Because of the residual damage due to possible rebar pullout and/or fracture prior to the static test, the ultimate load reached was much lower than that of slab 1 and 2. Figure 81 shows the load vs. deflection curve for the static loading. The ultimate load at complete failure was approximately 17.7 kips. Failure was determined at the point when the specimen exhibited yielding behavior, was unable to sustain any increasing load, and exhibited concrete crushing at the top compression fiber. The final residual deflection after static loading was 2.26 in., which is much higher than for slab 1 and slab 2. Much like the reduced flexural capacity, this increased residual deflection is likely due to damage done to the specimen during fatigue loading.

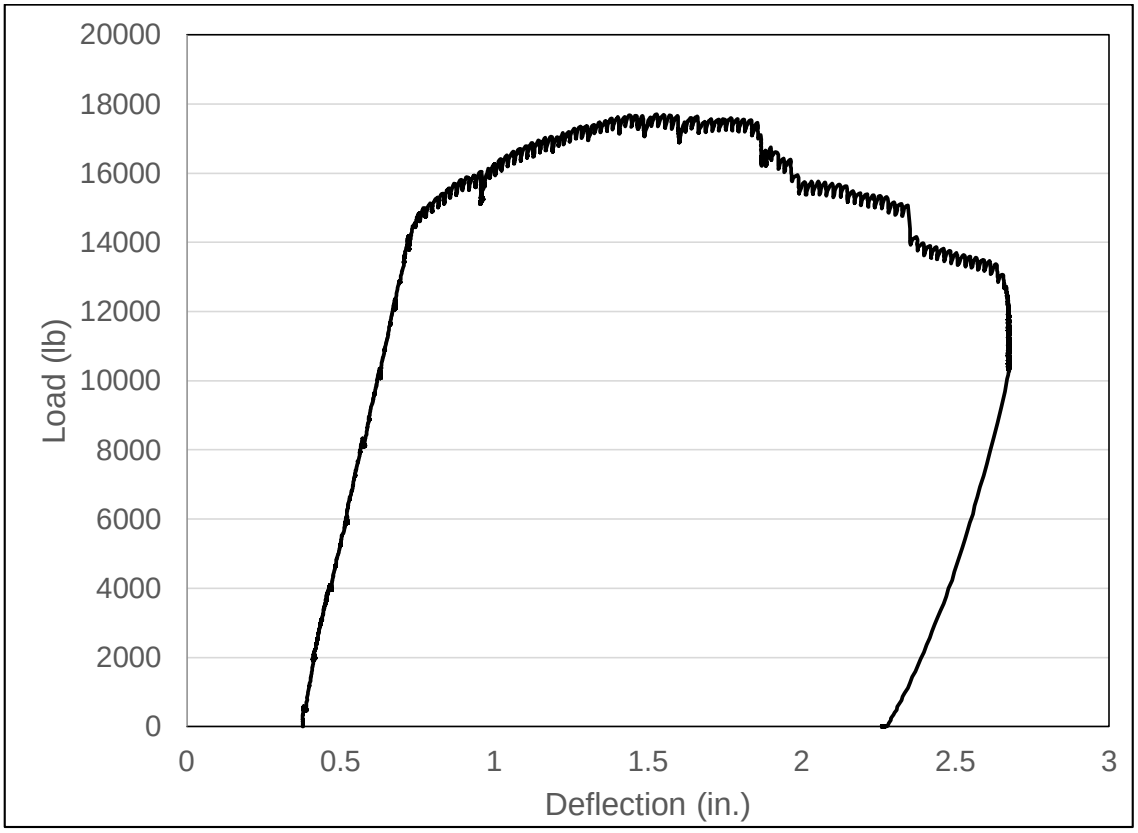

Figure 81. Load vs. Deflection for slab 3 static loading

The interface between the UHPC and NSC closest to the load point had a visible separation of approximately 0.1 in. on the south side of slab and 1.2 in. on the north side. After the final static loading, one of the rebar that extended into the joint was fractured, and another piece of rebar on the north side of slab had been pulled out of the UHPC connection. This likely occurred during fatigue loading and became visible after the cracks were widened during the final static test. The stress in the steel during fatigue loading at 14.6 kips was calculated to be 47.5 ksi, which was well above the fatigue limit. This calculation can be found in Appendix C. The cracking after the final static loading is shown in

Figures 82-85. There was also crushing of the concrete on the top of the slab adjacent to the load point, as seen in Figure 86.

Figure 82. Crack at interface on north side of slab after final static loading and crushing of the top compression fiber in the base concrete

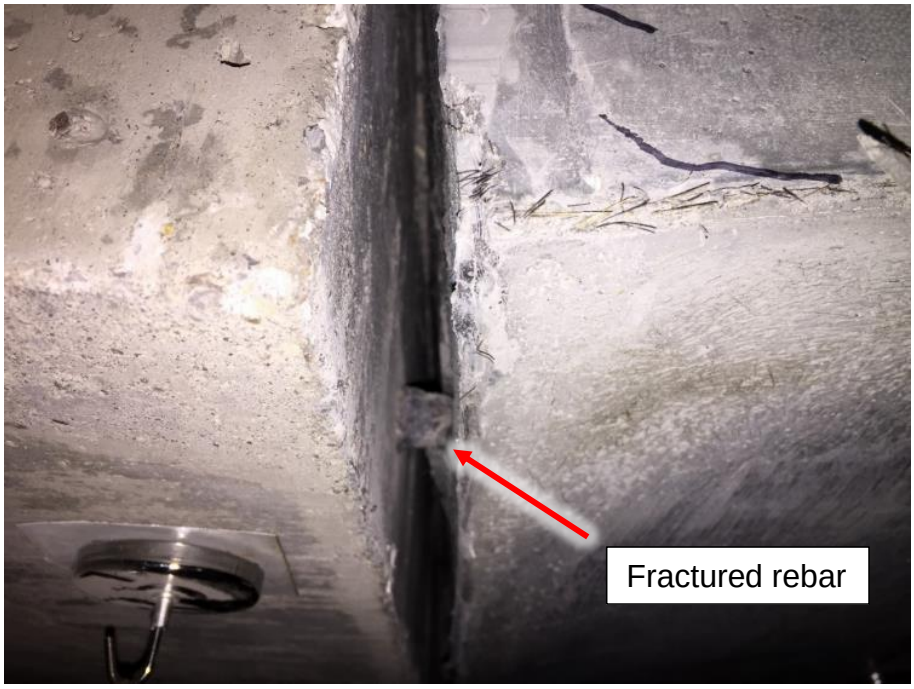

Figure 83. Crack at interface on north side of slab from underneath

Figure 84. Crack in base concrete on south side and crushing of the top compression fiber after final static loading

Figure 85. Crack in base concrete on south side from underneath

Figure 86. Crushing of concrete on top of slab after final static loading

4.4.4 Comparison of Slabs 1, 2, and 3

There are a few key items to be taken from these results. Slab 1 and 2 had much higher ultimate flexural capacities than expected. This could be attributed to the higher tensile and compressive strength of the UHPC which may have caused stress redistribution away from the load point, increasing the strength of the specimens as a whole. It is also possible that the UHPC joint caused the specimens to be slightly stiffer than monolithic NSC slab specimens with the same dimensions and reinforcement. This was not the case for slab 3, which failed prematurely due to fatigue of the steel and damage to the specimen over time. Figure 87 depicts the load vs. deflection curves for all 3

slabs for the initial portion of loading. Slabs 1 and 2 had very similar slopes, which is to be expected. Slab 3 had a slope that was less steep than the other two slabs. This is due to the premature cracking of the specimen before decreasing the magnitude of the cyclic load. Figure 88 depicts the load vs. deflection curves for all the slabs during ultimate static loading to failure. Slabs 1 and 2 both reached an ultimate flexural strength of more than 36 kips. Slab 2 had a higher residual deflection than slab 1, indicating either that it may not have been as stiff, or was loaded further past yielding. Slab 3 had a much lower stiffness due to the prior fatigue loading and damage to the specimen.

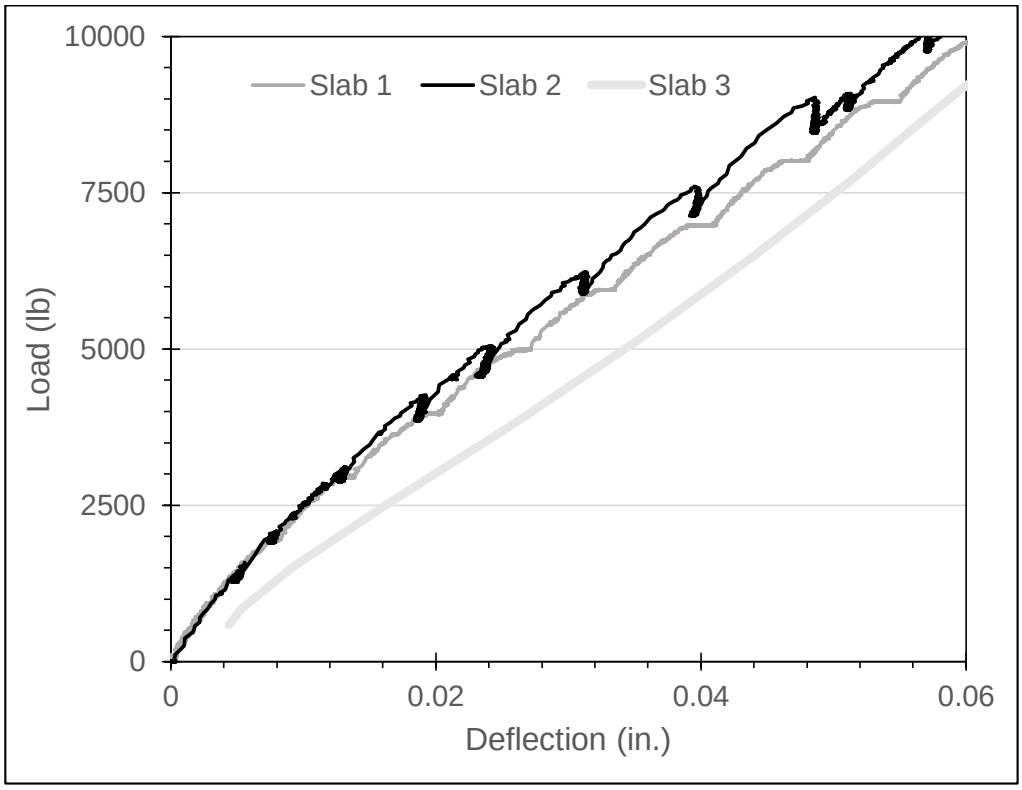

Figure 87. Load vs. Deflection curve for initial portion of loading for all 3 slabs

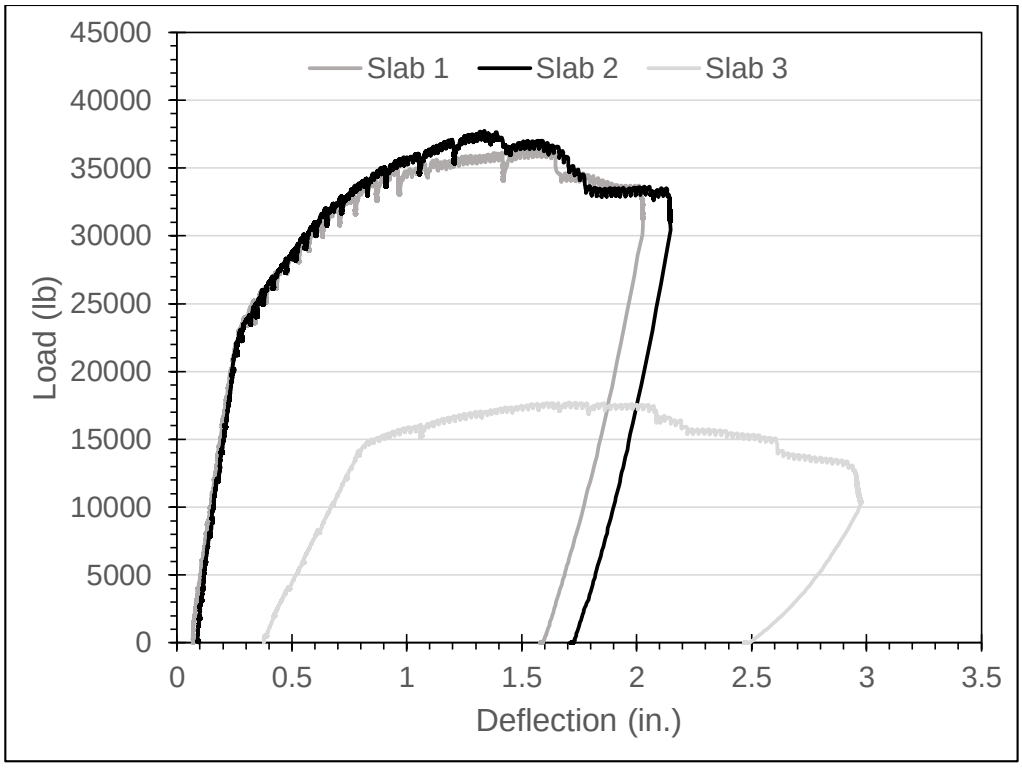

Figure 88. Load vs. Deflection curve for static testing for all 3 slabs

For slabs 1 and 2, it can be said that the development length was adequate. The steel provided the expected contribution based on the assumption that the steel yields. Because the steel may have been pulled out of the joint for slab 3, it is uncertain whether the specimen failed because the steel yielded or because the connection was damaged from fatigue loading.

Because there was essentially no surface preparation for the slab joints, they most closely resemble the 90 degree wire brushed composite MOR specimens. Like the 90 degree wire brushed composite MOR specimens, the slab specimen UHPC joints cracked first in the base concrete and eventually exhibited some weakness at the interface.

5.0 Findings, Conclusions & Recommendations

The study described in this thesis included multiple tests to obtain more information about the bond strength of UHPC to NSC and assess its feasibility as a repair material for bridge joints. MOR tests were performed on composite specimens, and both static and cyclic flexural testing was performed on medium-scale slab joints.

5.1 Findings and Conclusions

Based on the results of the testing described in this thesis, several conclusions were made.

- In order to reach an acceptable strength in a limited amount of time, heat curing was required for the specific UHPC formulation tested.
- Slant shear tests revealed that the bond strength of the NSC to UHPC specimens examined was comparable to the bond strengths of other UHPC/NSC specimens found in the literature; however, the small number of specimens in this study does not allow generalized conclusions about a correlation between slant shear bond strength and flexural strength.
- The MOR tests revealed that, for most composite specimens, the interface between the UHPC and NSC performed similarly, and failed in the base concrete. Based on normalized results, the exposed aggregate surface preparation performed the best and sustained the highest stresses for most interface configurations.

This surface preparation would likely perform best in the field when implementation is feasible.

- When comparing the normalized flexural stress coefficients from the composite specimens, the 60 degree interface specimens reached a higher flexural stress as a whole. For these specimens, the wire-brushed and sand-blasted surfaces performed better than the exposed aggregate surfaces. When implementing replacement UHPC joints in the field, it may be most beneficial to use a 60° cut angle when removing the current joint. Utilizing a typical roughness (resulting from removing the current joint with saw cuts) could potentially produce comparable flexural strengths to the values found in this study.
- All of the flexural strengths observed during testing of the composite specimens were at least as large as the calculated flexural strengths for a monolithic NSC specimen. Approximately 91.7% of the composite specimens fractured within the base concrete, indicating that the bond between the two materials was at least as strong as the base concrete, and the interface between the two materials did not weaken the specimen (in terms of maximum flexural stress).
- Based on the results from the first two medium-scale slab specimens, the overall measured flexural load capacity of the specimens (approximately 37 kips) far exceeded the calculated

flexural load capacity of a monolithic NSC slab with the same dimensions and reinforcement (23.5 kips). This may be an indication that the UHPC joints in this study may have provided additional flexural strength to the specimens by resisting cracking and redirecting stresses away from the load point.

- The measured cracking load for slab 1 (10.9 kips) was slightly less than the calculated cracking load for a monolithic NSC slab with the same dimensions and reinforcement (11.7 kips). The cracking loads for slabs 2 and 3 (13.1 and 12.5 kips respectively) were at least as high as the calculated cracking load (11.7 kips). All initial cracks occurred in the base concrete.
- The flexural stiffness measured for slab 3 steadily decreased throughout the course of fatigue loading, and sharply decreased when the magnitude of the load was increased. It is not clear whether initial cracking at 12.5 kips accelerated the rate of decrease for the slab stiffness.
- Testing of slab 3 under fatigue loading revealed an increase in residual deflection over time, which tracks with the reduced stiffness over time. This specimen, after initial cracking, was more susceptible to decreased stiffness and flexural capacity under fatigue loading.
- The results for static loading of slab 3 revealed a flexural strength (17.7 kips) that was less than the calculated flexural strength for a

monolithic NSC slab with the same dimensions and reinforcement (23.5 kips). While this value is not extremely far in magnitude from the expected flexural capacity, it is more than 50% less than the flexural capacities exhibited by slabs 1 and 2.

- All slabs experienced some degree of separation at the interface between the UHPC and the NSC closest to the load point, indicating that this location may be a weak point for these specimens. Although the specimens experienced interface separation, for slabs 1 and 2 the main cause of failure was cracking and crushing in the base concrete at the load point. Slab 3 likely failed due to a combination of interface failure, rebar fracture and fatigue, and base concrete cracking and crushing at the load point.

5.2 Recommendations and Future Work

Based on the results of this research and the processes involved, the following recommendations are made for similar research and potential future projects relating to this subject.

- Because the external strain gages performed poorly and did not consistently give a clear picture of the strain behavior of the slab specimens, it is recommended that future studies of this type should include internal strain gages placed on the rebar in order to obtain more useful information.

- The magnitude of the load for cyclic testing should be based on the calculated cracking load for a monolithic NSC specimen or the graphically determined cracking load of previous specimens—basing this value on the visually observed values of previous specimens can be more variable and less accurate. This practice may prevent premature cracking in fatigue loading specimens. Similar studies should be performed to replicate the test program of slab 3, taking care to prevent any cracking prior to fatigue loading in order to determine the true effect of fatigue loading on the stiffness and flexural capacity of an uncracked section.
- Studies should be performed to assess bond strength and performance of both UHPC repair joints and composite MOR joints for specimens with a dampened surface to determine the effects of moisture on the bond.
- The results of this research indicate that UHPC is a promising repair material for bridge joints; in any case, more research should be conducted to determine the best practices for heat curing in the field (where heat lamps may not be feasible) and the behavior of a replacement UHPC joint in a fully operational bridge deck system.
- Because Ductal® is a relatively expensive material, more research should be conducted for less expensive types of UHPC and their performance in the same testing scenarios outlined in this study.

References

American Concrete Institute (ACI). (2006). “Guide for the selection of materials for the repair of concrete.” ACI 546.3R-06, Farmington Hills, MI.

Anon [Internet], “North American Ductal® Bridge Projects.” Available at www.ductal-lafarge.com [Cited November 28, 2017].

ASTM. (2013). “Standard Test Method for Bond Strength of Epoxy-Resin Systems used with Concrete by Slant Shear,” C882-13, ASTM International, West Conshohocken, PA.

ASTM. (2015). “Standard Test Method For Measuring Pavement Macrotexture Depth Using a Volumetric Technique,” E965-15, ASTM International, West Conshohocken, PA.

ASTM. (2015). “Standard Test Method for Slump of Hydraulic-Cement Concrete,” C143-15, ASTM International, West Conshohocken, PA.

ASTM. (2016). “Standard Test Method For Flexural Strength of Concrete (Using Simple Beam with Third-Point Loading),” C78-16, ASTM International, West Conshohocken, PA.

ASTM. (2017). “Standard Test Method For Splitting Tensile Strength of Cylindrical Concrete Specimens,” C496 -17, ASTM International, West Conshohocken, PA.

ASTM. (2017). “Standard Test Method for Compressive Strength of Cylindrical Concrete Specimens,” C39-17, ASTM International, West Conshohocken, PA.

ASTM. (2017). “Standard Test Method for Air Content of Freshly Mixed Concrete by the Pressure Method,” C231-17, ASTM International, West Conshohocken, PA.

ASTM. (2017). “Standard Test Method for Temperature of Freshly Mixed Hydraulic-Cement Concrete,” C1064-17, ASTM International, West Conshohocken, PA.

Bierwagen, D. et al., “Ultra-High Performance Concrete Waffle Slab Bridge Deck for Wapello County, Iowa,” HPC Bridge Views, Issue No. 65, January/February 2011. Available at http://www.hpcbridgeviews.org [Cited November 28, 2017].

Bornstedt, G. “Connecting Precast Concrete Bridge Deck Panels with Ultra High Performance Concrete (UHPC),” Western Bridge Engineer’s Seminar, Phoenix, AZ, September 25–28, 2011. Abstract only.

British Standard. (1999). “Products and systems for the protection and repair of concrete structures. Test methods. Determination of slant shear strength.” BS EN 12615:1999, British Standards Institution, 12.

Carbonell Munoz, M. A., Harris, D. K., Ahlborn, T. M., and Froster, D. C., “Bond Performance between Ultrahigh-Performance Concrete and Normal-Strength Concrete,” *ASCE Journal of Materials in Civil Engineering*, Vol. 26, No.8, Aug 2014.

Climaco, J. C. T. S., and Regan, P. E. (2001). "Evaluation of bond strength between old and new concrete in structural repairs." Magazine of Concrete Research, 53(6), pp. 377-390.

Denarie, E., and Bruhwiler, E., “Structural Rehabilitations with Ultra-High Performance Fibre Reinforced Concretes (UHPFRC),” *Restoration of Buildings and Monuments*, Vol. 12, No. 5/6, 2006, pp. 453-468

Diab, A. M., Eldin, M. R. T., and Elmoaty, A. E. M. A., “Slant Shear Bond Strength Between Self Compacting Concrete and Old Concrete,” *Construction and Building Materials* 130, 12 November 2016, pp.73-82.

Floyd, R.W., and Volz, J. S., “ODOT Research Project Proposal: Evaluation of Ultra-High Performance Concrete for Use in Bridge Connections and Repair,” The Board of Regents of the University of Oklahoma, July 2016.

Graybeal, B. (2010) “Behavior of Field-Cast Ultra-High Performance Concrete Bridge Deck Connections Under Cyclic and Static Structural Loading,” FHWA-HRT-11-023, Federal Highway Administration, McLean, VA.

Graybeal, B., “Tech Note | Ultra-High Performance Concrete,” FHWA-HRT-11-038, March 2011, Federal Highway Administration, McLean, VA.

Graybeal, B., “Ultra-High Performance Concrete: A State-of-the-Art Report for the Bridge Community,” FHWA-HRT-13-060, June 2013, Federal Highway Administration, McLean, VA.

Graybeal, B., “Design and Construction of Field-Cast UHPC Connections,” FHWA-HRT-14-084, 2014, Federal Highway Administration, McLean, VA.

Habel, K., Denarie, E., and Bruhwiler, E., “Structural response of composite ‘UHPFRC-concrete’ members under bending,” Proceedings of the International Symposium on Ultra High Performance Concrete, Kassel, Germany, September 13-15, 2004.

Keierleber, B. et al., “FHWA, Iowa Optimize Pi Girder,” ASPIRE, Winter 2010, pp. 24–26. Available at http://www.aspirebridge.org [Cited November 28, 2017].
Momayez, A., Ehsani, M. R., Ramezanianpour, A. A., and Rajaie, H., “Comparison of Methods for Evaluating Bond Strength Between Concrete Substrate and Repair Materials”, *Cement and Concrete Research*, Vol. 35, No. 4, April 2005, pp. 748-757.

Moore, B., “Little Cedar Creek Bridge—Big Innovation,” ASPIRE, Spring 2012, p. 27. Available at http://www.aspirebridge.org [Cited November 28, 2017].

Oklahoma Department of Transportation, “ODOT Standard Specifications,” Transportation Commission, 2009, pp. 551.

Ozyildirim, H.C. and Volgyi, J.F.J., “Virginia’s Developments in the Use of Concrete in Bridges,” ASPIRE, Winter 2008, pp. 50–52. Available at http://www.aspirebridge.org [Cited November 28, 2017].

Royce, M.C., “Concrete Bridges in New York State,” ASPIRE, Fall 2011, pp. 46–48. Available at http://www.aspirebridge.org. [Cited November 28, 2017].

Sarkar, J., “Characterization of the Bond Strength between Ultra High Performance Concrete Bridge Deck Overlays and Concrete Substrates,” Michigan Technological University, 2010.

Shutt, C.A., “UHPC Joint Provides New Solutions,” ASPIRE, Fall 2009, pp. 28–30. Available at http://www.aspirebridge.org [Cited November 28, 2017].

Tayeh, B. A., Abu Bakar, B. H., Mehat Johari, M. A., and Voo, Y. L., "Evaluation of bond strength between normal concrete substrate and ultra-high performance fiber concrete as a repair material," Procedia Engineering 54, 2013, pp. 554-563.

Appendix A: Tables

Table 17. Compressive Strength Results for all Cylinders

Name	12 Hour (psi)	1-Day (psi)	3-Day (psi)	7-Day (psi)	28-Day (psi)	Test Day (psi)
Trial Batch – Mix Design 1	N/A	4125	N/A	6590	7890	N/A
	N/A	-	N/A	6300	8020	N/A
	N/A	-	N/A	6995	8160	N/A
Trial Batch – Mix Design 2	N/A	2080	N/A	3390	3510	N/A
	N/A	2175	N/A	3415	3795	N/A
	N/A	2215	N/A	3455	3795	N/A
Trial Batch – Mix Design 3	N/A	3525	N/A	-	6840	N/A
	N/A	3490	N/A	-	7115	N/A
	N/A	3445	N/A	-	6740	N/A
Trial Batch – Mix Design 4	N/A	2190	N/A	3670	4660	N/A
	N/A	2065	N/A	3935	4100	N/A
	N/A	2310	N/A	3825	4310	N/A
Batch N1	N/A	2430	3780	N/A	4990	N/A
	N/A	2345	-	N/A	4985	N/A
	N/A	2280	-	N/A	-	N/A
Batch N2	N/A	1755	N/A	N/A	3585	N/A
	N/A	1710	N/A	N/A	3465	N/A
	N/A	1715	N/A	N/A	3600	N/A
Batch N3	N/A	2395	N/A	N/A	4500	N/A
	N/A	2335	N/A	N/A	4815	N/A
	N/A	2445	N/A	N/A	4645	N/A
Batch N4	N/A	3080	N/A	N/A	5610	N/A
	N/A	2745	N/A	N/A	6120	N/A
	N/A	3055	N/A	N/A	5810	N/A
Batch U1	N/A	N/A	11,910	N/A	21,080	21,080
	N/A	N/A	10,660	N/A	22,165	22,165
	N/A	N/A	12,280	N/A	21,975	21,975
Batch U2	N/A	N/A	9200	N/A	21,255	21,255
	N/A	N/A	12,620	N/A	22,870	22,870
	N/A	N/A	13,130	N/A	21,995	21,995

Table 17. Compressive Strength Results for all Cylinders, Continued

Name	12 Hour (psi)	1-Day (psi)	3-Day (psi)	7-Day (psi)	28-Day (psi)	Test Day (psi)
Batch U3	N/A	N/A	12,710	N/A	22,080	22,080
	N/A	N/A	11,980	N/A	21,340	21,340
	N/A	N/A	12,380	N/A	21,640	21,640
Batch U4	N/A	N/A	12,910	N/A	22,180	22,180
	N/A	N/A	12,115	N/A	20,985	20,985
	N/A	N/A	12,770	N/A	21,735	21,735
Medium-scale slab NSC	N/A	3065	N/A	4950	5460	N/A
	N/A	3080	N/A	4455	6150	N/A
	N/A	3105	N/A	4965	6320	N/A
Slab Joint 1 UHPC	22,640	N/A	N/A	N/A	22,185	23,355
	20,690	N/A	N/A	N/A	23,505	22,000
	20,955	N/A	N/A	N/A	22,923	-
Slab Joint 2 UHPC	15,700	N/A	N/A	N/A	19,185	26,410
	18,030	N/A	N/A	N/A	25,065	22,895
	15,445	N/A	N/A	N/A	17,125	23,764
Slab Joint 3 UHPC	17,645	N/A	N/A	N/A	24,440	21,945
	17,090	N/A	N/A	N/A	18,045	24,520
	17,200	N/A	N/A	N/A	19,280	22,520

Table 18. NSC Fresh Concrete Properties

Batch	Temperature (°F)	Air Content (%)	Slump (in.)	Unit Weight (lb/ft^3)
N1	67.6	8.00	4.25	142.2
N2	68.5	7.00	5.25	133.9
N3	70.9	7.00	5.25	142.0
N4	67.0	6.60	3.00	145.9
Slab NSC	85.1	1.80	2.25	-

Appendix B: Additional Photos of Specimens and Test Setup

Figure 89. Wooden MOR form inserts coated with sugar for exposed aggregate specimens

Figure 90. NSC cylinders after grinding prior to compressive strength testing

Figure 91. Steel fibers being added to UHPC mixture

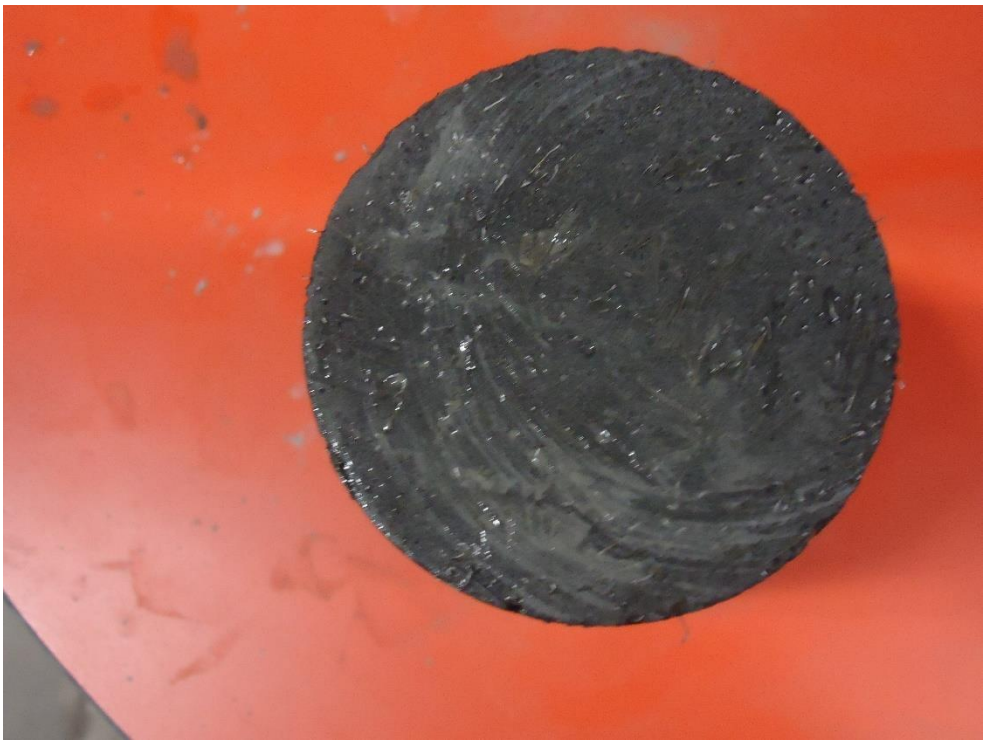

Figure 92. Top surface of UHPC cylinder after grinding prior to compressive strength testing

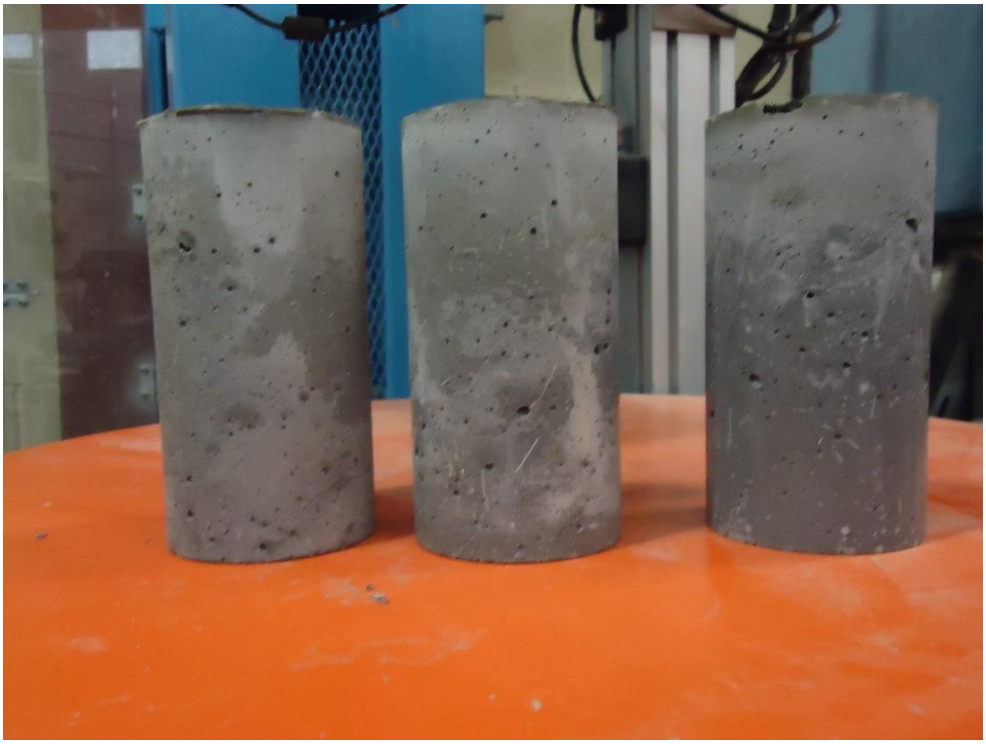

Figure 93. UHPC cylinders prior to grinding

Figure 94. Composite MOR specimen prior to testing

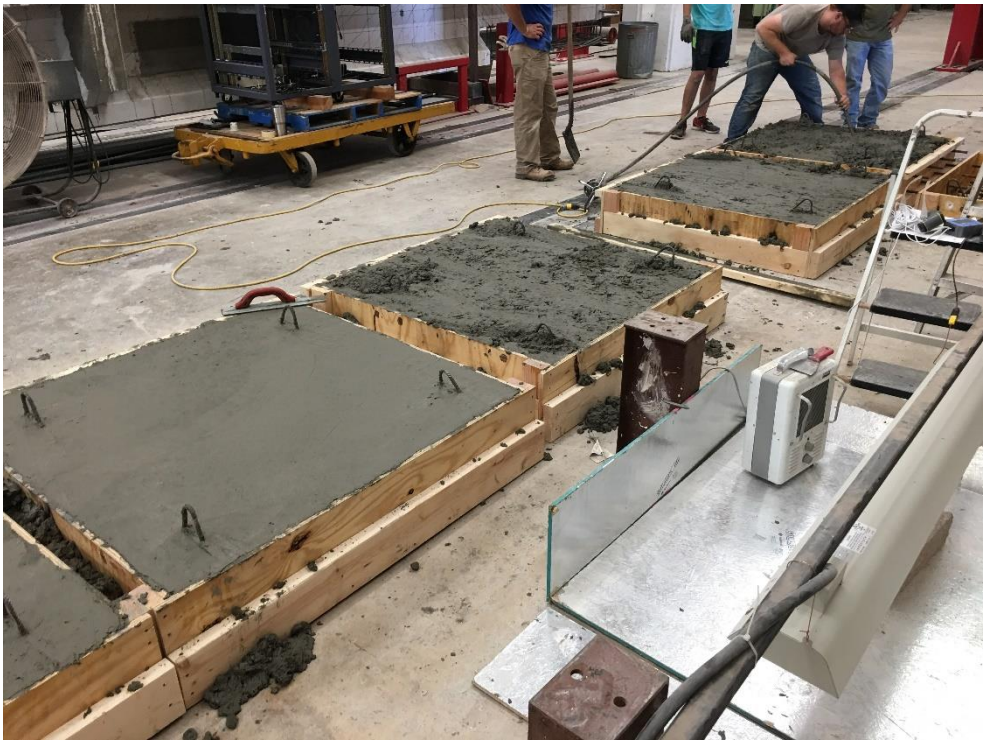

Figure 95. Slab panels during finishing process

Figure 96. Slab panels with exposed rebar prior to casting of the UHPC joint

Figure 97. Heat lamp and medium-scale slab with UHPC joint during heat curing process

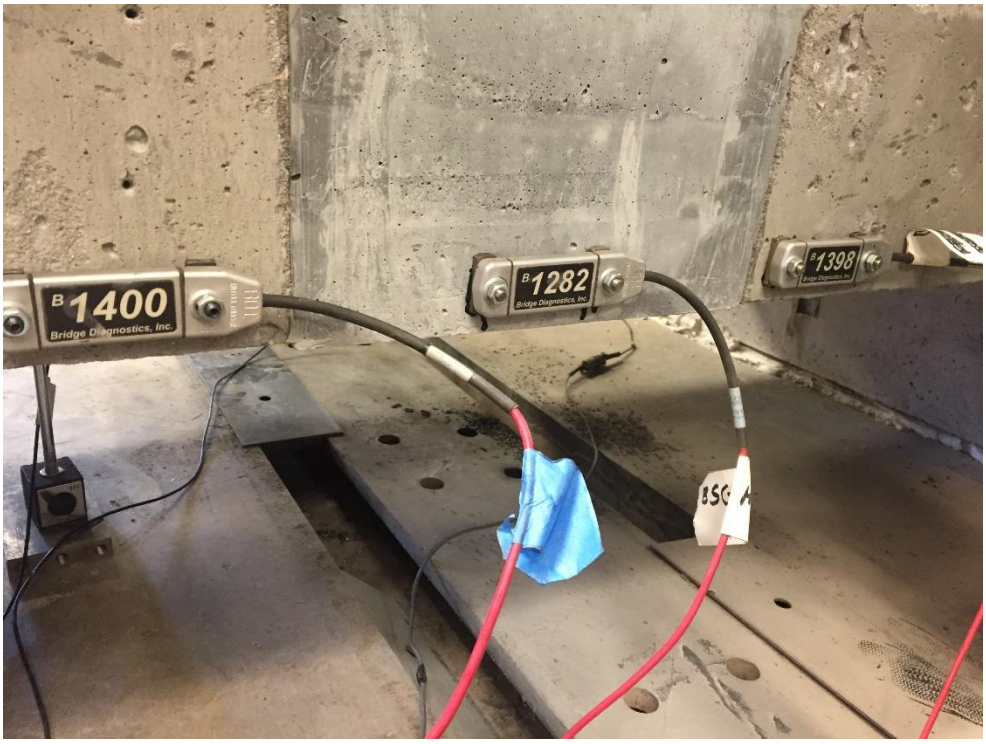

Figure 98. Strain gages on south side of slab prior to testing

Figure 99. LVDT on underside of slab prior to testing

Figure 100. Wire potentiometer attached to underside of slab prior to testing

Figure 101. Hydraulic cylinder and load cell prior to attachment to hand pump; used for part 2 of static testing

Appendix C: Calculations

Cracking Moment and Corresponding Load for Slabs

$$M_{cr} = \frac{f_r I_s}{y_t}$$

Where

$f_r = 7.5\sqrt{f'c} = 7.5\sqrt{5500\ psi} = 556.2\ psi$

$I_s = \frac{bh^3}{12} = \frac{(48\ in.)(8\ in.)^3}{12} = 2{,}048\ in.^4$

$y_t = 4\ in.$

So,

$$M_{cr} = \frac{f_r I_s}{y_t} = \frac{(556.2\ psi)(2{,}048\ in.^4)}{4\ in.} = 284{,}774\ lb \cdot in. = 23.73\ kip \cdot ft$$

To find the corresponding point load for a non-symmetric simple span of length L = A + B:

$$P = \frac{ML}{AB} = \frac{(23.73\ kip \cdot ft)(8.5\ ft)}{(5.167\ ft)(3.333\ ft)} = 11.7\ kips$$

Note that

M_{cr} = cracking moment, lb-in.

f_r = modulus of rupture of concrete, psi

I_s = moment of inertia of gross section of slab about centroidal axis, in.^{4}

b = width of compression face of member, in.

h = overall depth of member, in.

y_t = distance from the centroid of the cross section to the tension face, in.

f'_c = compressive strength of concrete, psi

Flexural Capacity and Corresponding Load for Slabs

Assuming both layers of steel are in tension during loading,

$$M_n = A_{s1} f_y \left(d_1 - \frac{c}{2}\right) + A_{s2} f_y \left(d_2 - \frac{c}{2}\right)$$

Where

$A_{s1} = A_{s2} = 4(0.31\ in.^2) = 1.24\ in.^2$

$f_y = 60\ ksi$

$d_1 = 6.063\ in.$

$d_2 = 2.44\ in.$

$$a = \frac{2A_s f_y}{0.85 f'_c b} = \frac{2(1.24\ in.^2)(60\ ksi)}{0.85(5.5\ ksi)(48\ in.)} = 0.66\ in.$$

$$c = \frac{a}{\beta_1} = \frac{0.66\ in.}{0.80} = 0.825\ in.$$

Checking the assumption that the steel yields:

$$\varepsilon_{s1} = \frac{0.003}{c}(d_1 - c) = \frac{0.003}{0.825}(6.063 - 0.825) = 0.019 > 0.00205$$

$$\varepsilon_{s2} = \frac{0.003}{c}(d_2 - c) = \frac{0.003}{0.825}(2.44 - 0.825) = 0.006 > 0.00205$$

So,

$$M_n = (1.24\ in.^2)(60\ ksi)\left[\left(6.063\ in. - \frac{0.825\ in.}{2}\right) + \left(2.44\ in. - \frac{0.825\ in.}{2}\right)\right]$$

$$= 571.2\ kip \cdot in. = 47.6\ kip \cdot ft$$

To find the corresponding point load for a non-symmetric simple span of length L = A + B:

$$P = \frac{ML}{AB} = \frac{(47.6\ kip \cdot ft)(8.5\ ft)}{(5.167\ ft)(3.333\ ft)} = 23.5\ kips$$

Note that

M_n = nominal flexural strength at section, lb-in.

A_{s1} = area of the bottom layer of longitudinal tension reinforcement, in.^{2}

A_{s2} = area of the top layer of longitudinal tension reinforcement, in.^{2}

f_y = specified yield strength of reinforcement, ksi

d_1 = distance from extreme compression fiber to centroid of bottom layer of longitudinal tension reinforcement, in.

d_2 = distance from extreme compression fiber to centroid of top layer of longitudinal tension reinforcement, in.

a = depth of equivalent rectangular stress block, in.

c = distance from extreme compression fiber to neutral axis, in.

ε_{s1} = value of net tensile strain in the bottom layer of longitudinal tension reinforcement, in./in.

ε_{s2} = value of net tensile strain in the top layer of longitudinal tension reinforcement, in./in.

Fatigue Stress in Steel for Slab 3

$$f_s = n\frac{My}{I_{cr}}$$

$$\rho_1 = \frac{A_s}{bd} = \frac{4(0.31\ in.^2)}{48\ in.(6.063\ in.)} = 0.0043$$

$$\rho_2 = \frac{A_s}{bd} = \frac{8(0.31\ in.^2)}{48\ in.(4.25\ in.)} = 0.0122$$

$$n = \frac{E_s}{E_c} = \frac{29{,}000\ ksi}{4227\ ksi} = 6.86$$

$$k_1 = \sqrt{2\rho n + (\rho n)^2} - \rho n = \sqrt{2(.0043)(6.86) + (.0043 * 6.86)^2} - (.0043 * 6.86)$$

$$= 0.212$$

$$k_2 = \sqrt{2\rho n + (\rho n)^2} - \rho n = \sqrt{2(.0122)(6.86) + (.0122 * 6.86)^2} - (.0122 * 6.86)$$

$$= 0.333$$

$$k_2 d = (0.333)(4.25\ in.) = 1.42\ in.$$

$$A_{str} = A_s n = 4(0.31 in.^2)(6.86) = 8.51\ in.^2$$

$$I_{cr} = \frac{1}{12}(48\ in.)(1.42\ in.)^3 + 48\ in.(1.42\ in.)\left(\frac{1.42\ in.}{2}\right)^2$$

$$+ 8.51\ in.^2(6.063\ in. - 1.42\ in.)^2 + 8.51\ in.(2.44\ in. - 1.42\ in.)^2$$

$$= 238.113\ in.^4$$

$$M = \frac{Pab}{L} = \frac{14.6\ kips(5.167\ ft)(3.333\ ft)}{8.5\ ft} = 29.58\ kip \cdot ft = 354.97\ kip \cdot in.$$

$$y = 6.063\ in. - 1.42\ in. = 4.643\ in.$$

$$f_s = (6.86)\frac{(354.97\ kip \cdot in.)(4.643\ in.)}{238.113\ in.^4} = 47.5\ ksi$$

Note that

M = applied moment, lb-in.

A_s = area of longitudinal tension reinforcement, in.^{2}

A_{str} = transformed area of longitudinal tension reinforcement, in.^{2}

ρ_1 = reinforcement ratio for bottom layer of steel

ρ_1 = reinforcement ratio for top layer of steel

f_s = stress in steel reinforcement under load, ksi

I_{cr} = cracked moment of inertia, in.^{4}

n = ratio of steel modulus of elasticity to concrete modulus of elasticity

d = effective depth to centroid of longitudinal tension reinforcement, in.

kd = depth from top of section to cracked neutral axis, in.